Higher Order Corrections to Top-Quark Pair Production

Dissertation

zur
Erlangung der naturwissenschaftlichen Doktorwürde
(Dr. sc. nat.)
vorgelegt der
Mathematisch-Naturwissenschaftliche Fakultät
der
Universität Zürich
von

Cedric Studerus

von
Waldkirch, SG

Promotionskomitee

Prof. Dr. Thomas Gehrmann
Prof. Dr. Daniel Wyler
Prof. Dr. Ben Moore
Prof. Dr. Ulrich Straumann

Zürich, 2010

Zusammenfassung

Diese Dissertation beinhaltet drei Projekte: Das Hauptprojekt ist die Berechnung von Zwei-Loop-Korrekturen zur Top-Quark-Paarproduktion in störungstheoretischer QCD. Das zweite Projekt ist die Reduktion von Drei-Loop-Feynman-Integralen in der Berechnung von Quark- und Gluon- Formfaktoren. Das dritte Projekt ist die Entwicklung des Computerprogramms `Reduze`, um Reduktionen von Multi-Loop-Feynman-Integralen durchzuführen. Der Code ist erfolgreich für die Reduktionen in den vorher genannten Projekten benutzt worden.

Zuerst berechnen wir die fermionischen Zwei-Loop-Korrekturen und die planaren Zwei-Loop-Diagramme, die zum führenden Farbkoeffizienten des Wirkungsquerschnitts von Top-Antitop-Quark-Produktion durch Quark-Antiquark-Streuung beitragen. Wir erhalten analytische Ergebnisse, die für beliebige Werte der Mandelstam-Invarianten s und t und der Top-Quark-Masse m gültig sind. Unsere Ergebnisse bestätigen schon bekannte Resultate, wie die analytische Berechnung im Limes verschwindender Masse und die numerischen Werte für die exakte Amplitude. Ferner stellen wir die Entwicklung der Zwei-Loop-Amplitude an der Produktionsschwelle $s \gtrsim 4m^2$ zur Verfügung.

Zweitens beschreiben wir die Berechnung der Drei-Loop-QCD-Korrekturen für Quark- und Gluon- Formfaktoren. Die relevanten Drei-Loop-Feynman-Diagramme werden ausgerechnet und die resultierenden Drei-Loop-Integrale mit Hilfe der Integration-by-Parts-Identities auf einen kleinen Satz bekannter Master-Integrale reduziert. Unsere Berechnungen bestätigen die kürzlich von Baikov et al. veröffentlichten Ergebnisse für die Drei-Loop-Formfaktoren. Zusätzlich leiten wir die $\mathcal{O}(\epsilon)$-Terme von den Fermion-Loop-Beiträge der Drei-Loop-Formfaktoren her, die für die Berechnung der fermionischen Beiträge zu der kollinear anomalen Dimensionen von Quarks und Gluons auf Vier-Loop-Level benötigt werden. Der endliche Anteil der Formfaktoren wird benutzt, um die harten Matching-Koeffizienten für den Drell-Yan-Prozess und die inklusive Higgs-Produktion in soft-kollinear effektiver Theorie zu bestimmen.

Schliesslich stellen wir `Reduze` vor, ein Computerprogramm, um Feynman-Integrale mit Hilfe der Integration-by-Parts-Identities und des Laporta-Algorithmus auf Master-Integrale zu reduzieren. Das Programm ist in C++ geschrieben und benutzt von der `GiNaC`-library zur Verfügung gestellte Klassen, um die algebraischen Vorfaktoren im Gleichungssystem zu vereinfachen. `Reduze` bietet die Möglichkeit, Reduktionen parallel durchzuführen.

Abstract

This thesis consists of three projects: the main project is the calculation of two-loop corrections to top-quark pair production in perturbative QCD. The second project is the reduction of Feynman integrals in the calculation of quark and gluon form factors at three loop. The third project is the development of the computer code `Reduze` to perform reductions of multi-loop Feynman integrals. The code has been used successfully for the reductions in the projects mentioned before.

First, we evaluate the fermionic two-loop QCD corrections and the planar two-loop QCD diagrams contributing to the leading color coefficient of the heavy-quark pair production cross section in the quark-antiquark channel. We obtain analytic results which are valid for any value of the Mandelstam invariants s and t, and of the heavy quark mass m. Our findings confirm previous results for the analytic evaluation in the small-mass limit and numerical results for the exact amplitude. We furthermore provide the expansion of the two-loop amplitude at the production threshold $s \gtrsim 4m^2$.

Second, we describe the calculation of the three-loop QCD corrections to quark and gluon form factors. The relevant three-loop Feynman diagrams are evaluated and the resulting three-loop Feynman integrals are reduced to a small set of known master integrals by using integration-by-parts relations. Our calculation confirms the recent results by Baikov et al. for the three-loop form factors. In addition, we derive the subleading $\mathcal{O}(\epsilon)$ terms for the fermion-loop type contributions to the three-loop form factors which are required for the extraction of the fermionic contributions to the four-loop quark and gluon collinear anomalous dimensions. The finite parts of the form factors are used to determine the hard matching coefficients for the Drell-Yan process and inclusive Higgs-production in soft-collinear effective theory.

Finally, we present `Reduze` which is a computer program for reducing Feynman integrals to master integrals employing a Laporta algorithm. The program is written in C++ and uses classes provided by the `GiNaC` library to perform the simplifications of the algebraic prefactors in the system of equations. `Reduze` offers the possibility to run reductions in parallel.

Acknowledgements

From the beginning of my PhD position I started working on top-quark pair production in collaboration with my supervisor Dr. Prof. Thomas Gehrmann and Roberto Bonciani, Andrea Ferroglia and Daniel Maître. I am very grateful to Thomas for giving me this opportunity and thank him very much. The collaboration with Thomas, Roberto, Andrea and Daniel was and still is a pleasure! On the other side, I got the time to work on my own project, the reduction code `Reduze`, which then became useful also in the top-quark production project. Here I want to thank again Daniel, for all his help setting up a software project and hints in C++ programming. Great thanks also goes to Doug Potter who always supported me with information about operating systems and shell-scripting. The `Reduze`-project made great progress when Andreas von Manteuffel got involved. It would not have been possible to fully parallelize the code without him. I thank Andreas very much for all discussions and the fruitful collaboration.

Special thank goes to all my colleagues and friends at the institute, particularly to Tobias Motz, Katja and Pedro Schwaller, Antoine Klein, Christine Moran, Nico Greiner, Marc Gillioz, Gionata Luisoni, Erich Weihs, Beat Tödtli, Nico Hamaus, Lucas Lombriser, Aurel Schneider, Pedro Jiménez-Delgado. We had a great time playing Doppelkopf and having Separata-parties.

I thank Christine, Andreas and Thomas for reading the manuscript. I also thank the University of Zurich, particularly the Institute of Physics and the Institute of Theoretical Physics for the education in physics and science during all the years of study. This research was supported by the Forschungskredit der Universität Zürich.

Contents

List of Figures

List of Tables

LIST OF TABLES

1

Introduction

This doctoral thesis is the summary of the work I have done as a PhD student in the last three years at the Institute of Theoretical Physics at University of Zurich. The thesis consists of three projects: the main project is the calculation of two-loop corrections to top-quark pair production in perturbative QCD. The second project is the reduction of Feynman integrals in the calculation of quark and gluon form factors at three loop. The third project is the development of the computer code `Reduze` to perform reductions of multi-loop Feynman integrals. The code has been used successfully for the reductions in the projects previously mentioned.

The thesis is organized as follows: in this chapter a short overview about quantum theory, the standard model of particle physics, quantum chromodynamics and physics at hadron colliders will be given. It is mostly based on the books [1–8]. In Chapter 2 we will discuss the calculation of two-loop corrections to top-quark pair production and in Chapter 3 the calculation of the three-loop quark and gluon form factors is presented. In Chapter 4 we will have a closer look on how reductions are performed and explain the computer program `Reduze`.

1.1 Quantum Theory

The main goals of classical physics are the predictions of position and momentum of a collection of particles at any time assuming these values are known at one point in time. The physical forces that cause the change of the system can be described with a Hamiltonian, a function depending on the position and momentum of the particles.

In describing the microscopic world of atoms and the fundamental particles the classical description breaks down. Various observed quantities have discrete values: the spin of an electron, leading to a magnetic moment, has only two different values and the spectrum of the hydrogen atom consists of discrete steps. The energy and spin are quantized. Furthermore, the double-slit experiment showed that particles like

electrons, neutrons and even atoms behave like a wave as well. On the other hand, light can be regarded as consisting of energy quanta, namely photons, which was the correct assumption to derive the law for black body radiation and the explanation of the photoelectric effect. This wave-particle dualism does have a solution with the notion of a quantum mechanical state.

The mathematical concepts of quantum physics are quite abstract. Instead of concentrating on the phase space of position and momentum of a particle one considers a particle as a vector $|\Psi\rangle$ of an abstract Hilbert space and calls it a state. The measurable quantities of a state, like energy, are the eigenvalues of a self adjoint operator acting on the state. Those states which are eigenvectors of a self adjoint operator are called pure states. In general, a state can be a superposition of some basis states. Then one can calculate a mean value, the expectation value, of this state using the scalar product of the Hilbert space.

$$\langle A \rangle_\Psi = \langle \Psi | A | \Psi \rangle \ . \tag{1.1}$$

For pure normalized states $\langle \Psi | \Psi \rangle = 1$ which are eigenstates of a self adjoint operator A, $|A\Psi\rangle = a\,|\Psi\rangle$, the expectation value becomes $\langle A \rangle_\Psi = a$ the eigenvalue. The time evolution of a state is governed by a unitary operator $U(t, t_0)$ which transforms a state $|\Psi\rangle\,(t_0)$ at time t_0 to the state $|\Psi\rangle\,(t - t_0) = U(t, t_0)\,|\Psi\rangle\,(t_0)$ at time $t - t_0$.

A great success of the quantum theory was the Schrödinger equation

$$i\hbar\,\frac{\partial}{\partial t}\Psi(\vec{x}, t) = H(\vec{x})\ \Psi(\vec{x}, t) \tag{1.2}$$

where the Hilbert space is the space of the square-integrable functions $L^2(R^3)$ and the time independent self adjoint Hamiltonian is given by:

$$H(\vec{x}) = -\frac{\hbar^2}{2m}\,\triangle_x + V(\vec{x})\ . \tag{1.3}$$

The Schrödinger equation describes a particle with mass m in a potential $V(\vec{x})$. The famous example is the calculation of the discrete energy spectrum of the hydrogen atom, assuming an electron in the electric field of the nucleus, by solving the eigenvalue equation

$$H(\vec{x})\ \Psi(\vec{x}) = E\ \Psi(\vec{x})\ . \tag{1.4}$$

The unitary time evolution operator $U(t, t_0)$ which fulfills $U(t, t_0)\,\Psi(\vec{x}, t_0) = \Psi(\vec{x}, t - t_0)$ is formally given by

$$U(t, t_0) = \exp\left(\frac{-i}{\hbar}\,H(\vec{x})\ (t - t_0)\right) \tag{1.5}$$

The Schrödinger equation can also describe scattering of particles on an external potential. In scattering theory the squared amplitude

$$|\langle \Psi | U | \Phi \rangle|^2 \tag{1.6}$$

is interpreted as the probability that the state $|\Phi\rangle$ after evolving in time by the unitary operator U is equal to the state $|\Psi\rangle$

The Schrödinger equation describes non-relativistic particles. But for high energy experiments we need a relativistic description as well as a formalism that is able to predict particle creation and annihilation. This extension is sometimes called second quantization and leads from quantum mechanics to quantum field theories.

The relativistic wave functions of free particles with different spin are characterized by their transformation properties under the different spinor representations of the Lorentz group. The differential equations the wave functions fulfill are obtained as the simplest possible differential equations which are invariant under the corresponding representation. The most important relativistic invariant equations for a spin 0 and a spin 1/2 particle are the Klein-Gordon equation and the Dirac equation. The free Klein-Gordon equation reads

$$\Box_x \Psi(x) + \frac{m^2\, c^2}{\hbar^2}\, \Psi(x) = 0 \tag{1.7}$$

and the free Dirac equation

$$i\,\hbar\,\gamma^\mu\,\partial_\mu\,\Psi(x) = m\,c\,\Psi(x)\ . \tag{1.8}$$

The γ^μ are the Dirac matrices, $\hbar$ the Planck constant and c the speed of light in vacuum. The equation for a spin 1 vector field A^μ is the Klein-Gordon equation for each component of A^μ.

For the description of particle creation and annihilation, a multi-particle Hilbert space, the Fock space F, is constructed by the direct sum of all n-particle Hilbert spaces H_n

$$F = \bigoplus_{n=0}^{\infty} H_n\ , \tag{1.9}$$

where the n-particle spaces are defined as tensor products of the one particle space.

$$H_n = \bigotimes_{k=1}^{n} H\ , \qquad H_0 = \mathbb{C}\ . \tag{1.10}$$

The space H_0 contains the vacuum Ω. The Fock space F can be decomposed into $F = F^- + F^+$, where $F^\pm = S^\pm F$ are the projections to the antisymmetric and symmetric states. The most important operators that one defines on the Fock space are the so-called emission or creation operators $a^\dagger(f)$ and the annihilation or absorption operators $a(f)$. The emission operator creates a particle state with wave function f from the vacuum state $\Omega = (1, 0, 0\ldots) \in F$ and the absorption operator is its adjoint. These two operators fulfill

$$\begin{aligned} [a(f), a^\dagger(g)]_\pm &= (f, g) \\ [a(f), a(g)]_\pm = [a^\dagger(f), a^\dagger(g)]_\pm &= 0\ , \end{aligned} \tag{1.11}$$

where the subscript $\pm$ means the anti-commutator (for antisymmetric states) or the commutator (for symmetric states), respectively. One also introduces the operator valued distributions that express the mapping of a function to the operators:

$$a^\dagger(f) = \int a^\dagger(\vec{x})\ f(\vec{x})\,\mathrm{d}^3\vec{x} = \int \hat{a}^\dagger(\vec{k})\ \hat{f}(\vec{k})\,\mathrm{d}^3\vec{k} \tag{1.12}$$

and

$$a(f) = \int f^*(\vec{x})\ a(\vec{x})\,\mathrm{d}^3\vec{x} = \int \hat{f}^*(\vec{k})\ \hat{a}(\vec{k})\,\mathrm{d}^3\vec{k}\ . \tag{1.13}$$

From equation (1.11) it follows that they fulfill

$$\begin{aligned} [a(k), a^\dagger(k')]_\pm &= \delta^3(k-k') \\ [a(k), a(k')]_\pm &= [a^\dagger(k), a^\dagger(k')]_\pm = 0\ . \end{aligned} \tag{1.14}$$

These are the canonical commutation and anticommutation relations. To arrive at a relativistic invariant formulation one introduces the so-called field operators. For a free real scalar field (without spin) in x-space they are defined through the following distributional Fourier transform:

$$\begin{aligned} \Psi^+(\mathbf{x},t) &= \int \frac{\mathrm{d}^3\mathbf{p}}{(2\pi)^3}\frac{1}{\sqrt{2E_\mathbf{p}}}a^\dagger(\mathbf{p})e^{ipx} \\ \Psi^-(\mathbf{x},t) &= \int \frac{\mathrm{d}^3\mathbf{p}}{(2\pi)^3}\frac{1}{\sqrt{2E_\mathbf{p}}}a(\mathbf{p})e^{-ipx}\ . \end{aligned} \tag{1.15}$$

The spin-statistics theorem states that for quantization of physical fields, the commutation relations have to be used for particles with integer spin (bosons) and anticommutation relations for particles with half integer spin (fermions).

So far, only free fields and field equations have been introduced but we are interested in the description of the physical interacting fields. Here enters the beautiful and successful concept of gauge invariance. The observation is that e.g. the Dirac equation is invariant under a global phase transformation $\Psi(x) \to \exp(i\,\Lambda)\,\Psi(x)$ but not under a local phase transformation or gauge transformation $\Psi(x) \to \exp(i\,\Lambda(x))\,\Psi(x)$ since this transformation adds a term $\partial_\mu\Lambda(x)$. But this unwanted term can be compensated by introducing an additional field A^μ, a gauge field, into the Dirac equation that transforms under the gauge transformation as $A^\mu \to A^\mu - \partial_\mu\,\Lambda(x)$. This additional field has the same gauge transformation as the vector field in classical electrodynamics (ED) and therefore can be identified as the photon field. The correct coefficients of the gauge field A^μ contain the speed of light in vacuum c and the electro-magnetic coupling constant e. The Dirac equation with the additional source term reads:

$$\gamma^\mu\ \left(i\,\hbar\,\partial_\mu - \frac{e}{c}\,A^\mu\right)\ \Psi(x) = m\,c\,\Psi(x)\ . \tag{1.16}$$

The field equations for interacting fields can also be derived from a gauge invariant Lagrangian by a variational principle.

$$L(\Psi, \bar{\Psi}, A^\mu) = \bar{\Psi} \left(\gamma^\mu \left(i \hbar \partial_\mu - \frac{e}{c} A^\mu \right) - m c \right) \Psi(x) - \frac{1}{4} F^{\mu\nu} F_{\mu\nu} . \tag{1.17}$$

$F^{\mu\nu} = \partial_\mu A_\nu - \partial_\nu A_\mu$ is the field strength tensor and $\bar{\Psi}$ is the Dirac conjugated field of Ψ. The three Euler-Lagrange equations then lead to the Dirac equation, conjugated Dirac equation and the Maxwell equations.

The Dirac equation with the local phase transformation of the gauge group U(1) essentially defines quantum electrodynamics (QED). If one takes a non-abelian gauge group as SU(3), one gets the non-abelian gauge theory quantum chromodynamics (QCD).

1.2 Perturbation Theory

Information about the fundamental forces the physical particles feel is given by scattering experiments where one beam of particles strikes a fixed target or two beams are collided. The observables that can be measured in such an experiment are the energy of the particles and their trajectories. From these measurements one can deduce the particle type as well as its mass, spin, charge etc. In theory one wants to predict these results, particularly the angular and energy distribution of the scattered particles. For this, a quantum mechanical amplitude has to be calculated. The probability that a given free ingoing particle state is transformed by the interaction to a certain free outgoing state is given by the square of the scalar product

$$\langle \Psi_{out} \mid S \mid \Psi_{in} \rangle , \tag{1.18}$$

where S is the so-called scattering operator or S-matrix. The problem is that this scattering operator has never been shown to exist for physically relevant interactions. However, this scattering operator can be expanded around a small coupling constant g. This expansion can be defined as a formal power series (convergence has not been proved). The amazing fact, at least for QED, is that the lowest order contributions predict amplitudes which are very accurate when compared with experimental measurements. Higher order corrections improve the theoretical predictions and become smaller and smaller.

The S-Matrix is usually split into a non-interacting and an interacting part

$$S = 1 + i T . \tag{1.19}$$

For a $2 \to n$ process with two incoming particles with momenta p_1 and p_2 and n outgoing momenta with momenta q_i we construct the free asymptotic states $\mid p \rangle = a^\dagger(p)\Omega$. The

matrix elements of S are related to the invariant matrix element M by

$$\begin{aligned}\langle q_1, \ldots, q_n, \mid i\,T \mid p_1, p_2 \rangle =& (2\pi)^4\, \delta^{(4)}\left(p_1 + p_2 - \sum q_i\right) \times \\ & i\,M(p_1, p_2 \to q_1, \ldots, q_n)\,.\end{aligned} \tag{1.20}$$

The matrix element M is the scattering amplitude analogous to the quantum mechanical amplitude of the one particle theory.

The perturbative expansion of the amplitude M in the coupling constant has a descriptive interpretation as a sum of Feynman diagrams, where each diagram represents incoming particles which undergo an interaction and then leave the process as outgoing particles. External legs carry incoming or outgoing momenta in such a way that energy-momentum conservation is fulfilled. An edge of a diagram is identified with a propagating particle and a node with a vertex where the interaction takes place. At any vertex the momenta have to be conserved, and if the diagram has closed loops, some loop momenta must be introduced which are then integrated over. The particular model that one uses determines the set of allowed propagators and interaction vertices. The external legs, propagators and vertices correspond to mathematical expressions which are, together with the prescription of how to combine them, the Feynman rules. For QCD the Feynman rules can be found in Figure 1.2. Every vertex introduces a factor of a coupling constant to the analytical expression of a diagram and determines its order in the perturbation series of the amplitude. The simplest Feynman diagrams are the tree level diagrams as in Figure 2.1. In the next order of the perturbative expansion in the coupling constant the contributing diagrams usually have one closed loop and going to higher orders introduces more and more loops. According to the Feynman rules, every loop in the diagram introduces a four dimensional integration over the loop momenta. These integrals are called Feynman integrals.

With the Feynman rules the amplitude of scattering and decay processes can be calculated perturbatively. From the amplitude, measurable quantities like decay widths and cross sections together with their differential distributions can then be obtained by a phase space integration.

1.3 Renormalization

The Feynman integrals are plagued by divergences and have to be regularized. There are two types of divergences that can occur. These are the so-called ultraviolet (UV) and infrared (IR) divergences. The reason for the UV divergences is the fact that in quantum field theory the field operators are operator valued distributions and one cannot simply multiply them at the same space-time point. One can get rid of those divergences by renormalization. The IR divergences arise when the gauge bosons are massless and the initial or final states of a process contain charged particles. The IR divergences cancel

if physical quantities like cross sections are calculated and all contributing diagrams are taken into account. For explicit calculations of Feynman diagrams the method of dimensional regularization is often used. This method continues the four dimensional space-time to the complex plane and introduces dimension dependent measures for the Feynman integrals. This way, both the UV and IR divergences are regularized.

By renormalization, the UV divergences of Feynman integrals are turned into finite expressions which are not uniquely determined but depend on so-called renormalization constants. These constants can be fixed by the symmetries of the theory and a few renormalization conditions. They relate the free parameters of the theory with the experimentally measured values. There exist several renormalization schemes, from which the $\overline{\text{MS}}$ scheme is widely used in quantum chromodynamics.

1.4 Standard Model of Particle Physics

The standard model of particle physics (SM) is the quantum field theory which describes the interaction of the fundamental particles in the electro-magnetic, weak and strong interaction. The gravitational force is not included. On the one side there are theoretical problems quantizing gravity, but on the other side its contribution to measurable quantities is negligibly small in today's collider experiments. The SM is a gauge theory with the gauge group $\mathrm{U(1)_Y} \times \mathrm{SU(2)_L} \times \mathrm{SU(3)_C}$, where $\mathrm{U(1)_Y} \times \mathrm{SU(2)_L}$ is the unified electroweak sector and $\mathrm{SU(3)_C}$ the strong sector described by quantum chromodynamics.

The fundamental constituents of matter are the fermions. All fermions feel the weak interaction. The fermions that also feel the strong interaction are called quarks and the others leptons. The left-handed components of the fermions form weak isospin doublets under the transformation group $\mathrm{SU(2)_L}$, like an electron with its neutrino and an up-type quark with a down-type quark, whereas the right-handed components transform as singlets. The quarks have baryon number $B = 1/3$ and lepton number $L = 0$ and the leptons $B = 0$ and $L = 1$. For each particle there also exist a corresponding antiparticle with the same mass and opposite quantum numbers. Quarks and leptons come in three generations as listed in Figure 1.1.

The gauge bosons are the particles that mediate the forces between the fermions. The massless photon is responsible for the electro-magnetic force, the massive Z- and W-bosons mediate the weak interaction and the massless gluons the strong force. Every generator of a transformation group leads to a massless gauge field. In the case of $\mathrm{SU(3)_C}$ this are the eight gluon fields. In the electroweak sector the physical gauge fields of the Z- and W-bosons get their mass by the Higgs mechanism through spontaneous symmetry breaking. This mechanism introduces the Higgs boson. Up to now, the Higgs

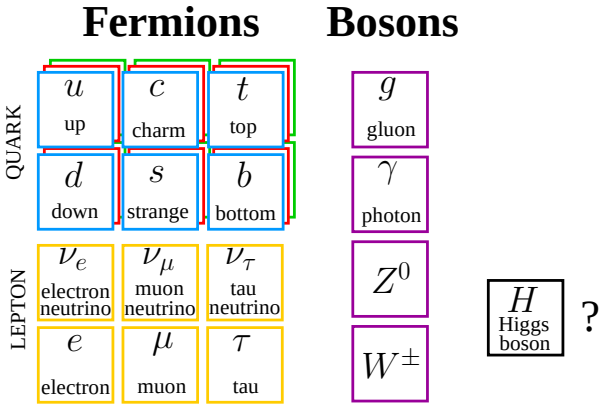

Figure 1.1: Particles and forces described by the Standard Model. Fermions are present in three different quark and lepton families. Furthermore, the six quark flavors can have three different colors.

boson has not been found experimentally. Higgs searches are underway at Tevatron and at LHC.

The weak interaction allows for flavor changing transition like $t \to b$ emitting the charged W^+-boson. The strength of this flavor mixing current is given by the entry V_{tb} of the unitary Cabibbo-Kobayashi-Maskawa (CKM) matrix. This matrix relates the mass eigenstates of the quarks to their flavor eigenstates.

1.5 Quantum Chromodynamics

Quantum chromodynamics (QCD) is the quantum field theory which describes the strong interaction. It is a non-abelian field theory with gauge group SU(3). The gauge fields are the eight gluons which mediate the strong force. The fermions interacting with the gluons are the quarks. Beside the color charge the quarks also carry a weak charge and an electric charge, which is a fraction of the elementary electron charge. The up-type quarks are called up (u), charm (c) and top (t) and the down-type quarks are down (d), strange (s) and bottom (b). The top quark is the heaviest quark. Unlike the photons in QED, the gluons carry a color charge. This is the reason for the opposite behavior of the strong coupling constant which gets large at low energy scales (confinement) and small at high energies (asymptotic freedom). Confinement refers to the fact that quarks and gluons are never observed as free particles but are confined in hadrons like protons or pions. Asymptotic freedom, on the other hand, means that at high energies quarks and gluons interact very weakly. In this region, where the coupling constant is small, perturbative calculations can be performed.

The Lagrangian for this theory consists of three terms:

$$\mathcal{L}_{QCD} = \mathcal{L}_{\text{inv.}} + \mathcal{L}_{\text{gauge-fixing}} + \mathcal{L}_{\text{ghost}} \,. \tag{1.21}$$

The first term $\mathcal{L}_{\text{inv.}}$ is invariant under local SU(3)$_C$ gauge transformations and defines the kinetic terms of the quark and gluon fields and all quark-gluon and gluon-gluon interactions. It is written as

$$\mathcal{L}_{\text{inv.}} = \sum_f \bar{q}_{f_i} \left(i \not{D} - m_q \right)_{ij} q_{f_j} - \frac{1}{4} F^{\mu\nu,\,a} F^a_{\mu\nu} \,, \tag{1.22}$$

where the sum runs over all quark flavors f. The field strength tensor $F^a_{\mu\nu}$ and the covariant derivative $\not{D}$ have the form:

$$F^a_{\mu\nu} = \partial_\mu A^a_\nu - \partial_\nu A^a_\mu + g_s f^{abc} A^b_\mu A^c_\nu \,, \tag{1.23}$$

$$\not{D}_{ij} = (\gamma^\mu D_\mu)_{ij} = \gamma^\mu \left(\delta_{ij} \partial_\mu - i\, g_s\, T^a_{ij}\, A^a_\mu \right) \,, \tag{1.24}$$

$$(m_q)_{ij} = m_q \delta_{ij} \,. \tag{1.25}$$

In the above equations, g_s is the bare gauge coupling, T^a_{ij} the generators of the SU(3) gauge group in the fundamental representation and f^{abc} the structure constants.

The QCD Lagrangian requires two more terms. Within the path integral quantization, the functional integral must be restricted to sections transversal to the gauge orbits by choosing a gauge fixing. This leads to the Faddeev-Popov determinant which can be attributed to the ghost fields. The ghost fields are scalar anticommuting fields and not physical particles, as they have the wrong relation between spin and statistics.

$$\mathcal{L}_{\text{gauge-fixing}} = -\frac{1}{2\xi} \left(\partial^\mu A^a_\mu \right)^2 \,, \tag{1.26}$$

$$\mathcal{L}_{\text{ghost}} = \tilde{c}^a \left(-\partial^2 \delta^{ac} - g_s\, \partial^\mu f^{abc} A^b_\mu \right) c^c \,. \tag{1.27}$$

From this Lagrangian, the Feynman rules for perturbative calculations in the strong coupling constant can be derived. They are listed in Figure 1.2. Instead of the coupling constant g_s we often use the parameter

$$\alpha_s = \frac{g_s^2}{4\pi} \,. \tag{1.28}$$

With the Feynman rules one can calculate the amplitude for the scattering of quarks and gluons and then a partonic cross section. In nature, however, there exists only hadrons, bounded states of partons (quarks and gluons), like the proton. The connection between the hadronic cross section and the partonic cross section is given by a convolution of the partonic cross section with the so-called parton distribution functions (PDF). The PDF $f(x, \mu_F)$ gives the probability density to find a particular parton in a hadron with the longitudinal momentum fraction x of the hadron at the factorization scale μ_F. PDFs are universal, meaning that they have to be determined once

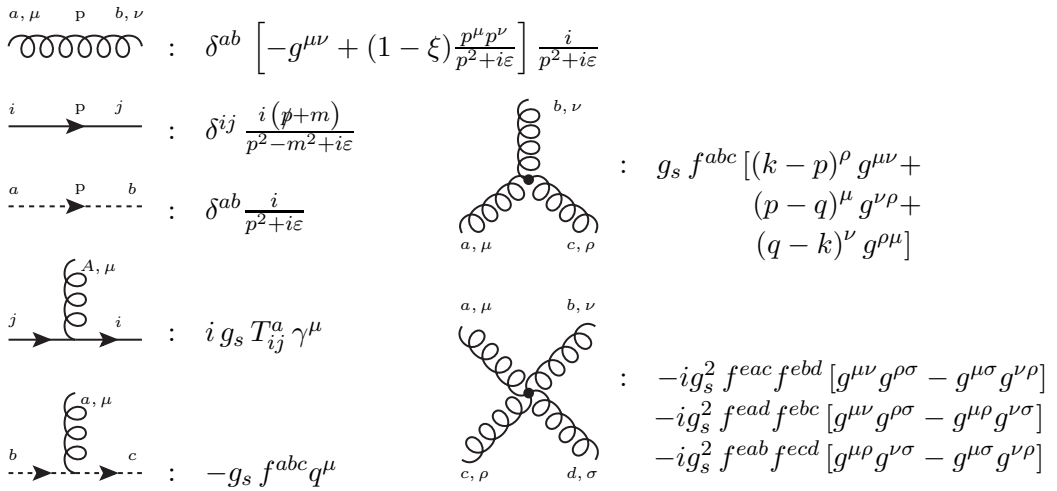

Figure 1.2: QCD Feynman rules for the matrix element $i\,M$.

by experiments and then can be used to make other predictions. For a process of two colliding beams of hadrons with energy

$$s_{\text{had}} = (p_{h_1} + p_{h_2})^2 \ , \tag{1.29}$$

the underlying process is the scattering of two partons with an energy fraction

$$\hat{s} = x_1 x_2 s_{\text{had}} \tag{1.30}$$

of the hadronic energy. Then the hadronic cross section is given by

$$\sigma_{h_1,h_2}(s_{\text{had}}) = \sum_{i,j}\int_0^1 \mathrm{d}x_1 \int_0^1 \mathrm{d}x_2\; f_i^{h_1}(x_1,\mu_F)\; f_j^{h_2}(x_2,\mu_F)\; \hat{\sigma}_{ij}\left(\hat{s},\alpha_s(\mu_R),\mu_R,\mu_F\right) \ , \tag{1.31}$$

where the sum runs over all partons and $\hat{\sigma}_{ij}$ is the partonic cross section of the partons i and j at the renormalization scale μ_R and factorization scale μ_F.

1.6 Precision Physics at Hadron Colliders

With the upcoming measurements at the Large Hadron Collider (LHC), a new era of particle physics will begin. Two proton beams are collided with a center of mass energy up to 14 TeV and a luminosity of order $10^{34}\text{cm}^{-2}\text{s}^{-1}$. In collisions at such high energies new heavy particles could be produced and the high luminosities will give large statistics in quite a short time: the LHC is a discovery machine. The LHC will give

more insight in the properties and interactions of the fundamental particles and it is hoped that it will discover the Higgs boson. Because of the hadronic initial states, there will be a large hadronic activity in the detectors which comes from soft and hard scattering of the partons. Since the latter can be calculated in perturbative QCD, the findings at LHC will also serve as precision tests for QCD.

In the following we will give an overview of some processes for which the higher order calculations in Chapter 2 and 3 are needed.

1.6.1 Higgs Production and Drell-Yan Process

One of the main goals of the LHC is the detection of the Higgs boson, the last particle predicted by the SM that has not yet been found experimentally. The Higgs field is responsible for the origin of the particle masses, particularly it gives masses to the W- and Z-bosons by the Higgs mechanism through spontaneous symmetry breaking. Higgs-boson production is an electroweak process and at LHC the dominant reaction is gluon-gluon fusion where the Higgs is emitted from an intermediate top-quark loop, and weak gauge-boson fusion where the Higgs is created by annihilating two weak gauge bosons. Depending on the mass of the Higgs boson, it decays dominantly to a b-quark pair or to a W- and Z-boson pair if its mass is above those particle pair production threshold.

Even though the Higgs production is an electroweak process, the QCD corrections can be quite large. Within effective field theory, where the heavy quarks (the top quark) are integrated out, the gluon-gluon fusion Higgs-production process can be represented by an effective Lagrangian and makes the computation of this process much simpler. The form factor of the effective gluon-gluon-Higgs vertex, where the Higgs is off-shell, is the coefficient function of the amplitude of this vertex.

The Drell-Yan process is a scattering process where a quark-antiquark pair annihilates to an off-shell photon or Z- or W-boson. The same vertex also appears in deep inelastic scattering where electrons are scattered on protons. These processes are used for the determination of the parton distribution functions of the proton and the determination of the electroweak parameters (gauge boson masses, weak mixing angle).

1.6.2 Top-Quark Pair Production

The top quark was detected more than 15 years ago at the proton-antiproton collider Tevatron [9, 10], where its mass has been determined very accurately to 173 GeV with an error of less than one percent. The top quark is the weak-isospin partner of the bottom quark and has spin 1/2 and an electric charge of 2/3 of the positron charge. Since its extremely short mean lifetime of order 10^{-25}s is smaller than the typical hadronization time of order 10^{-24}s, the top quark cannot form hadronic bound states. With its large

mass the top decay $t \to bW^+$ is kinematically allowed and is even the dominant channel, since decays to d- and s-quarks are suppressed by the CKM matrix. At hadron colliders top quarks are mainly produced in pairs in the strong interaction. On the parton level, the two leading-order production channels are quark-antiquark annihilation $q\bar{q} \to t\bar{t}$ and gluon-gluon fusion $gg \to t\bar{t}$. At Tevatron, quark annihilation accounts for 85% of the final production cross section, whereas gluon fusion is dominant to 90% at LHC. According to the decay modes of the W boson to a lepton and an antineutrino or an quark-antiquark pair, the top-antitop pairs finally decay in three different channels, all-jet, lepton-jet and dilepton, which all have been studied at Tevatron.

While at the Tevatron a few thousand top quarks have been detected, the LHC will be an authentic top-quark factory, since it will already produce millions of top quarks in the first low-luminosity phase. The great wealth of data that will be obtained at the LHC will allow precise measurements of the top-quark related observables. This includes a precise mass determination and more accurate measurements of the production cross section and its differential distributions. Besides the hadronic production of top-quark pairs, also the weak process of single top production can be studied. This process is important for the determination of the CKM matrix element V_{tb}. The study of the SM structure and the strength of the Wtb vertex is also of great interest, since it is sensitive to deviations from the SM-Higgs mechanism and possible new physics. Further studies include top-spin correlations and potential new non-SM top production- and decay-channels.

The precise measurements of the top-quark related observables must be matched by equally precise calculations of the relevant cross sections and differential distributions in perturbative QCD.

1.7 Anatomy of Higher Order Corrections

Calculations of higher order corrections have become an important subject in theoretical particle physics due to the need to predict observables with accurate precision and also the developments and improvements of the mathematical techniques and computer programs to make these huge calculations feasible. The first step to calculate a cross section of a process with n particles in the final state is the calculation of the squared amplitude $|M^{(n)}|^2$ which is expanded in a coupling constant α.

$$\begin{aligned} |M^{(n)}|^2 &= \left| \sum_{i=0}^{\infty} \alpha^{i+1} M_i^{(n)} \right|^2 \\ &= \alpha^2 \left| M_0^{(n)} \right|^2 + \alpha^3 \, 2\,\Re\left(M_1^{(n)} \, \overline{M}_0^{(n)} \right) \\ &\quad + \alpha^4 \left(\left| M_1^{(n)} \right|^2 + 2\,\Re\left(M_2^{(n)} \, \overline{M}_0^{(n)} \right) \right) + O(\alpha^5) \,, \end{aligned} \tag{1.32}$$

where the amplitude $M_i^{(n)}$ consist of all i-loop diagrams with the n particles in the final state. For the cancellation of the infrared divergences in the virtual corrections the so-called Bremsstrahlung diagrams or real corrections, which have additional particles in the final state, have to be computed as well. For an $(n+1)$-particle final state, each diagram gets an additional factor of $\sqrt{\alpha}$ and the expansion is given as

$$|M^{(n+1)}|^2 = \alpha^3 \left|M_0^{(n+1)}\right|^2 + \alpha^4\, 2\,\Re\left(M_1^{(n+1)}\,\overline{M}_0^{(n+1)}\right) + O(\alpha^5)\,, \tag{1.33}$$

whereas the expansion for a $(n+2)$-particle final state reads

$$|M^{(n+2)}|^2 = \alpha^4 \left|\overline{M}_0^{(n+2)}\right|^2 + O(\alpha^5)\,. \tag{1.34}$$

The squared amplitude $|M|^2$ of the full process with the real radiation included is then given as the sum of the virtual part $|M^{(n)}|^2$ and the real and mixed virtual-real parts $|M^{(n+j)}|^2$ with integers j, depending on the order of expansion. The leading order (LO) of the squared amplitude $|M|^2$ consists of the tree-level diagrams $M_0^{(n)}$ only. The next-to-leading order (NLO) corrections contain the virtual one-loop diagrams $M_1^{(n)}$ and the real diagrams $M_0^{(n+1)}$ with one additional particle in the final state at leading order. At next-to-next-to-leading order (NNLO) the pure virtual contributions come from the two-loop diagrams $M_2^{(n)}$ and the squared one-loop diagrams $M_1^{(n)}$, the mixed virtual-real from the one-loop diagrams in $M_1^{(n+1)}$ and the real corrections from the tree-level diagrams $M_0^{(m+2)}$ with two additional particles. Each of these contributions are infrared-divergent. The IR-poles must be extracted from the real radiation by subtraction or dedicated phase space integration (sector decomposition).

The crucial ingredients in higher order corrections are the virtual loop-diagrams interfered with the tree-level diagrams. The general steps in the analytical calculation are to generate the relevant diagrams, to square them, and finally to calculate the Dirac/Lorentz- and color-structure until one ends up with a sum of terms on which the remaining loop-integration has to be performed. The large number of unknown integrals need not to be calculated explicitly as one can use linear equations (integration-by-parts- and Lorentz-invariant- identities) which relate different integrals and set up a homogeneous system of linear equations which can be reduced with the Laporta algorithm (see Chapter 4). This way all integrals can be expressed as a linear combination of a few so-called master integrals. The reduction is a very time consuming task since the coefficients in the system of equations are rational polynomials in multiple variables. The use of computer algebra systems becomes unavoidable.

A master integral is a d-dimensionally regularized integral over a ratio of Lorentz invariant scalar products of loop and external momenta and so-called propagators which are differences of the squared momentum and the squared mass of an internal edge

of a Feynman diagram. The value of a master integral depends on the external kinematics, i.e. on a set of Mandelstam invariants, built from the external momenta, and masses. The master integrals have to be calculated explicitly. The aim is to expand the integral in the dimension d around the physical dimension 4 so that the divergent structure becomes visible as a Laurent series around $\epsilon = (4-d)/2$, and to bring the coefficient functions into a form suitable for numerical evaluation. There are two main strategies: one is the explicit integration of the loop integrals after transformation to one dimensional integrals (Feynman parameters) or complex contour integrals (Mellin-Barnes transformation). The other strategy is to derive a differential equation from the master integrals which can be expanded in ϵ and solved order by order up to integration constants. The undetermined constants often can be found by imposing a regularity condition at some specific value of the kinematic invariants. If no such conditions can be imposed, the constants can be found by comparing the expansion in a kinematic invariant to the expansion of the result in the Mellin-Barnes representation, where one does not have to perform all contour integrations but often only sum up residues.

The complexity of such calculations increases substantially with the number of loops and external legs. The state of the art in performing loop calculations are one-loop for $2 \to 4$, 2-loop for $2 \to 2$, 3-loop for $1 \to 2$ and 4-loop for $1 \to 1$ processes.

Bibliography

[1] M. E. Peskin and D. V. Schroeder, "An Introduction To Quantum Field Theory," *Reading, USA: Addison-Wesley (1995) 842 p.*

[2] S. Weinberg, "The Quantum theory of fields. Vol. 1: Foundations," *Cambridge, UK: Univ. Pr. (1995) 609 p.*

[3] C. Itzykson and J. B. Zuber, "Quantum Field Theory," *New York, Usa: Mcgraw-hill (1980) 705 p. (International Series In Pure and Applied Physics)*

[4] F. Halzen and A. D. Martin, "Quarks & Leptons: An Introductory Course in Modern Particle Physics," *John Wiley & Sons (1984) 396 p.*

[5] V. A. Smirnov, "Feynman integral calculus," *Berlin, Germany: Springer (2006) 283 p.*

[6] J. C. Collins, "Renormalization. An Introduction To Renormalization, The Renormalization Group, And The Operator Product Expansion," *Cambridge, Uk: Univ. Pr. (1984) 380 p.*

[7] G. Scharf, "Finite quantum electrodynamics," *Berlin, Germany: Springer (1989) 224 p. (Texts and monographs in physics)*

[8] G. Scharf, "Quantum gauge theories: A true ghost story," *New York, USA: Wiley (2001) 245 p.*

[9] W. Bernreuther, J. Phys. G **35**, (2008) 083001 [arXiv:0805.1333].

[10] F. Abe *et al.* [CDF Collaboration], Phys. Rev. Lett. **74** (1995) 2626 [hep-ex/9503002];
S. Abachi *et al.* [D0 Collaboration], Phys. Rev. Lett. **74**, (1995) 2632 [hep-ex/9503003].

BIBLIOGRAPHY

2

Top-Quark Pair Production

2.1 Introduction

The top quark, with a mass of approximately 173 GeV, is the heaviest elementary particle produced at colliders until now. So far, the study of the properties of the top-quark was only possible at the Tevatron [1], where the mass of this particle was measured with an accuracy of less than one percent. The production cross sections and decay widths are only known with larger uncertainties. Because of its large mass, the top quark is expected to couple strongly with the electroweak symmetry breaking sector. Therefore, the study of scattering and decay processes involving top quarks is expected to provide fundamental clues on the mechanism responsible for the origin of particle masses. This is one of the main goals of the Large Hadron Collider (LHC) physics program.

While the Tevatron produced a few thousand top quarks, the LHC will be an authentic top-quark factory, since it will produce millions of top quarks already in the first low-luminosity phase [51]. The great wealth of data that will be obtained at the LHC will allow precise measurements of the top-quark related observables. In turn, the latter must be matched by equally precise calculations of the relevant cross sections and differential distributions in perturbative QCD.

At Tevatron, top quarks are primarily produced in pairs with their antiparticles. The same situation will be encountered at the LHC, where experimental collaborations anticipate measurements of the total top-quark pair-production cross section with a relative error between 5% and 10%. On the theory side, the top-quark pair-production cross section was calculated at next-to-leading-order (NLO) in perturbative QCD [2–8, 52]. The NLO electroweak corrections were obtained in [15, 16, 53]. The resummation of logarithmic terms, which become large near the production threshold, was extensively studied in [12–14, 17–19, 54].

2. TOP-QUARK PAIR PRODUCTION

The current resummation-improved NLO predictions for the top-quark pair-production cross section at the LHC shows an uncertainty of about 15% [51]; the latter is dominated by the scale uncertainty. Therefore, in order to reduce the theoretical uncertainty at the same level of the expected experimental error, the calculation of the next-to-next-to-leading order (NNLO) perturbative QCD corrections is required.

The Feynman diagrams needed for the evaluation of the NNLO QCD corrections to the top-quark pair production can be grouped in three categories: i) two-loop corrections to the tree-level production channels $q\bar{q} \to t\bar{t}$ and $gg \to t\bar{t}$, ii) one-loop matrix elements with an additional parton in the final state, and iii) tree-level matrix elements with two additional partons in the final state. The last two sets of diagrams were already evaluated in the context of the calculation of the NLO corrections to the production of $t\bar{t} + 1j$ [10]. Contributions arising from the interference of one-loop diagrams in both the quark-antiquark and the gluon-fusion channels were studied in [25, 55–57]. The first steps toward the calculation of the two-loop corrections were taken in [20, 21]; in these papers all the relevant two-loop diagrams were evaluated in the limit $s, |t|, |u| \gg m^2$, where s is the squared center of mass energy, t is the squared momentum transfer, $u = 2m^2 - s - t$ and m is the heavy-quark mass. A full numerical calculation of the two-loop virtual corrections in the $q\bar{q} \to t\bar{t}$ channel was carried out in [24].

In this chapter we present the calculation of two subsets of diagrams in the $q\bar{q} \to t\bar{t}$ channel which were published in [58] and [59].

In Section 2.3 we compute all two-loop contributions to $q\bar{q} \to t\bar{t}$ arising from closed fermion loops in a compact analytic form, which provide a first independent validation of the recent results of [20, 24], allow for a fast numerical evaluation, and permit the analytical study of the behavior of the top quark production cross section at threshold.

In Section 2.4 we describe the calculation of a conspicuous subset of the two-loop planar diagrams in the $q\bar{q} \to t\bar{t}$ production channel. The calculation of these corrections allows us to obtain an analytic expression for the leading color coefficient in the interference of the two-loop matrix element with the tree-level amplitude. Our results are valid for generic values of the Mandelstam invariants s, t and of the heavy-quark mass m.

Both calculations were carried out by means of a technique based on the identification of a set of Master Integrals (MIs) through the Laporta algorithm [30], and on their subsequent evaluation by means of the differential equation method [40]. The results are written in terms of a suitable base of one- and two-dimensional Harmonic Polylogarithms (HPLs) described in Appendix A

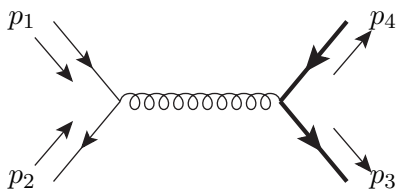

Figure 2.1: *Tree-level amplitude. Massive quarks are indicated by a thick line.*

2.2 Notation and Conventions

We consider the scattering process

$$q(p_1) + \overline{q}(p_2) \longrightarrow t(p_3) + \overline{t}(p_4)\,, \tag{2.1}$$

of an initial massless quark-antiquark pair to the heavy top-antitop pair in QCD. All quark masses except the top mass m are assumed to be zero. The on-shell conditions are $p_i^2 = 0$ for $i = 1, 2$ and $p_j^2 = m^2$ for $j = 3, 4$ and the Mandelstam variables are defined as follows

$$s = (p_1 + p_2)^2\,, \quad t = (p_1 - p_3)^2\,, \quad u = (p_1 - p_4)^2\,. \tag{2.2}$$

Conservation of momentum implies that $s + t + u = 2m^2$.

The squared matrix element (averaged over the spin and color of the incoming quarks and summed over the spin of the outgoing ones), calculated in $d = 4 - 2\varepsilon$ dimensions, can be expanded in powers of the strong coupling constant α_S as follows:

$$|\mathcal{M}|^2(s,t,m,\varepsilon) = \frac{4\pi^2\alpha_S^2}{N_c^2}\left[\mathcal{A}_0 + \left(\frac{\alpha_S}{\pi}\right)\mathcal{A}_1 + \left(\frac{\alpha_S}{\pi}\right)^2\mathcal{A}_2 + \mathcal{O}\left(\alpha_S^3\right)\right]. \tag{2.3}$$

The tree-level amplitude involves a single diagram (Fig. 2.1) and its contribution to Eq. (2.3) is given by

$$\mathcal{A}_0 = 4N_c\,C_F\left[\frac{(t-m^2)^2 + (u-m^2)^2}{s^2} + \frac{2m^2}{s} - \varepsilon\right], \tag{2.4}$$

where N_c is the number of colors and $C_F = (N_c^2 - 1)/2N_c$.

The $\mathcal{O}(\alpha_S)$ term $\mathcal{A}_1$ in Eq. (2.3) arises from the interference of one-loop diagrams with the tree-level amplitude [2–8]. The $\mathcal{O}(\alpha_S^2)$ term $\mathcal{A}_2$ consists of two parts, the interference of two-loop diagrams with the Born amplitude and the interference of one-loop diagrams among themselves:

$$\mathcal{A}_2 = \mathcal{A}_2^{(2\times0)} + \mathcal{A}_2^{(1\times1)}\,.$$

The latter term $\mathcal{A}_2^{(1\times1)}$ was studied extensively in [25, 55]. $\mathcal{A}_2^{(2\times0)}$, originating from the two-loop diagrams, can be decomposed according to color and flavor structures as follows:

$$\mathcal{A}_2^{(2\times0)} = N_c C_F \left[N_c^2 A + B + \frac{C}{N_c^2} + N_l \left(N_c D_l + \frac{E_l}{N_c} \right) + N_h \left(N_c D_h + \frac{E_h}{N_c} \right) + N_l^2 F_l + N_l N_h F_{lh} + N_h^2 F_h \right], \tag{2.5}$$

where N_l and N_h are the number of light- and heavy-quark flavors, respectively. The coefficients $A, B, \ldots, F_h$ in Eq. (2.5) are functions of s, t, and m, as well as of the dimensional regulator ε. These quantities were calculated in [20] in the approximation $s, |t|, |u| \gg m^2$. For a fully differential description of top quark pair production at NNLO, the complete mass dependence of $\mathcal{A}_2^{(2\times0)}$ is required. An exact numerical expression for it has been obtained in [24].

2.3 Two-Loop Fermionic Corrections to Heavy-Quark Pair Production: the Quark-Antiquark Channel

In this section, we provide independent confirmations of the recent results of [20, 24] by deriving exact analytic expressions for all the terms in Eq. (2.5) arising from two-loop diagrams involving at least a fermion loop (i.e. the coefficients D_i, E_i, F_j with $i = l, h$ and $j = l, h, lh$).

2.3.1 Calculation

The calculation starts from the two-loop Feynman diagrams for $q\bar{q} \to t\bar{t}$, which are generated using QGRAF [26], interfered with the tree-level amplitude, and simplified using FORM [27]. Out of the 218 two-loop diagrams contributing to the amplitude, 28 are proportional to N_l, 29 are proportional to N_h, 2 are proportional to $N_l N_h$, while just one contributes to the N_l^2 and N_h^2 parts. Most importantly, there is only one two-loop box topology contributing to the N_l part of the squared amplitude, and a single other two-loop box topology proportional to N_h. These two box topologies are very similar to the ones encountered in the evaluation of the two-loop QED corrections to Bhabha scattering [28, 29], and can be evaluated with the same techniques.

All two-loop integrals appearing in these amplitudes are reduced to a set of master integrals (MIs) by means of the standard method based on the Laporta algorithm [30]. The integrals are represented with the propagators of the two main auxiliary topologies listed in Table 2.1

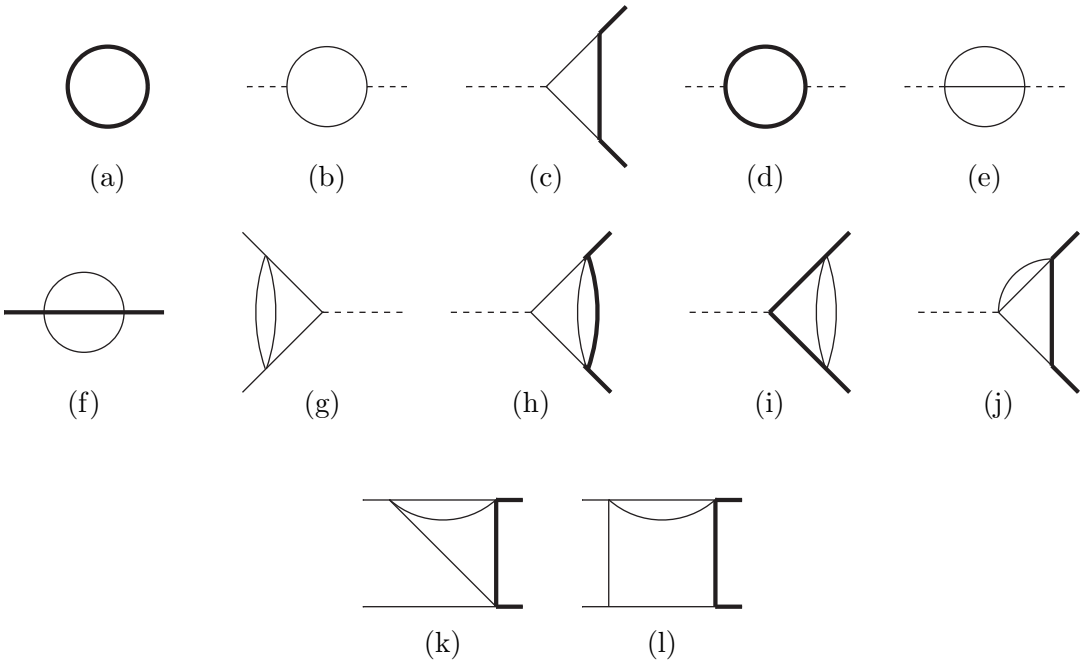

Figure 2.2: *Non-reducible topologies for the light quark corrections.*

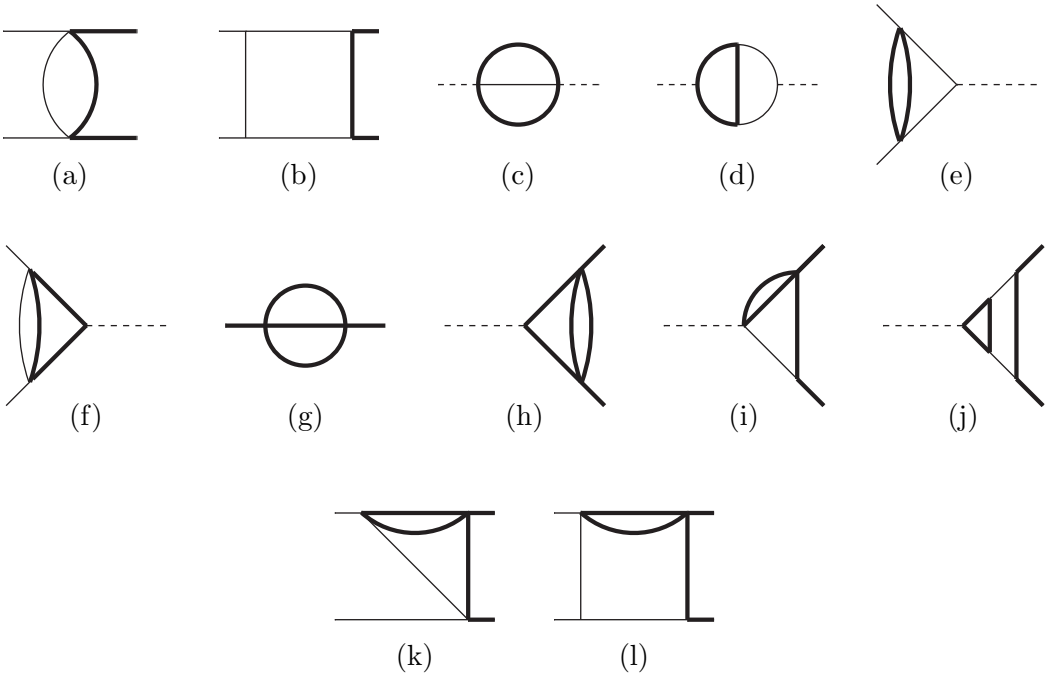

Figure 2.3: *Non-reducible topologies for the heavy quark corrections.*

Only part of these MIs were available in the literature [31–37] from previous two-loop calculations of the heavy quark form factors [38] and amplitudes for Bhabha scattering [28, 29, 39]. For the remaining integrals, we employed the differential equation method [40].

The reduction to MIs was carried out with `Reduze` (see Chapter 4) and large parts of it were cross checked with the `Maple` package `A.I.R.` [41]. The 12 irreducible topologies encountered in the calculation of the diagrams with a light quark loop are shown in Fig. 2.2. The diagrams proportional to N_h also contain 12 irreducible topologies, which can be found in Fig. 2.3. In both figures, thick internal lines indicate massive propagators, while thin lines indicate massless ones. An external dashed leg carries a squared momentum s; other external lines indicate particles on their mass-shell, where $p_i^2 = 0$ for thin lines and $p_i^2 = -m^2$ for thick lines.

The analytic expressions of the one-loop MIs in Fig. 2.2 and Fig. 2.3 are well known. The large majority of the two-loop MIs is also known in the literature: explicit analytic expressions for all the two-loop MIs with the exception of the ones belonging to topologies Fig. 2.2-(k), Fig. 2.2-(l), Fig. 2.3-(k), and Fig. 2.3-(l) can be found in [31–33, 35].

The MIs associated with topologies Fig. 2.2-(k), Fig. 2.2-(l), Fig. 2.3-(k), and Fig. 2.3-(l) that were not available in the literature are collected in Appendix A.3. In calculating the MIs by means of the differential equation method, it is crucial to fix the undetermined integration constant(s) appearing in the solution of the differential equations. While there is no general method available to fix such initial condition, it is usually sufficient to know the behavior of the MI in some particular kinematic point; for example, knowing that the integral is regular for a certain value of s, one can impose the regularity of the solution of the differential equation in that point. This can be sufficient to determine the integration constant. In our calculation, the initial conditions for the single master integral belonging to topology Fig. 2.2-(k) and the two MIs belonging to topology Fig. 2.3-(l) were determined by imposing the regularity of the solution of the differential equation in $t = 0$. However, this is not always sufficient. For topology Fig. 2.3-(k), which has two MIs, imposing the regularity of both MIs in $t = 0$ allowed to fix only one of the two initial conditions required. In order to fix the second integration constant, we had to use another piece of information, namely that the scalar integral with all the denominators raised to power one diverges at most logarithmically at the threshold $t = -m^2$. The final result for these two MIs was then checked by calculating their $t \to 0$ limit with the Mellin Barnes technique, using the `Mathematica` packages `Ambre` [42] and `MB` [43]. For what concerns the MI of the box topology in Fig. 2.2-(l), the initial conditions were defined calculating the integral in $t = 0$ with Mellin Barnes techniques.

All the MIs were calculated in the non-physical region $s < 0$, where they are real and can be conveniently written as functions of the dimensionless variables

$$x = \frac{\sqrt{-s+4m^2} - \sqrt{-s}}{\sqrt{-s+4m^2} + \sqrt{-s}}\,, \qquad y = \frac{-t}{m^2}\,, \qquad z = \frac{-u}{m^2}\,. \tag{2.6}$$

The MIs of the topology Fig. 2.3-(e) are an exception. In this case it is convenient to employ the variable

$$x_p = \frac{\sqrt{-s} - \sqrt{-s-4m^2}}{\sqrt{-s} + \sqrt{-s-4m^2}}\,. \tag{2.7}$$

The transcendental functions appearing in the MIs are one- and two-dimensional harmonic polylogarithms (HPLs).In the result one finds one-dimensional HPLs of maximum weight four and two-dimensional HPLs of maximum weight three. Both sets of functions can be rewritten in terms of conventional Nielsen's polylogarithms. In Appendix A.1, we briefly review the definition of the HPLs employed and we collect the expression of some of them in terms of Nielsen's polylogarithms.

Following the procedure outlined in the present section, it is possible to obtain the expression of the bare squared matrix elements involving diagrams proportional to N_l and/or N_h. After this goal is achieved, it is then necessary to renormalize the ultraviolet divergences. In the next section, we briefly discuss the renormalization procedure and we explicitly list the needed renormalization constants.

2.3.2 Renormalization

The renormalized QCD matrix element is obtained from the bare one by expanding the following expression :

$$\mathcal{A}_{\rm ren} = \prod_n Z_{{\rm WF},n}^{1/2}\, \mathcal{A}_{\rm bare}\left(\alpha_{S,\rm bare} \to Z_{\alpha_S}\alpha_S\,, m_{\rm bare} \to Z_m m\right)\,, \tag{2.8}$$

where $Z_{{\rm WF},n}$ is the external leg wave function renormalization factor, α_S is the renormalized coupling constant and m is the renormalized heavy quark mass. (In the rest of the section we suppress the subscript "S" in α_S).

We postpone the discussion of mass renormalization to the end of the section and we start by considering the coupling constant and wave function renormalization.

We introduce the following quantities:

$$a_0 = \frac{\alpha_{\rm bare}}{\pi}\,, \qquad \text{and} \qquad a = \frac{\alpha}{\pi}\,. \tag{2.9}$$

By expanding the amplitude and the wave function renormalization factor in a_0 we find:

$$\mathcal{A}_{\rm ren}(\alpha_{\rm bare}) \;=\; a_0\mathcal{A}_0 + a_0^2\mathcal{A}_1 + a_0^3\mathcal{A}_2 + \mathcal{O}(a_0^4)\,,$$

$$Z_{\mathrm{WF},n} = 1 + a_0 \delta Z^{(1)}_{\mathrm{WF},n} + a_0^2 \delta Z^{(2)}_{\mathrm{WF},n} + \mathcal{O}(a_0^3)\,. \tag{2.10}$$

The relation between a_0 and a is given by:

$$a_0 = a + a^2 \delta Z^{(1)}_{\alpha} + a^3 \delta Z^{(2)}_{\alpha} + \mathcal{O}(a^4)\,. \tag{2.11}$$

By employing Eqs. (2.10,2.11) in Eq. (2.8) we find

$$\begin{aligned}
\mathcal{A}_{\mathrm{ren}} &= a\mathcal{A}_0 + a^2 \mathcal{A}^{(1)}_{\mathrm{ren}} + a^3 \mathcal{A}^{(2)}_{\mathrm{ren}} + \mathcal{O}(a^4)\,, \\
\mathcal{A}^{(1)}_{\mathrm{ren}} &= \mathcal{A}_1 + \left(\sum_n \frac{1}{2} \delta Z^{(1)}_{\mathrm{WF},n} + \delta Z^{(1)}_{\alpha} \right) \mathcal{A}_0\,, \\
\mathcal{A}^{(2)}_{\mathrm{ren}} &= \mathcal{A}_2 + \left(\sum_n \frac{1}{2} \delta Z^{(1)}_{\mathrm{WF},n} + 2\delta Z^{(1)}_{\alpha} \right) \mathcal{A}_1 + \left(-\sum_n \frac{1}{8} \left(\delta Z^{(1)}_{\mathrm{WF},n} \right)^2 \right. \\
&\quad \left. + \sum_n \frac{1}{2} \delta Z^{(2)}_{\mathrm{WF},n} + \delta Z^{(1)}_{\alpha} \sum_n \delta Z^{(1)}_{\mathrm{WF},n} + \delta Z^{(2)}_{\alpha} \right) \mathcal{A}_0\,.
\end{aligned} \tag{2.12}$$

In the equations above, $\mathcal{A}_i$ represents the bare amplitude at i loops stripped of the factor a. In the case of the process $q\overline{q} \to t\bar{t}$, the wave function renormalization factors of massless quarks vanish at one loop, while the ones of the massive quarks in the on-shell renormalization scheme are given by

$$\delta Z^{(1)}_{\mathrm{WF},M} = C(\varepsilon) \left(\frac{\mu^2}{m^2} \right)^{\varepsilon} C_F \left(-\frac{3}{4\varepsilon} - \frac{1}{1-2\varepsilon} \right)\,, \tag{2.13}$$

where the subscript M indicates massive quarks and where $C(\varepsilon) = (4\pi)^{\varepsilon}\Gamma(1+\varepsilon)$. The one-loop renormalization constant for α in the $\overline{MS}$ scheme is given by

$$\delta Z^{(1)}_{\alpha} = C(\varepsilon) \frac{e^{-\gamma\varepsilon}}{\Gamma(1+\varepsilon)} \left(-\frac{\beta_0}{2\varepsilon} \right)\,, \tag{2.14}$$

where $\beta_0 = 11/6 C_A - 1/3(N_l + N_h)$ and γ is the Euler-Mascheroni constant $\gamma \approx 0.577216$.

Therefore, the overall one-loop counter term is given by

$$\delta Z^{(1)}_{\mathrm{WF},M} + \delta Z^{(1)}_{\alpha} = -\frac{C(\varepsilon)}{4\varepsilon} \left[2\beta_0 + \left(3 + 4\varepsilon + 3\varepsilon \ln\left(\frac{\mu^2}{m^2} \right) \right) C_F + \mathcal{O}\left(\varepsilon^2\right) \right]\,. \tag{2.15}$$

To renormalize the two-loop diagrams contributing to the N_l corrections of the partonic cross section it is necessary to extract from the last two lines in Eq. (2.12) the terms proportional to N_l. Taking into account the fact that the wave function renormalization factors are zero for the incoming particles and identical for the massive ones, we find that

$$\mathcal{A}^{(2,N_l)}_{\mathrm{ren}} = \mathcal{A}^{(N_l)}_2 + \left(\delta Z^{(1)}_{\mathrm{WF},M} + 2\delta Z^{(1,C_A)}_{\alpha} \right) \mathcal{A}^{(d_1)}_1 + 2\delta Z^{(1,N_l)}_{\alpha} \sum_{j=3}^{10} \mathcal{A}^{(d_j)}_1$$

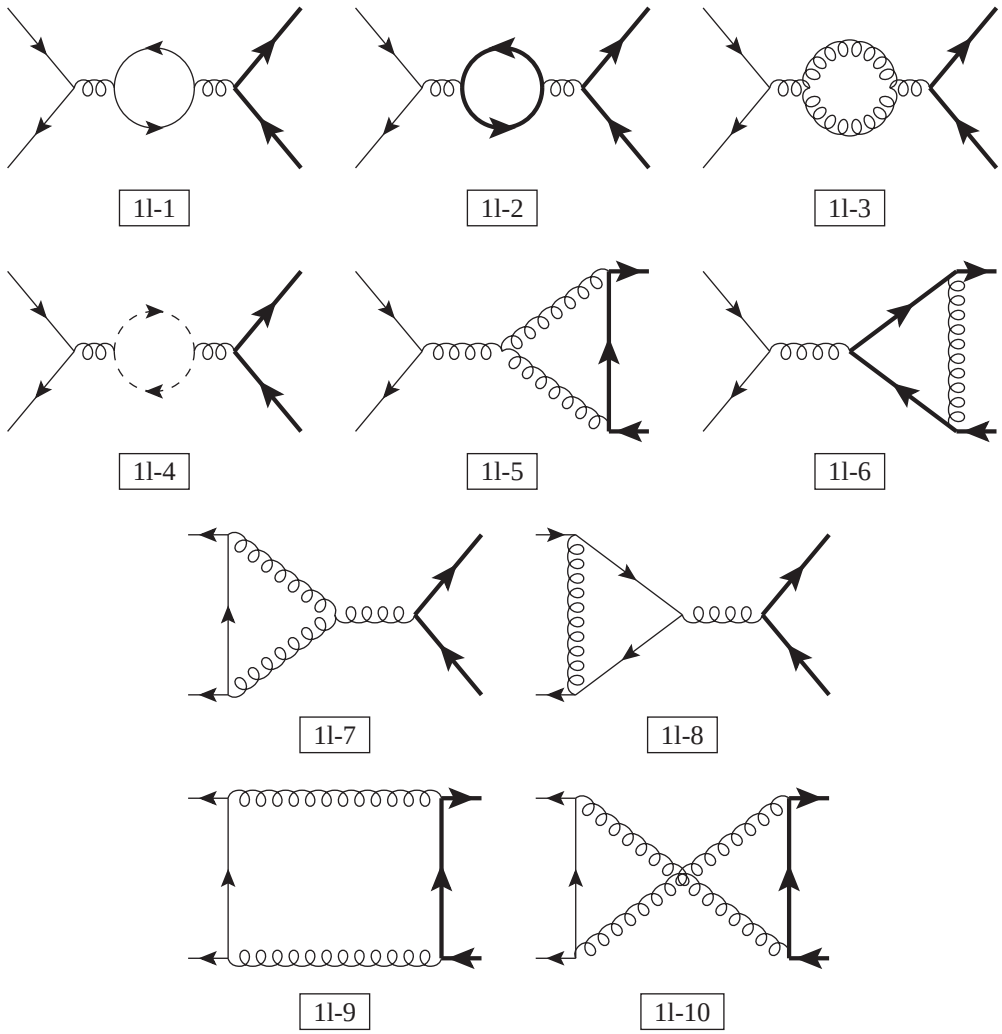

Figure 2.4: *One-loop diagrams. Thin arrow lines represent massless quarks, thick arrow line massive quarks, dashed arrow lines are Faddeev-Popov ghosts, and coiled lines are gluons.*

$$+\left(\delta Z_{\mathrm{WF},M}^{(2,N_l)}+2\delta Z_{\alpha}^{(1,N_l)}\delta Z_{\mathrm{WF},M}^{(1)}+\delta Z_{\alpha}^{(2,N_l)}\right)\mathcal{A}_0\,. \tag{2.16}$$

In Eq. (2.16), the quantity $\mathcal{A}_1^{(d_j)}$ is the amplitude of the j-th diagram in Fig. 2.4 (stripped of the factor a). The renormalization coefficients not previously defined are:

$$\begin{aligned}
\delta Z_{\alpha}^{(1,N_l)} &= C(\varepsilon)\,\frac{e^{-\gamma\varepsilon}}{\Gamma(1+\varepsilon)}\,\frac{N_l}{6\varepsilon}\,,\\
\delta Z_{\alpha}^{(1,C_A)} &= -C(\varepsilon)\,\frac{e^{-\gamma\varepsilon}}{\Gamma(1+\varepsilon)}\,C_A\frac{11}{12\varepsilon}\,,\\
\delta Z_{\alpha}^{(2,N_l)} &= C(\varepsilon)^2\left(\frac{e^{-\gamma\varepsilon}}{\Gamma(1+\varepsilon)}\right)^2\frac{N_l}{4\varepsilon}\left(\frac{5}{12}C_A+\frac{1}{4}C_F-\frac{11}{9\varepsilon}C_A\right)\,,\\
\delta Z_{\mathrm{WF},M}^{(2,N_l)} &= C(\varepsilon)^2\left(\frac{\mu^2}{m^2}\right)^{2\varepsilon}C_F N_l\left(\frac{1}{16\varepsilon^2}+\frac{9}{32\varepsilon}+\frac{59}{64}+\frac{\pi^2}{24}+\mathcal{O}\left(\varepsilon\right)\right)\,.
\end{aligned} \tag{2.17}$$

In order to renormalize the part of the squared matrix element proportional to N_h, one has to consider the terms proportional to N_h in the last two lines of Eq. (2.12), and to add the counter term for the on-shell mass renormalization:

$$\begin{aligned}
\mathcal{A}_{\mathrm{ren}}^{(2,N_h)} &= \mathcal{A}_2^{(N_h)}+\left(\delta Z_{\mathrm{WF},M}^{(1)}+2\delta Z_{\alpha}^{(1,C_A)}\right)\mathcal{A}_1^{(d_2)}+2\delta Z_{\alpha}^{(1,N_h)}\sum_{j=3}^{10}\mathcal{A}_1^{(d_j)}-2\delta Z_m^{(1)}\mathcal{A}_1^{(d_2,\text{mass ct})}\\
&\quad+\left(\delta Z_{\mathrm{WF},M}^{(2,N_h)}+\delta Z_{\mathrm{WF},m}^{(2,N_h)}+2\delta Z_{\alpha}^{(1,N_h)}\delta Z_{\mathrm{WF},M}^{(1)}+\delta Z_{\alpha}^{(2,N_h)}\right)\mathcal{A}_0\,.
\end{aligned} \tag{2.18}$$

It must be observed that in this case also the external massless legs acquire a non vanishing two-loop wave function renormalization factor indicated by $\delta Z_{\mathrm{WF},m}^{(2,N_h)}$. The quantity $\mathcal{A}^{(d_2,\text{mass ct})}$ indicates the second diagram in Fig. 2.4 with a mass counter term insertion in one of the internal heavy quark lines. The renormalization constant appearing for the first time in Eq. (2.18) are:

$$\begin{aligned}
\delta Z_{\alpha}^{(1,N_h)} &= C(\varepsilon)\,\frac{e^{-\gamma\varepsilon}}{\Gamma(1+\varepsilon)}\,\frac{N_h}{6\varepsilon}\,,\\
\delta Z_m^{(1)} &= \delta Z_{\mathrm{WF},M}^{(1)}\,,\\
\delta Z_{\alpha}^{(2,N_h)} &= C(\varepsilon)^2\left(\frac{e^{-\gamma\varepsilon}}{\Gamma(1+\varepsilon)}\right)^2\frac{1}{4\varepsilon}\left(\frac{5}{12}C_A N_h+\frac{1}{4}C_F N_h-\frac{11}{9\varepsilon}C_A N_h\right)\,,\\
\delta Z_{\mathrm{WF},M}^{(2,N_h)} &= C(\varepsilon)^2\left(\frac{\mu^2}{m^2}\right)^{2\varepsilon}C_F N_h\left(\frac{1}{8\varepsilon^2}+\frac{19}{96\varepsilon}+\frac{1139}{576}-\frac{\pi^2}{6}+\mathcal{O}\left(\varepsilon\right)\right)\,,\\
\delta Z_{\mathrm{WF},m}^{(2,N_h)} &= C(\varepsilon)^2\left(\frac{\mu^2}{m^2}\right)^{2\varepsilon}C_F N_h\left(\frac{1}{32\varepsilon}-\frac{5}{192}+\mathcal{O}\left(\varepsilon\right)\right)\,.
\end{aligned} \tag{2.19}$$

The renormalization coefficients in Eqs. (2.17,2.19) can be found in [20, 44].

The renormalization of the functions F_i $(i = l, h, lh)$ in Eq. (2.5) is trivial since the relevant two-loop diagrams are reducible and involve the insertion of two one-loop

fermionic vacuum polarization insertions on the gluon propagator in the diagram of Fig. 2.1.

2.3.3 Results

The main result of this section is an analytic, non-approximated expression for the coefficients $E_l, E_h, D_l, D_h, F_l, F_{lh}, F_h$ in Eq. (2.5). This result is too long to be explicitly printed here but one can find a text file with the complete result in the arXiv submission of [58]. The result is written in terms of one-dimensional HPLs of maximum weight four and two-dimensional HPLs of maximum weight three. Since the coefficients in Eq. (2.5) still contain infrared poles, the result is dependent on the choice of a global, ε-dependent normalization factor. With our choice, we factor out an overall coefficient

$$C^2(\varepsilon) = \left[(4\pi)^\varepsilon \, \Gamma(1+\varepsilon)\right]^2 \, . \tag{2.20}$$

We also provide two codes, one written in `Fortran`, the other as a `Mathematica` package, that numerically evaluate the analytic expression of the quantities listed above for arbitrary values of the mass scales involved in the calculation.

In order to cross check our results, we expanded them in the $s, |t|, |u| \gg m^2$ limit. The first term in the expansion agrees with the results published in [20]; the second order term agrees with the results found in the `Mathematica` files included in the arXiv version of [24]. We also find complete agreement with the numerical result of Table 3 in [24], corresponding to a phase space point in which the $s, |t|, |u| \gg m^2$ approximation cannot be applied.

It is straightforward to expand our result for values of the center of mass energy close to the production threshold. We define

$$\beta = \sqrt{1 - \frac{4m^2}{s}} \, , \qquad \xi = \frac{1-\cos\theta}{2} \, , \qquad L_\mu = \ln\left(\frac{\mu^2}{m^2}\right) \, , \qquad \ln_2 = \ln(2) \, , \tag{2.21}$$

where θ is the scattering angle in the partonic center of mass frame, and we expand our results in powers of the heavy quark velocity β, up to terms of order β^2. We find

$$\begin{aligned} D_l(\beta,\xi) \;=\; & \left(-\frac{1}{4} + \mathcal{O}\left(\beta^2\right)\right)\frac{1}{\varepsilon^3} + \left[\frac{19}{36} - \frac{\ln_2}{3} + \frac{L_\mu}{6} + \left(-\frac{1}{3} + \frac{2\xi}{3}\right)\beta + \mathcal{O}\left(\beta^2\right)\right]\frac{1}{\varepsilon^2} \\ & + \left\{2\ln_2^2 - \frac{37\ln_2}{9} - \frac{2\zeta(2)}{3} + \frac{589}{216} + \left(\frac{37}{18} - 2\ln_2\right)L_\mu + \frac{L_\mu^2}{2}\right. \\ & \left. + \left[2 - \frac{4\ln_2}{3} + \left(\frac{8\ln_2}{3} - 4\right)\xi + \left(\frac{2}{3} - \frac{4\xi}{3}\right)L_\mu\right]\beta + \mathcal{O}\left(\beta^2\right)\right\}\frac{1}{\varepsilon} \\ & + \left\{-\frac{32\ln_2^3}{9} + \frac{16\ln_2^2}{9} + \frac{14\zeta(2)\ln_2}{3} + \frac{475\ln_2}{54} - \frac{13\zeta(2)}{18} - \frac{79\zeta(3)}{18} - \frac{1211}{144}\right. \end{aligned}$$

$$
\begin{aligned}
&+\left(\frac{16\ln_2^2}{3}-\frac{4\ln_2}{3}-\frac{7\zeta(2)}{3}-\frac{163}{36}\right)L_\mu+\left(\frac{1}{9}-\frac{8\ln_2}{3}\right)L_\mu^2+\frac{4L_\mu^3}{9}\\
&+\left[\frac{20\ln_2^2}{9}-\frac{64\ln_2}{27}-\frac{26\zeta(2)}{9}+\frac{7}{27}+\left(-\frac{40\ln_2^2}{9}+\frac{128\ln_2}{27}+\frac{52\zeta(2)}{9}-\frac{14}{27}\right)\xi\right.\\
&\left.+\left(\frac{20}{9}-\frac{20\ln_2}{9}+\left(\frac{40\ln_2}{9}-\frac{40}{9}\right)\xi\right)L_\mu+\left(\frac{4}{3}-\frac{8\xi}{3}\right)L_\mu^2\right]\beta+\mathcal{O}\left(\beta^2\right)\Bigg\}+\mathcal{O}\left(\varepsilon\right)\ , \qquad (2.22)
\end{aligned}
$$

$$
\begin{aligned}
D_h(\beta,\xi) \;=\;& \left(\frac{8}{9}+\frac{2L_\mu}{3}+\mathcal{O}\left(\beta^2\right)\right)\frac{1}{\varepsilon^2}+\left\{-\frac{16\ln_2}{9}+\frac{\zeta(2)}{3}+\frac{88}{27}+\left(\frac{25}{9}-\frac{4\ln_2}{3}\right)L_\mu+L_\mu^2\right.\\
&\left.+\left[\frac{16}{9}-3\zeta(2)-\frac{32\xi}{9}+\left(\frac{4}{3}-\frac{8\xi}{3}\right)L_\mu\right]\beta+\mathcal{O}\left(\beta^2\right)\right\}\frac{1}{\varepsilon}+\left\{\frac{16\ln_2^2}{9}+\frac{55\zeta(2)\ln_2}{3}\right.\\
&-\frac{148\ln_2}{27}-\frac{857\zeta(2)}{72}+\frac{283\zeta(3)}{144}-\frac{209}{108}+\left(\frac{4\ln_2^2}{3}-\frac{14\ln_2}{9}-\frac{\zeta(2)}{3}-\frac{319}{54}\right)L_\mu\\
&+\left(\frac{5}{6}-2\ln_2\right)L_\mu^2+\frac{7L_\mu^3}{9}+\left[12\zeta(2)\ln_2+\frac{8\ln_2}{9}-\frac{131\zeta(2)}{18}+6\zeta(2)\ln(\beta)\right.\\
&+\frac{214}{27}+\left(-\frac{16\ln_2}{9}-\frac{58\zeta(2)}{9}-\frac{428}{27}\right)\xi+\left(\frac{4\ln_2}{9}-6\zeta(2)+\frac{16}{9}\right.\\
&\left.\left.\left.+\left(-\frac{8\ln_2}{9}-\frac{32}{9}\right)\xi\right)L_\mu+(2-4\xi)L_\mu^2\right]\beta+\mathcal{O}\left(\beta^2\right)\right\}+\mathcal{O}\left(\varepsilon\right)\ , \qquad (2.23)
\end{aligned}
$$

$$
\begin{aligned}
E_l(\beta,\xi) \;=\;& \left(\frac{1}{4}+\mathcal{O}\left(\beta^2\right)\right)\frac{1}{\varepsilon^3}+\left[\frac{\ln_2}{3}-\frac{25}{36}-\frac{L_\mu}{6}+\left(\frac{4}{3}-\frac{8\xi}{3}\right)\beta+\mathcal{O}\left(\beta^2\right)\right]\frac{1}{\varepsilon^2}\\
&+\left\{\frac{\zeta(2)}{\beta}-2\ln_2^2+\frac{31\ln_2}{9}+\frac{8\zeta(2)}{3}-\frac{373}{216}+\left(2\ln_2-\frac{31}{18}\right)L_\mu-\frac{L_\mu^2}{2}\right.\\
&+\left[\frac{16\ln_2}{3}+\zeta(2)-8+\left(-\frac{32\ln_2}{3}-2\zeta(2)+16\right)\xi+2\zeta(2)\xi^2\right.\\
&\left.+\left(-\frac{8}{3}+\frac{16\xi}{3}\right)L_\mu\right]\beta+\mathcal{O}\left(\beta^2\right)\Bigg\}\frac{1}{\varepsilon}+\Bigg\{\Bigg(-8\ln_2\zeta(2)-4\ln(\beta)\zeta(2)+4\zeta(2)\\
&+4\zeta(2)L_\mu\Bigg)\frac{1}{\beta}+\frac{32\ln_2^3}{9}-\frac{68\ln_2^2}{9}-\frac{50\zeta(2)\ln_2}{3}+\frac{643\ln_2}{54}+\frac{221\zeta(2)}{18}-\frac{10\zeta(3)}{9}\\
&-\frac{10285}{1296}+\left(-\frac{16\ln_2^2}{3}+\frac{68\ln_2}{9}+\frac{25\zeta(2)}{3}-\frac{787}{108}\right)L_\mu+\left(\frac{8\ln_2}{3}-\frac{17}{9}\right)L_\mu^2-\frac{4L_\mu^3}{9}\\
&+\Bigg[-\frac{80\ln_2^2}{9}-8\zeta(2)\ln_2+\frac{256\ln_2}{27}+\frac{158\zeta(2)}{9}-4\zeta(2)\ln(\beta)-\frac{28}{27}\\
&+\left(\frac{160\ln_2^2}{9}+16\zeta(2)\ln_2-\frac{512\ln_2}{27}-\frac{334\zeta(2)}{9}+8\zeta(2)\ln(\beta)+\frac{56}{27}\right)\xi
\end{aligned}
$$

$$+\Big(-16\ln_2\zeta(2)-8\ln(\beta)\zeta(2)+14\zeta(2)\Big)\xi^2+\Bigg(\frac{80\ln_2}{9}+4\zeta(2)-\frac{80}{9}+\Big(-\frac{160\ln_2}{9}$$
$$-8\zeta(2)+\frac{160}{9}\Big)\xi+8\zeta(2)\xi^2\Bigg)L_\mu+\left(-\frac{16}{3}+\frac{32\xi}{3}\right)L_\mu^2\Bigg]\beta+\mathcal{O}\left(\beta^2\right)\Bigg\}+\mathcal{O}\left(\varepsilon\right), \quad (2.24)$$

$$E_h(\beta,\xi) = \left(-\frac{8}{9}-\frac{2L_\mu}{3}+\mathcal{O}\left(\beta^2\right)\right)\frac{1}{\varepsilon^2}+\Bigg\{\frac{16\ln_2}{9}+\frac{7\zeta(2)}{6}-\frac{64}{27}+\left(\frac{4\ln_2}{3}-\frac{19}{9}\right)L_\mu-L_\mu^2$$
$$+\left[6\zeta(2)-\frac{64}{9}+\frac{128\xi}{9}+\left(-\frac{16}{3}+\frac{32\xi}{3}\right)L_\mu\right]\beta+\mathcal{O}\left(\beta^2\right)\Bigg\}\frac{1}{\varepsilon}$$
$$+\Bigg\{\left(\frac{8\zeta(2)}{3}+2\zeta(2)L_\mu\right)\frac{1}{\beta}-\frac{16\ln_2^2}{9}-\frac{43\zeta(2)\ln_2}{3}+\frac{343\ln_2}{27}+\frac{61\zeta(2)}{9\sqrt{2}}$$
$$+\frac{841\zeta(2)}{72}-\frac{83\zeta(3)}{18}-12\zeta(2)\ln(\beta)-\frac{5}{12}\mathrm{Li}_3\left(3-2\sqrt{2}\right)-\frac{61\mathrm{Li}_2\left(3-2\sqrt{2}\right)}{9\sqrt{2}}$$
$$+\frac{5}{18}\ln^3\left(1+\sqrt{2}\right)-\frac{61\ln^2\left(1+\sqrt{2}\right)}{9\sqrt{2}}-\frac{5}{6}\zeta(2)\ln\left(1+\sqrt{2}\right)-\frac{6703}{324}$$
$$+\left(-\frac{4\ln_2^2}{3}+\frac{38\ln_2}{9}+\frac{16\zeta(2)}{3}-\frac{463}{54}\right)L_\mu+\left(2\ln_2-\frac{41}{18}\right)L_\mu^2-\frac{7L_\mu^3}{9}$$
$$+\Bigg[-24\zeta(2)\ln_2-\frac{32\ln_2}{9}+\frac{7\zeta(2)}{9}-12\zeta(2)\ln(\beta)-\frac{856}{27}+\Bigg(\frac{64\ln_2}{9}+\frac{184\zeta(2)}{9}$$
$$+\frac{1712}{27}\Bigg)\xi+\frac{16\zeta(2)\xi^2}{3}+\Bigg(-\frac{16\ln_2}{9}+14\zeta(2)-\frac{64}{9}+\left(\frac{32\ln_2}{9}-4\zeta(2)+\frac{128}{9}\right)\xi$$
$$+4\zeta(2)\xi^2\Bigg)L_\mu+\left(-8+16\xi\right)L_\mu^2\Bigg]\beta+\mathcal{O}\left(\beta^2\right)\Bigg\}+\mathcal{O}\left(\varepsilon\right), \quad (2.25)$$

$$F_l(\beta,\xi) = \frac{2}{81}\left[(5-6\ln_2)^2-54\zeta(2)\right]+\mathcal{O}\left(\beta^2\right)+\mathcal{O}\left(\varepsilon\right), \quad (2.26)$$

$$F_h(\beta,\xi) = \frac{128}{81}+\mathcal{O}\left(\beta^2\right)+\mathcal{O}\left(\varepsilon\right), \quad (2.27)$$

$$F_{lh}(\beta,\xi) = \left(\frac{160}{81}-\frac{64\ln_2}{27}\right)-4\zeta(2)\beta+\mathcal{O}\left(\beta^2\right)+\mathcal{O}\left(\varepsilon\right). \quad (2.28)$$

These expansions could be used in the future in the calculation of logarithmically enhanced terms at production threshold.

2.4 Two-Loop Planar Corrections to Heavy-Quark Pair Production in the Quark-Antiquark Channel

In this section, we provide an exact analytic expression for the coefficient A in Eq. (2.5), which arises from planar Feynman diagrams only.

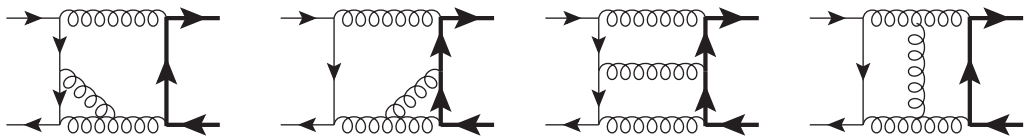

Figure 2.5: *Some of the two-loop planar box diagrams involved in the calculation.*

2.4.1 Calculation

The package QGRAF [26] generates 218 two-loop Feynman diagrams contributing to the process $q\bar{q} \to t\bar{t}$. After treating the QGRAF output with FORM [27] in order to carry out the color (and Dirac) algebra, one finds that there are 44 non-vanishing diagrams contributing to the leading color coefficient in Eq. (2.5). Some of the box diagrams involved in the calculation are shown in Fig. 2.5. All the two-loop graphs encountered in our calculation can be treated by employing the technique based upon the Laporta algorithm for the reduction to a set of Master Integrals (MIs). The MIs are then evaluated by means of the differential equation method. All appearing integrals are represented by the propagators of the auxiliary topology AuxTopo A listed in Table 2.1.

A subset of the MIs needed in the calculation were available in the literature [31–34, 36, 37]. They were employed in previous two-loop calculations of the heavy-quark form factors [38], amplitudes for Bhabha scattering [28], heavy-to-light quark transitions [61], and in the calculation of the fermionic corrections to $q\bar{q} \to t\bar{t}$ in the previous section. The MIs not included in this subset are a part of the original findings of this work.

The reduction to MIs was carried out with `Reduze` (see Chapter 4) and large parts of it were cross checked with the `Maple` package `A.I.R.` [41]. The six so far unknown irreducible topologies encountered in the calculation of the planar diagrams are shown in Fig. 2.6. In the figure, thick internal lines indicate massive propagators, while thin lines indicate massless ones. An external dashed leg carries a squared momentum $(p_1 + p_2)^2 = s$; other external lines indicate particles on their mass-shell, where $p_i^2 = 0$ for thin lines and $p_i^2 = m^2$ for thick lines. The calculation of the master integrals is performed by the method of differential equation and the integration constants are fixed by regularity conditions of the integrals and explicit calculation with Mellin-Barnes techniques. The MIs in Fig. 2.6 are collected in Appendix A.4 and in a file included with the arXiv submission of the publication [59].

In order to numerically check the analytic calculation of the MIs, we employed the sector decomposition technique [45], implemented in the `Mathematica` package `FIESTA` [63].

All the MIs were calculated in the non-physical region $s < 0$, where they are real and can be conveniently written as functions of the dimensionless variables defined in 2.6. The transcendental functions appearing in the results are one- and two-dimensional

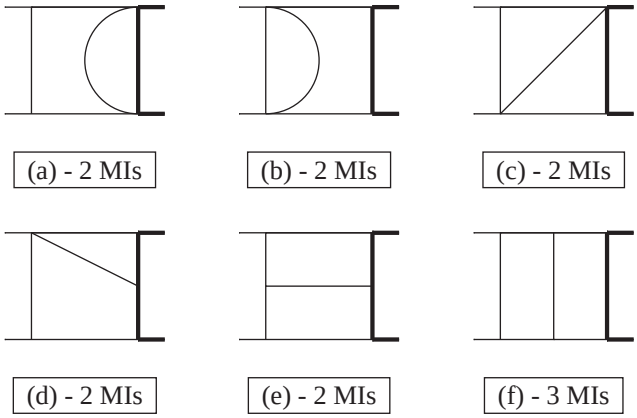

Figure 2.6: *New non-reducible topologies encountered in the calculation of the planar diagrams. The number of Master Integrals related to each topology is indicated in the figure.*

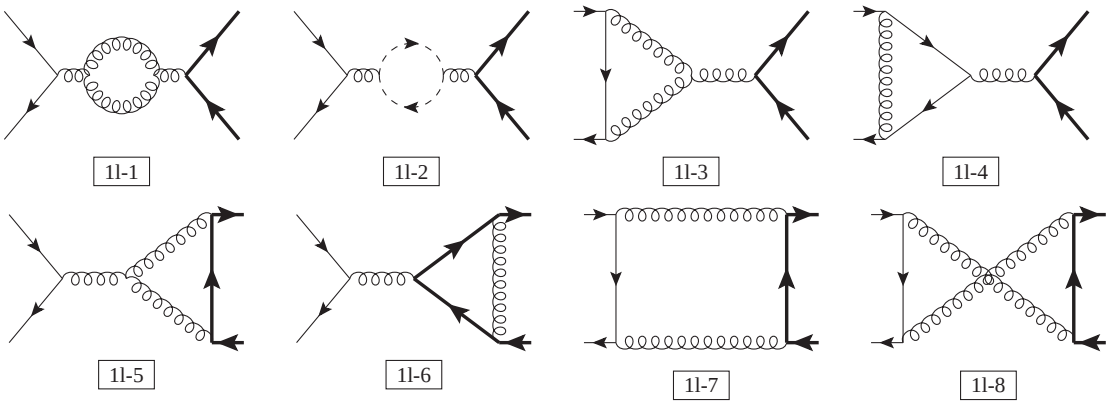

Figure 2.7: *One-loop diagrams (excluding the diagrams with closed quark loops). Thin arrow lines represent massless quarks, thick arrow line massive quarks, dashed arrow lines are Faddeev-Popov ghosts, and coiled lines are gluons.*

harmonic polylogarithms (HPLs) of maximum weight four. In Appendix A.1, we briefly review the definition of the HPLs appearing in the calculation. All the HPLs appearing in the analytic expression of the coefficient A can be evaluated numerically with arbitrary precision by employing the methods and codes described in [60].

Following the procedure outlined in the present section, it is possible to obtain the expression of the bare squared matrix elements involving planar two-loop diagrams. The renormalization of the ultraviolet divergences is discussed in the next section.

2.4.2 Renormalization

Here we are interested in finding the ultraviolet counterterm needed to renormalize the two-loop diagrams not involving closed quark loops. The part of this counterterm needed to renormalize the leading color structure in Eq. (2.5) can then be trivially extracted. Taking into account the fact that the wave function renormalization factors are zero for the incoming particles and identical for the massive ones, one finds that the renormalized amplitude (excluding quark-loop diagrams) is

$$\begin{aligned}\mathcal{A}_{\text{ren}}^{(2,\text{g})} &= \mathcal{A}_2^{(\text{g})} + \left(\delta Z_{\text{WF},M}^{(1)} + 2\delta Z_\alpha^{(1,C_A)}\right) \sum_{j=1}^{8} \mathcal{A}_1^{(d_j)} - \delta Z_m^{(1)} \sum_{l=5}^{8} \mathcal{A}_1^{(d_l,\,\text{mass CT})} \\ &\quad + \left(\delta Z_{\text{WF},M}^{(2,\text{g})} + 2\delta Z_\alpha^{(1,C_A)} \delta Z_{\text{WF},M}^{(1)} + \delta Z_\alpha^{(2,\text{g})}\right) \mathcal{A}_0 \,. \end{aligned} \tag{2.29}$$

In Eq. (2.29), the quantity $\mathcal{A}_1^{(d_j)}$ is the amplitude of the j-th diagram in Fig. 2.7 (stripped of the factor a). The quantity $\mathcal{A}^{(d_l,\,\text{mass CT})}$ indicates the l-th diagram in Fig. 2.7 with a mass counter term insertion in one of the internal heavy quark lines. The renormalization coefficients not previously defined are:

$$\begin{aligned}\delta Z_m^{(1)} &= \delta Z_{\text{WF},M}^{(1)} \,, \\ \delta Z_\alpha^{(1,C_A)} &= -C(\varepsilon)\, \frac{e^{-\gamma\varepsilon}}{\Gamma(1+\varepsilon)}\, C_A \frac{11}{12\varepsilon} \,, \\ \delta Z_\alpha^{(2,\text{g})} &= C(\varepsilon)^2 \left(\frac{e^{-\gamma\varepsilon}}{\Gamma(1+\varepsilon)}\right)^2 \frac{1}{4\varepsilon} \left[\left(\frac{11}{6}\right)^2 \frac{C_A^2}{\varepsilon} - \frac{17}{12} C_A^2\right] \,, \\ \delta Z_{\text{WF},M}^{(2,\text{g})} &= C(\varepsilon)^2 \left(\frac{\mu^2}{m^2}\right)^{2\varepsilon} C_F \left[C_F \left(\frac{9}{32\varepsilon^2} + \frac{51}{64\varepsilon} + \frac{433}{128} - \frac{3}{2}\zeta(3) + \pi^2 \ln 2 - \frac{13}{16}\pi^2\right)\right. \\ &\quad \left. + C_A \left(-\frac{11}{32\varepsilon^2} - \frac{101}{64\varepsilon} - \frac{803}{128} + \frac{3}{4}\zeta(3) - \frac{\pi^2}{2}\ln 2 + \frac{5}{16}\pi^2\right) + \mathcal{O}(\varepsilon)\right] \,, \end{aligned} \tag{2.30}$$

and they can be found in [20, 44].

2.4.3 Results

The main result of this section is an analytic, non-approximated expression for the coefficient A in Eq. (2.5). Since such a result is too long to be explicitly printed here, we included in the arXiv submission of the publication [59] a text file with the complete result, which is written in terms of one- and two-dimensional HPLs of maximum weight four. Since the coefficients in Eq. (2.5) still contain infrared poles, the result is dependent on the choice of a global, ε-dependent normalization factor. With our choice, we factor out an overall coefficient as defined in Eq. 2.20. We also provide a code that

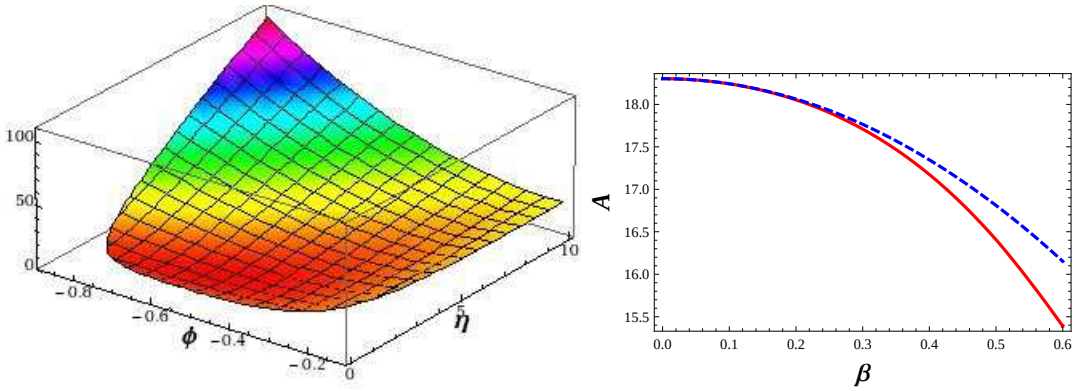

Figure 2.8: *Left: finite part of the coefficient A as a function of the variables η and ϕ. Right: the exact value of $A^{(0)}$ as a function of β (red solid curve) versus its expansion close to threshold up to terms of order β^2 (blue dashed curve). Both curves are plotted for $\xi = 1/2$. In both cases we used the normalization adopted in [24] to facilitate comparisons.*

numerically evaluates the analytic expression of the quantities listed above for arbitrary values of the mass scales involved in the calculation. The code is written in `C++` and uses the package for the evaluation of multiple polylogarithms within `GiNaC` [60].

In order to cross check our results, we expanded them in the $s, |t|, |u| \gg m^2$ limit. The first term in the expansion agrees with the results published in [20]; the second order term agrees with the results found in the `Mathematica` files included in the arXiv version of [24]. We also find complete agreement with the numerical result of Table 3 in [24], corresponding to a phase-space point in which the $s, |t|, |u| \gg m^2$ approximation cannot be applied. With our code it is also possible to reproduce the first plot in Figure 4 of [24], where the finite part of A is shown as a surface depending on the variables η and ϕ, defined as

$$\eta = \frac{s}{4m^2} - 1\,, \quad \phi = -\frac{t-m^2}{s}\,, \quad \frac{1}{2}\left(1 - \sqrt{\frac{\eta}{1+\eta}}\right) \leq \phi \leq \frac{1}{2}\left(1 + \sqrt{\frac{\eta}{1+\eta}}\right). \quad (2.31)$$

This surface is shown on the left side of Figure 2.8.

Furthermore, it is possible to expand our result for values of the center of mass energy close to the production threshold. With the definitions in Eq. 2.21 we expand our results in powers of the heavy quark velocity β, up to terms of order β^2. The coefficients of this expansion contain transcendental constants which originate from one- and two-dimensional HPLs evaluated at $x = 1$. Since we did not find a satisfactory analytical representation for all of these constants, in the formulae below we present them in a numerical form. We find:

$$A(\beta,\xi) \;=\; \frac{A^{(-4)}(\beta,\xi)}{\varepsilon^4} + \frac{A^{(-3)}(\beta,\xi)}{\varepsilon^3} + \frac{A^{(-2)}(\beta,\xi)}{\varepsilon^2} + \frac{A^{(-1)}(\beta,\xi)}{\varepsilon} + A^{(0)}(\beta,\xi) + \mathcal{O}(\varepsilon)\,,$$

$$
\begin{aligned}
A^{(-4)} &= 0.25 - 0.5\beta^2\,(1-\xi)\,\xi + \mathcal{O}\left(\beta^3\right) , \\
A^{(-3)} &= 1.68185 + 0.5L_\mu + \beta(1-2\xi) - \beta^2\Big[0.5 + \xi(1-\xi)(5.86371 + L_\mu)\Big] + \mathcal{O}\left(\beta^3\right) , \\
A^{(-2)} &= -2.67119 - 0.302961L_\mu + 0.5L_\mu^2 + \beta\Big[1.84475 + 2L_\mu - \xi(3.68951 + 4L_\mu)\Big] \\
&\quad +\beta^2\Big[0.777936 - L_\mu - \xi(1-\xi)(7.03784 + 4.39408L_\mu + L_\mu^2)\Big] + \mathcal{O}\left(\beta^3\right) , \\
A^{(-1)} &= -8.15701 - 5.7593L_\mu - 2.13629L_\mu^2 + 0.333333L_\mu^3 + \beta\Big[-9.83935 - 3.64382L_\mu \\
&\quad +2L_\mu^2 + \xi\big(19.6787 + 7.28765L_\mu - 4L_\mu^2\big)\Big] + \beta^2\Big[2.78693 + 5.22254L_\mu \\
&\quad -L_\mu^2 + \xi(1-\xi)(46.7006 + 8.75816L_\mu - 0.727411L_\mu^2 - 0.666667L_\mu^3)\Big] + \mathcal{O}\left(\beta^3\right) , \\
A^{(0)} &= 23.5701 + 7.82592L_\mu + 0.754463L_\mu^2 - 2.03531L_\mu^3 + 0.166667L_\mu^4 + \\
&\quad \beta\Big[0.505501 - 11.5953L_\mu - 7.31049L_\mu^2 + 1.33333L_\mu^3 + \xi\big(-1.011 + 23.1906L_\mu \\
&\quad +14.621L_\mu^2 - 2.66667L_\mu^3\big)\Big] + \beta^2\Big[-4.351 - 3.60348L_\mu + 7.05587L_\mu^2 \\
&\quad -0.666667L_\mu^3 + \xi(1-\xi)\big(-5.36823 + 43.1864L_\mu + 6.73063L_\mu^2 + 0.737281L_\mu^3 \\
&\quad -0.333333L_\mu^4\big)\Big] + \mathcal{O}\left(\beta^3\right) . \qquad (2.32)
\end{aligned}
$$

Note that the dependence on β and on ξ in the formulae above is only polynomial. All the logarithmic terms $\ln\beta$, $\ln\xi$, $\ln(1-\xi)$, $\ln(1-2\,\xi)$, ..., which are indeed present in the expansion of individual HPLs, cancel out in the final expressions. The coefficient A is finite at threshold. The expansion presented here could be used in the future for the calculation of logarithmically enhanced terms near the $t\bar{t}$ production threshold. On the right hand side of Fig. 2.8, we compare the exact expression of the coefficient $A^{(0)}$ with the expansion in powers of β including up to terms of order β^2 (in the plot we set $\xi = 1/2$).

2.5 Conclusions and Outlook

In this chapter, we presented the analytic calculation of the two-loop fermionic corrections and the leading color coefficient in Eq. (2.5) to the heavy-quark production amplitude for $q\bar{q} \to t\bar{t}$, retaining the exact heavy-quark mass dependence. Our work serves as an independent confirmation of recent results obtained analytically as small-mass expansions [20] and numerically [24]. We also provide new results on the threshold expansion of the amplitude.

Our result represents a gauge invariant sub-set of the full two-loop corrections to the partonic process $q\overline{q} \to t\bar{t}$. In order to complete the analytic calculation of the two-loop corrections, it is necessary to calculate the non-planar diagrams. Likewise, analytic results for the two-loop amplitude for $gg \to t\bar{t}$ could be obtained in the same

calculational framework [64]. However, some of the two-loop diagrams appearing in the gluon fusion channel cannot be expressed in terms of two-dimensional HPLs. In fact, their reduction to MIs involves a "sunrise"-type subtopology with three equal massive propagators and an external momentum which is not on the mass shell of the internal propagators. It is known that already such a three-propagator graph involves elliptic integrals [65].

In order to obtain NNLO predictions for the total $t\bar{t}$ production cross section and for differential distributions, it is necessary to combine the two-loop virtual corrections with the already available [10] one-loop corrections to the $t\bar{t}$+(1 parton) process and with the tree-level $t\bar{t}$+(2 partons) process. These diagrams with additional partons in the final state contribute to infrared-divergent configurations where up to two partons can become unresolved. Their implementation requires the application of a NNLO subtraction method. The methods presently available [45–47] have been applied up to now [48–50, 66] to at most $1 \to 3$ processes in e^+e^- annihilation and $2 \to 1$ processes at hadron colliders. A calculation of a hadronic $2 \to 2$ process, involving massive partons, will represent a new step in complexity, potentially requiring further refinements of the methods available to date.

AuxTopo A	AuxTopo B
k_1^2	k_1^2
k_2^2	$k_2^2 - m_t^2$
$(k_1 - k_2)^2$	$(k_1 - k_2)^2 - m_t^2$
$(k_1 - p_1)^2$	$(k_1 - p_1)^2$
$(k_2 - p_1)^2$	$(k_2 - p_1)^2 - m_t^2$
$(k_1 - p_1 - p_2)^2$	$(k_1 - p_1 - p_2)^2$
$(k_2 - p_1 - p_2)^2$	$(k_2 - p_1 - p_2)^2 - m_t^2$
$(k_1 - p_3)^2 - m_t^2$	$(k_1 - p_3)^2 - m_t^2$
$(k_2 - p_3)^2 - m_t^2$	$(k_2 - p_3)^2$

Table 2.1: Propagators in the two different auxiliary topologies used to represent most of the two-loop integrals in the fermionic and planar corrections to top-quark pair production.

Bibliography

[1] F. Abe *et al.* [CDF Collaboration], Phys. Rev. Lett. **74** (1995) 2626 [hep-ex/9503002];
S. Abachi *et al.* [D0 Collaboration], Phys. Rev. Lett. **74**, (1995) 2632 [hep-ex/9503003].

[2] P. Nason, S. Dawson and R.K. Ellis, Nucl. Phys. B **303** (1988) 607.

[3] P. Nason, S. Dawson and R.K. Ellis, Nucl. Phys. B **327** (1989) 49 [Erratum-ibid. B **335** (1990) 260].

[4] W. Beenakker, H. Kuijf, W.L. van Neerven and J. Smith, Phys. Rev. D **40** (1989) 54.

[5] W. Beenakker, W.L. van Neerven, R. Meng, G.A. Schuler and J. Smith, Nucl. Phys. B **351** (1991) 507.

[6] M.L. Mangano, P. Nason and G. Ridolfi, Nucl. Phys. B **373** (1992) 295.

[7] J.G. Körner and Z. Merebashvili, Phys. Rev. D **66** (2002) 054023 [hep-ph/0207054].

[8] W. Bernreuther, A. Brandenburg, Z.G. Si and P. Uwer, Nucl. Phys. B **690** (2004) 81 [hep-ph/0403035].

[9] B.W. Harris, E. Laenen, L. Phaf, Z. Sullivan and S. Weinzierl, Phys. Rev. D **66** (2002) 054024 [hep-ph/0207055].

[10] S. Dittmaier, P. Uwer and S. Weinzierl, Phys. Rev. Lett. **98** (2007) 262002 [arXiv:hep-ph/0703120].

[11] A. Lazopoulos, T. McElmurry, K. Melnikov and F. Petriello, arXiv:0804.2220.

[12] N. Kidonakis and G. Sterman, Nucl. Phys. B **505** (1997) 321 [hep-ph/9705234].

[13] R. Bonciani, S. Catani, M.L. Mangano and P. Nason, Nucl. Phys. B **529** (1998) 424 [hep-ph/9801375].

[14] M. Cacciari, S. Frixione, M.L. Mangano, P. Nason and G. Ridolfi, JHEP **0404** (2004) 068 [hep-ph/0303085].

[15] J.H. Kühn, A. Scharf and P. Uwer, Eur. Phys. J. C **45** (2006) 139 [hep-ph/0508092]; Eur. Phys. J. C **51** (2007) 37 [hep-ph/0610335].

[16] W. Bernreuther, M. Fücker and Z.G. Si, Phys. Rev. D **74** (2006) 113005 [hep-ph/0610334]; arXiv:0804.1237.

[17] S. Moch and P. Uwer, Phys. Rev. D **78** (2008) 034003 [arXiv:0804.1476].

[18] M. Cacciari, S. Frixione, M. L. Mangano, P. Nason and G. Ridolfi, JHEP **0809** (2008) 127 [arXiv:0804.2800].

[19] N. Kidonakis and R. Vogt, Phys. Rev. D **78** (2008) 074005 [arXiv:0805.3844].

[20] M. Czakon, A. Mitov and S. Moch, Phys. Lett. B **651** (2007) 147 [arXiv:0705.1975].

[21] M. Czakon, A. Mitov and S. Moch, Nucl. Phys. B **798** (2008) 210 [arXiv:0707.4139].

[22] Z. Bern, L.J. Dixon and A. Ghinculov, Phys. Rev. D **63** (2001) 053007 [hep-ph/0010075];
C. Anastasiou, E.W.N. Glover, C. Oleari and M.E. Tejeda-Yeomans, Nucl. Phys. B **601** (2001) 318 [hep-ph/0010212];
E.W.N. Glover, JHEP **0404** (2004) 021 [hep-ph/0401119].

[23] C. Anastasiou, E.W.N. Glover, C. Oleari and M.E. Tejeda-Yeomans, Nucl. Phys. B **605** (2001) 486 [hep-ph/0101304];
E.W.N. Glover and M.E. Tejeda-Yeomans, JHEP **0306** (2003) 033 [hep-ph/0304169];
Z. Bern, A. De Freitas and L.J. Dixon, JHEP **0306** (2003) 028 [hep-ph/0304168].

[24] M. Czakon, Phys. Lett. B **664** (2008) 307 [arXiv:0803.1400].

[25] J. G. Korner, Z. Merebashvili and M. Rogal, Phys. Rev. D **73** (2006) 034030 [arXiv:hep-ph/0511264].

[26] P. Nogueira, J. Comput. Phys. **105** (1993) 279.

[27] J.A.M. Vermaseren, Symbolic Manipulation with `FORM`, Version 2, CAN, Amsterdam, 1991; "New features of FORM" [math-ph/0010025].

[28] R. Bonciani, A. Ferroglia, P. Mastrolia, E. Remiddi and J. J. van der Bij, Nucl. Phys. B **681** (2004) 261 [Erratum-ibid. B **702** (2004) 364] [hep-ph/0310333]; R. Bonciani and A. Ferroglia, Phys. Rev. D **72** (2005) 056004 [hep-ph/0507047]; R. Bonciani, A. Ferroglia and A.A. Penin, Phys. Rev. Lett. **100** (2008) 131601 [arXiv:0710.4775]; JHEP **0802** (2008) 080 [arXiv:0802.2215]; S. Actis, M. Czakon, J. Gluza and T. Riemann, Nucl. Phys. B **786** (2007) 26 [arXiv:0704.2400]; Phys. Rev. Lett. **100** (2008) 131602 [arXiv:0711.3847]; Phys. Rev. D **78** (2008) 085019 [arXiv:0807.4691].

[29] R. Bonciani, A. Ferroglia and A.A. Penin, Phys. Rev. Lett. **100** (2008) 131601 [arXiv:0710.4775]; JHEP **0802** (2008) 080 [arXiv:0802.2215];
S. Actis, M. Czakon, J. Gluza and T. Riemann, Nucl. Phys. B **786** (2007) 26 [arXiv:0704.2400]; Phys. Rev. Lett. **100** (2008) 131602 [arXiv:0711.3847].

[30] S. Laporta and E. Remiddi, Phys. Lett. B **379** (1996) 283 [hep-ph/9602417].
S. Laporta, Int. J. Mod. Phys. A **15** (2000) 5087 [hep-ph/0102033].
F.V. Tkachov, Phys. Lett. B **100** (1981) 65.
K.G. Chetyrkin and F.V. Tkachov, Nucl. Phys. B **192** (1981) 159.

[31] M. Argeri, P. Mastrolia and E. Remiddi, Nucl. Phys. B **631** (2002) 388 [hep-ph/0202123].

[32] R. Bonciani, P. Mastrolia and E. Remiddi, Nucl. Phys. B **661** (2003) 289 [Erratum-ibid. B **702** (2004) 359] [hep-ph/0301170]; Nucl. Phys. B **690** (2004) 138 [hep-ph/0311145].

[33] J. Fleischer, A.V. Kotikov and O.L. Veretin, Nucl. Phys. B **547** (1999) 343 [hep-ph/9808242].
U. Aglietti and R. Bonciani, Nucl. Phys. B **668** (2003) 3 [hep-ph/0304028].

[34] A.I. Davydychev and M.Y. Kalmykov, Nucl. Phys. B **699** (2004) 3 [hep-th/0303162].

[35] R. Bonciani, P. Mastrolia and E. Remiddi, Nucl. Phys. B **690** (2004) 138 [hep-ph/0311145].

[36] U. Aglietti and R. Bonciani, Nucl. Phys. B **698** (2004) 277 [hep-ph/0401193].

[37] M. Czakon, J. Gluza and T. Riemann, Phys. Rev. D **71** (2005) 073009 [hep-ph/0412164].

[38] W. Bernreuther, *et al.*, Nucl. Phys. B **706** (2005) 245 [hep-ph/0406046]; Nucl. Phys. B **712** (2005) 229 [hep-ph/0412259]; Nucl. Phys. B **723** (2005) 91 [hep-ph/0504190]; Phys. Rev. D **72** (2005) 096002 [hep-ph/0508254]; Phys. Rev. Lett. **95** (2005) 261802 [hep-ph/0509341]; J. Gluza, A. Mitov, S. Moch and T. Riemann, arXiv:0905.1137.

[39] R. Bonciani and A. Ferroglia, Phys. Rev. D **72** (2005) 056004 [hep-ph/0507047].

[40] A.V. Kotikov, Phys. Lett. B **254** (1991) 158; Phys. Lett. B **259** (1991) 314; Phys. Lett. B **267** (1991) 123;
E. Remiddi, Nuovo Cim. A **110** (1997) 1435. [hep-th/9711188];
M. Caffo, H. Czyz, S. Laporta and E. Remiddi, Acta Phys. Polon. B **29** (1998) 2627; [hep-th/9807119]; Nuovo Cim. A **111** (1998) 365. [hep-th/9805118];
T. Gehrmann and E. Remiddi, Nucl. Phys. B **580** (2000) 485 [hep-ph/9912329];
M. Argeri and P. Mastrolia, Int. J. Mod. Phys. A **22** (2007) 4375 [arXiv:0707.4037].

[41] C. Anastasiou and A. Lazopoulos, JHEP **0407** (2004) 046 [hep-ph/0404258].

[42] J. Gluza, K. Kajda and T. Riemann, Comput. Phys. Commun. **177** (2007) 879 [arXiv:0704.2423].

[43] M. Czakon, Comput. Phys. Commun. **175** (2006) 559 [hep-ph/0511200].

[44] K. Melnikov and T. van Ritbergen, Nucl. Phys. B **591** (2000) 515 [hep-ph/0005131].

[45] T. Binoth and G. Heinrich, Nucl. Phys. B **585** (2000) 741 [hep-ph/0004013]; Nucl. Phys. B **693** (2004) 134 [hep-ph/0402265]; G. Heinrich, Nucl. Phys. Proc. Suppl. **116** (2003) 368 [hep-ph/0211144]; Nucl. Phys. Proc. Suppl. **135** (2004) 290 [hep-ph/0406332]; Eur. Phys. J. C **48** (2006) 25 [hep-ph/0601062]; Int. J. Mod. Phys. A **23** (2008) 1457 [arXiv:0803.4177]; A. Gehrmann-De Ridder, T. Gehrmann and G. Heinrich, Nucl. Phys. B **682** (2004) 265 [hep-ph/0311276]; C. Anastasiou, K. Melnikov and F. Petriello, Phys. Rev. D **69** (2004) 076010 [hep-ph/0311311].

[46] D.A. Kosower, Phys. Rev. D **67** (2003) 116003 [hep-ph/0212097]; A. Daleo, T. Gehrmann and D. Maître, JHEP **0704** (2007) 016 [hep-ph/0612257]; A. Gehrmann-De Ridder and M. Ritzmann, arXiv:0904.3297; A. Gehrmann-De Ridder, T. Gehrmann and E.W.N. Glover, JHEP **0509** (2005) 056 [hep-ph/0505111].

[47] S. Catani and M. Grazzini, Phys. Rev. Lett. **98** (2007) 222002 [hep-ph/0703012].

[48] C. Anastasiou, K. Melnikov and F. Petriello, Phys. Rev. Lett. **93** (2004) 262002 [hep-ph/0409088]; Nucl. Phys. B **724** (2005) 197 [hep-ph/0501130]; JHEP **0709** (2007) 014 [hep-ph/0505069];
K. Melnikov and F. Petriello, Phys. Rev. Lett. **96** (2006) 231803 [hep-ph/0603182]; Phys. Rev. D **74** (2006) 114017 [hep-ph/0609070];
C. Anastasiou, G. Dissertori and F. Stöckli, JHEP **0709** (2007) 018 [arXiv:0707.2373].

[49] A. Gehrmann-De Ridder, T. Gehrmann, E.W.N. Glover and G. Heinrich, Phys. Rev. Lett. **99** (2007) 132002 [arXiv:0707.1285]; JHEP **0711** (2007) 058 [arXiv:0710.0346]; JHEP **0712** (2007) 094 [arXiv:0711.4711]; Phys. Rev. Lett. **100** (2008) 172001 [arXiv:0802.0813]; JHEP **0905** (2009) 106 [arXiv:0903.4658].

[50] M. Grazzini, JHEP **0802** (2008) 043 [arXiv:0801.3232]; D. de Florian and M. Grazzini, Phys. Lett. B **674** (2009) 291 [arXiv:0901.2427]; S. Catani, L. Cieri, G. Ferrera, D. de Florian and M. Grazzini, arXiv:0903.2120.

[51] J. Phys. G **35**, (2008) 083001 [arXiv:0805.1333].

[52] M. Czakon and A. Mitov, Nucl. Phys. B **824** (2010) 111 [arXiv:0811.4119 [hep-ph]].

[53] W. Beenakker, A. Denner, W. Hollik, R. Mertig, T. Sack and D. Wackeroth, Nucl. Phys. B **411** (1994) 343 .

[54] M. Czakon and A. Mitov, Phys. Lett. B **680** (2009) 154 [arXiv:0812.0353 [hep-ph]].

[55] J. G. Körner, Z. Merebashvili and M. Rogal, Phys. Rev. D **77** (2008) 094011 [arXiv:0802.0106].

[56] C. Anastasiou and S. M. Aybat, Phys. Rev. D **78** (2008) 114006 [arXiv:0809.1355].

[57] B. Kniehl, Z. Merebashvili, J. G. Korner and M. Rogal, Phys. Rev. D **78** (2008) 094013 [arXiv:0809.3980].

[58] R. Bonciani, A. Ferroglia, T. Gehrmann, D. Maitre and C. Studerus, "Two-Loop Fermionic Corrections to Heavy-Quark Pair Production: the Quark-Antiquark Channel," JHEP **0807** (2008) 129 [arXiv:0806.2301 [hep-ph]].

[59] R. Bonciani, A. Ferroglia, T. Gehrmann and C. Studerus, "Two-Loop Planar Corrections to Heavy-Quark Pair Production in the Quark-Antiquark Channel," JHEP **0908** (2009) 067 [arXiv:0906.3671 [hep-ph]].

[60] J. Vollinga and S. Weinzierl, Comput. Phys. Commun. **167** (2005) 177 [hep-ph/0410259].

[61] R. Bonciani and A. Ferroglia, JHEP **0811** (2008) 065 [arXiv:0809.4687]; H. M. Asatrian, C. Greub and B. D. Pecjak, Phys. Rev. D **78** (2008) 114028 [arXiv:0810.0987]; M. Beneke, T. Huber and X. Q. Li, Nucl. Phys. B **811** (2009) 77 [arXiv:0810.1230]; G. Bell, Nucl. Phys. B **812** (2009) 264 [arXiv:0810.5695].

[62] V. A. Smirnov, Phys. Lett. B **460** (1999) 397 [hep-ph/9905323]; J. B. Tausk, Phys. Lett. B **469**, 225 (1999) [hep-ph/9909506].

[63] A. V. Smirnov and M. N. Tentyukov, Comput. Phys. Commun. **180** (2009) 735 [arXiv:0807.4129].

[64] R. Bonciani, A. Ferroglia, T. Gehrmann, and C. Studerus, work in progress.

[65] S. Laporta and E. Remiddi, Nucl. Phys. B **704** (2005) 349 [hep-ph/0406160].

[66] S. Weinzierl, Phys. Rev. Lett. **101** (2008) 162001 [arXiv:0807.3241]; JHEP **0906** (2009) 041 [arXiv:0904.1077]; arXiv:0904.1145.

3

Quark and Gluon Form Factors

3.1 Introduction

The form factors are basic vertex functions, and are as such fundamental ingredients for many precision calculations in QCD. They couple an external, colour-neutral off-shell current to a pair of partons: the quark form factor is the coupling of a virtual photon to a quark-antiquark pair, while the gluon form factor is the coupling of a Higgs boson to a pair of gluons through an effective Lagrangian. They appear as virtual higher-order corrections in coefficient functions for the inclusive Drell-Yan process [2, 3] and the inclusive Higgs production cross section [4–6]. In these observables, the infrared poles of the form factors cancel with infrared singularities from real radiation corrections. Consequently, it is possible to relate the coefficients of the infrared poles of the form factors to the coefficients of large logarithmic terms in the corresponding real radiation processes [7, 8]. A framework for combining the resummation of logarithmically enhanced terms at all orders with fixed-order results is provided in an effective field theory expansion [9] of QCD, which is systematized by soft-collinear effective theory [10]. In this context, the pole terms of the form factors yield the anomalous dimensions of the effective operators, while their finite terms determine the matching coefficients to a given order [11–13].

The form factors are actually the simplest QCD objects that display a non-trivial infrared pole structure. As such, their infrared pole coefficients can be used to extract fundamental constants: the cusp anomalous dimensions [14] which control the structure of soft divergences and the collinear quark and gluon anomalous dimensions. From the calculation [15, 16] of the pole terms of the three-loop form factors (and finite plus subleading terms in the two-loop and one-loop form factors [17–19]), these anomalous dimensions [15, 20, 21] are now known to three-loop order. An important observation is the agreement (up to an overall colour factor) of the cusp anomalous dimension for the quark and gluon, the so-called Casimir scaling [22]. Casimir scaling has been verified to

three-loops [23, 24], but it is an open question whether it holds at four loops and beyond [25]. From non-perturbative arguments, the Casimir scaling is expected to break down at some loop order [26].

Based on the observation that infrared singularities of massless on-shell amplitudes in QCD are related to ultraviolet singularities of operators in soft-collinear effective field theory [14, 27], the pole structure of these amplitudes can be analyzed using operator renormalization. The singularity structure of arbitrary multi-leg massless QCD amplitudes is determined by an anomalous dimension matrix. The terms allowed in this anomalous dimension matrix are strongly constrained by relations between soft and collinear terms, from non-abelian exponentiation and from soft and collinear factorization. Independently, Becher and Neubert [21] and Gardi and Magnea [28] have proposed a remarkable all-loops conjecture that describes the pole structure of massless on-shell multi-loop multi-leg QCD amplitudes (generalizing earlier results at two [29] and three loops [30]) in terms of the cusp anomalous dimensions and the collinear anomalous dimensions. In this conjecture, the colour matrix structure of the soft anomalous dimension generated by soft gluons is simply a sum over two-body interactions between hard partons, and thus the matrix structure at any loop order is the same as at one loop. This result builds on the earlier work of Refs. [31, 32] which showed the colour matrix structure of the soft anomalous dimension at two loops is identical to that at one loop. There may be additional colour correlations at three loops or beyond, which cannot be excluded at present. However strong arguments for the absence of these terms are given in Refs. [21, 33]. If the all-order conjecture [21, 28] holds, the calculation of the pole parts of the form factors to a given loop order (and of the finite and subleading parts at fewer loops) would be sufficient to determine the infrared poles of all massless on-shell QCD amplitudes to this order.

The calculation of the three-loop form factors requires two principal ingredients: the algebraic reduction of all three-loop integrals appearing in the relevant Feynman diagrams to master integrals, and the analytical calculation of these master integrals. The reduction of integrals to master integrals exploits linear relations among different integrals, and is done based on a lexicographic ordering of the integrals (the Laporta algorithm [34]). Several dedicated computer-algebra implementations of the Laporta algorithm are available [34–37]. The reduction of the integrals relevant to the three-loop form factors is among the most challenging applications of the Laporta algorithm to date: due to the very large number of interconnected integrals to be reduced, the linear systems to be solved are often containing tens of thousand equations with a similar number of unknowns.

The master integrals in the three-loop form factors were identified already several years ago [38]. Their analytical calculation proved to be a major computational challenge, which was completed only in several steps. The one-loop bubble insertions

into two-loop vertex integrals as well as the two-loop bubble insertions into one-loop vertex integrals were derived using standard Feynman parameter integrals [38], while the genuine three-loop integrals required an extensive use of Mellin-Barnes integration techniques [39–41].

A first calculation of the three-loop form factors (based in part on numerical results for some of the expansion coefficients of the master integrals) was accomplished by Baikov et al. [42] in 2009. The analytical calculation of the last remaining master integrals was only completed recently [41]. It is the purpose of this chapter to validate the three-loop form factor results of Ref. [41, 42] by an independent calculation, and to extend them in in part to a higher order in the expansion in the dimensional regularization parameter $\epsilon = 2 - d/2$. These further expansion terms will be needed for an extraction of the quark and gluon collinear anomalous dimensions from the single pole pieces of the four-loop form factors.

We define the quark and gluon form factors in Section 3.2, where we also discuss their UV-renomalization and summarize existing results at one- and two-loops. The reduction of the form factors to master integrals is described in Section 3.3, and the three-loop master integrals are discussed in Section 3.4. Explicit analytical expressions for them are collected in the appendix of the publication [1]. Our results for the three-loop form factors are presented in Section 3.5, and supplemented by the appendix in [1]. The infrared structure of the QCD form factors up to four-loops is analyzed in Section 3.6. The three-loop hard matching coefficients for Drell-Yan and Higgs production in soft-collinear effective theory are determined from the form factors in Section 3.7. An outlook on future applications is contained in Section 3.8.

3.2 Quark and gluon form factors in perturbative QCD

The form factors are the basic vertex functions of an external off-shell current (with virtuality $q^2 = s_{12}$) coupling to a pair of partons with on-shell momenta p_1 and p_2. One distinguishes time-like ($s_{12} > 0$, i.e. with partons both either in the initial or in the final state) and space-like ($s_{12} < 0$, i.e. with one parton in the initial and one in the final state) configurations. The form factors are described in terms of scalar functions by contracting the respective vertex functions (evaluated in dimensional regularization with $d = 4 - 2\epsilon$ dimensions) with projectors. For massless partons, the full vertex function is described with only a single form factor.

The quark form factor is obtained from the photon-quark-antiquark vertex $\Gamma^{\mu}_{q\bar{q}}$ by

$$\mathcal{F}^q = -\frac{1}{4(1-\epsilon)q^2} \mathrm{T}r\left(\not{p}_2 \Gamma^{\mu}_{q\bar{q}} \not{p}_1 \gamma_\mu\right) , \tag{3.1}$$

while the gluon form factor relates to the effective Higgs-gluon-gluon vertex $\Gamma_{gg}^{\mu\nu}$ as

$$\mathcal{F}^g = \frac{p_1 \cdot p_2\, g_{\mu\nu} - p_{1,\mu} p_{2,\nu} - p_{1,\nu} p_{2,\mu}}{2(1-\epsilon)}\, \Gamma_{gg}^{\mu\nu}\,. \tag{3.2}$$

The form factors are expanded in perturbative QCD in powers of the coupling constant, with each power corresponding to a virtual loop. We denote the unrenormalized form factors by $\mathcal{F}^a$ and the renormalized form factors by F^a with $a = q, g$.

At tree level, the Higgs boson does not couple either to the gluon or to massless quarks. In higher orders in perturbation theory, heavy quark loops introduce a coupling between the Higgs boson and gluons. In the limit of infinitely massive quarks, these loops give rise to an effective Lagrangian [43] mediating the coupling between the scalar Higgs field and the gluon field strength tensor:

$$\mathcal{L}_{\text{int}} = -\frac{\lambda}{4} H F_a^{\mu\nu} F_{a,\mu\nu}\,. \tag{3.3}$$

The coupling λ has inverse mass dimension. It can be computed by matching [44, 45] the effective theory to the full standard model cross sections [5].

Evaluation of the Feynman diagrams, contributing to the vertex functions at a given loop order yields the bare (unrenormalised) form factors,

$$\mathcal{F}_b^q(\alpha_s^b, s_{12}) = 1 + \sum_{n=1}^{\infty} \left(\frac{\alpha_s^b}{4\pi}\right)^n \left(\frac{-s_{12}}{\mu_0^2}\right)^{-n\epsilon} S_\epsilon^n\, \mathcal{F}_n^q, \tag{3.4}$$

$$\mathcal{F}_b^g(\alpha_s^b, s_{12}) = \lambda^b \left(1 + \sum_{n=1}^{\infty} \left(\frac{\alpha_s^b}{4\pi}\right)^n \left(\frac{-s_{12}}{\mu_0^2}\right)^{-n\epsilon} S_\epsilon^n\, \mathcal{F}_n^g\right), \tag{3.5}$$

where μ_0^2 is the mass parameter introduced in dimensional regularisation to maintain a dimensionless coupling in the bare Lagrangian density and where

$$S_\epsilon = e^{-\epsilon\gamma}(4\pi)^\epsilon, \qquad \text{with the Euler constant } \gamma = 0.5772\ldots \tag{3.6}$$

The renormalization of the form factor is carried out by replacing the bare coupling α^b with the renormalized coupling $\alpha_s \equiv \alpha_s(\mu^2)$ evaluated at the renormalization scale μ^2

$$\alpha_s^b \mu_0^{2\epsilon} = Z_{\alpha_s} \mu^{2\epsilon} \alpha_s(\mu^2). \tag{3.7}$$

For simplicity we set $\mu^2 = |s_{12}|$ so that in the $\overline{\text{MS}}$ scheme [46],

$$\begin{aligned} Z_{\alpha_s} = S_\epsilon^{-1} \Bigg[& 1 - \frac{\beta_0}{\epsilon}\left(\frac{\alpha_s}{4\pi}\right) + \left(\frac{\beta_0^2}{\epsilon^2} - \frac{\beta_1}{2\epsilon}\right)\left(\frac{\alpha_s}{4\pi}\right)^2 \\ & - \left(\frac{\beta_0^3}{\epsilon^3} - \frac{7}{6}\frac{\beta_1\beta_0}{\epsilon^2} + \frac{1}{3}\frac{\beta_2}{\epsilon}\right)\left(\frac{\alpha_s}{4\pi}\right)^3 + \mathcal{O}(\alpha_s^4)\Bigg], \end{aligned} \tag{3.8}$$

where β_0, β_1 and β_2 are [47–49]

$$\beta_0 = \frac{11C_A}{3} - \frac{2N_F}{3}, \tag{3.9}$$

$$\beta_1 = \frac{34C_A^2}{3} - \frac{10C_AN_F}{3} - 2C_FN_F, \tag{3.10}$$

$$\beta_2 = \frac{2857C_A^3}{54} + C_F^2N_F - \frac{205C_FC_AN_F}{18} - \frac{1415C_A^2N_F}{54} + \frac{11C_FN_F^2}{9} + \frac{79C_AN_F^2}{54} \tag{3.11}$$

The renormalization relation for the effective coupling λ^b in the $\overline{\rm MS}$ scheme is given by,

$$\lambda^b = Z_\lambda \lambda \tag{3.12}$$

with

$$\begin{aligned} Z_\lambda = 1 &- \frac{\beta_0}{\epsilon}\left(\frac{\alpha_s}{4\pi}\right) + \left(\frac{\beta_0^2}{\epsilon^2} - \frac{\beta_1}{\epsilon}\right)\left(\frac{\alpha_s}{4\pi}\right)^2 \\ &- \left(\frac{\beta_0^3}{\epsilon^3} - \frac{2\beta_1\beta_0}{\epsilon^2} + \frac{\beta_2}{\epsilon}\right)\left(\frac{\alpha_s}{4\pi}\right)^3 + \mathcal{O}(\alpha_s^4)\,. \end{aligned} \tag{3.13}$$

The i-loop contribution to the unrenormalized coefficients is $\mathcal{F}_i^a$, while the renormalised coefficient is denoted by F_i^a where $a = q, g$. If s_{12} is space-like, the form factors are real, while they acquire imaginary parts for time-like s_{12}. These imaginary parts (and corresponding real parts) arise from the ϵ-expansion of

$$\Delta(s_{12}) = (-\mathrm{sgn}(s_{12}) - i0)^{-\epsilon} \tag{3.14}$$

so that the renormalized form factors are given by,

$$F^q(\alpha_s(\mu^2), s_{12}, \mu^2 = |s_{12}|) = 1 + \sum_{n=1}^{\infty}\left(\frac{\alpha_s(\mu^2)}{4\pi}\right)^n F_n^q, \tag{3.15}$$

$$F^g(\alpha_s(\mu^2), s_{12}, \mu^2 = |s_{12}|) = \lambda\left(1 + \sum_{n=1}^{\infty}\left(\frac{\alpha_s(\mu^2)}{4\pi}\right)^n F_n^g\right). \tag{3.16}$$

Up to three loops, the renormalized coefficients for the quark form factor (with $\mu^2 = |s_{12}|$) are then obtained as,

$$\begin{aligned} F_1^q &= \mathcal{F}_1^q\Delta(s_{12}), \\ F_2^q &= \mathcal{F}_2^q\left(\Delta(s_{12})\right)^2 - \frac{\beta_0}{\epsilon}\mathcal{F}_1^q\Delta(s_{12}), \\ F_3^q &= \mathcal{F}_3^q\left(\Delta(s_{12})\right)^3 - \frac{2\beta_0}{\epsilon}\mathcal{F}_2^q\left(\Delta(s_{12})\right)^2 - \left(\frac{\beta_1}{2\epsilon} - \frac{\beta_0^2}{\epsilon^2}\right)\mathcal{F}_1^q\Delta(s_{12}), \end{aligned} \tag{3.17}$$

while those for the gluon form factor are given by,

$$F_1^g = \mathcal{F}_1^g\Delta(s_{12}) - \frac{\beta_0}{\epsilon},$$

$$
\begin{aligned}
F_2^g &= \mathcal{F}_2^g\left(\Delta(s_{12})\right)^2 - \frac{2\beta_0}{\epsilon}\mathcal{F}_1^g\Delta(s_{12}) - \left(\frac{\beta_1}{\epsilon} - \frac{\beta_0^2}{\epsilon^2}\right), \\
F_3^g &= \mathcal{F}_3^g\left(\Delta(s_{12})\right)^3 - \frac{3\beta_0}{\epsilon}\mathcal{F}_2^g\left(\Delta(s_{12})\right)^2 - \left(\frac{3\beta_1}{2\epsilon} - \frac{3\beta_0^2}{\epsilon^2}\right)\mathcal{F}_1^g\Delta(s_{12}) - \left(\frac{\beta_2}{\epsilon} - \frac{2\beta_1\beta_0}{\epsilon^2} + \frac{\beta_0^3}{\epsilon^3}\right).
\end{aligned}
\tag{3.18}
$$

Unless explicitly stated otherwise, the renormalized form factors are given in the space-like case in the following sections.

The one-loop and two-loop form factors were computed in many places in the literature [15–19]. All-order expressions in terms of one-loop and two-loop master integrals are given in [19], and are summarized below.

3.2.1 Results at one-loop

Written in terms of the one-loop bubble integral, which is normalized to the factor

$$
S_\Gamma = \frac{(4\pi)^\epsilon}{16\pi^2\Gamma(1-\epsilon)}, \tag{3.19}
$$

the unrenormalised one-loop form factors are given by

$$
\mathcal{F}_1^q/S_R = \quad C_F\, B_{2,1}\left(\frac{4}{(D-4)} + D - 3\right), \tag{3.20}
$$

$$
\mathcal{F}_1^g/S_R = \quad C_A\, B_{2,1}\left(\frac{4}{(D-4)} - \frac{4}{(D-2)} + 10 - D\right), \tag{3.21}
$$

where

$$
S_R = \frac{16\pi^2 S_\Gamma}{S_\epsilon} = \frac{\exp(\epsilon\gamma)}{\Gamma(1-\epsilon)}. \tag{3.22}
$$

Eqs. (3.20) and (3.21) agree with eqs. (8) and (9) of ref. [19] respectively.

Inserting the expansion of the one-loop master integrals and keeping terms through to $\mathcal{O}(\epsilon^5)$, we find that

$$
\begin{aligned}
\mathcal{F}_1^q = C_F\Bigg[& -\frac{2}{\epsilon^2} - \frac{3}{\epsilon} + (\zeta_2 - 8) + \epsilon\left(\frac{3\zeta_2}{2} + \frac{14\zeta_3}{3} - 16\right) + \epsilon^2\left(\frac{47\zeta_2^2}{20} + 4\zeta_2 + 7\zeta_3 - 32\right) \\
& + \epsilon^3\left(\frac{141\zeta_2^2}{40} - \frac{7\zeta_2\zeta_3}{3} + 8\zeta_2 + \frac{56\zeta_3}{3} + \frac{62\zeta_5}{5} - 64\right) \\
& + \epsilon^4\left(\frac{949\zeta_2^3}{280} + \frac{47\zeta_2^2}{5} - \frac{7\zeta_2\zeta_3}{2} - \frac{49\zeta_3^2}{9} + 16\zeta_2 + \frac{112\zeta_3}{3} + \frac{93\zeta_5}{5} - 128\right) \\
& + \epsilon^5\Bigg(\frac{2847\zeta_2^3}{560} + \frac{94\zeta_2^2}{5} - \frac{329\zeta_2^2\zeta_3}{60} - \frac{28\zeta_2\zeta_3}{3} - \frac{31\zeta_2\zeta_5}{5} - \frac{49\zeta_3^2}{6} \\
& \qquad + 32\zeta_2 + \frac{224\zeta_3}{3} + \frac{248\zeta_5}{5} + \frac{254\zeta_7}{7} - 256\Bigg)\Bigg],
\end{aligned}
\tag{3.23}
$$

$$\mathcal{F}_1^g = C_A\Bigg[-\frac{2}{\epsilon^2} + \zeta_2 + \epsilon\left(\frac{14\zeta_3}{3} - 2\right) + \epsilon^2\left(\frac{47\zeta_2^2}{20} - 6\right) + \epsilon^3\left(-\frac{7\zeta_2\zeta_3}{3} + \zeta_2 + \frac{62\zeta_5}{5} - 14\right) + \epsilon^4\left(\frac{949\zeta_2^3}{280} - \frac{49\zeta_3^2}{9} + 3\zeta_2 + \frac{14\zeta_3}{3} - 30\right) + \epsilon^5\left(\frac{47\zeta_2^2}{20} - \frac{329\zeta_2^2\zeta_3}{60} - \frac{31\zeta_2\zeta_5}{5} + 7\zeta_2 + 14\zeta_3 + \frac{254\zeta_7}{7} - 62\right)\Bigg] \tag{3.24}$$

where the gluon form factor agrees with eq. (7) of ref. [16] through to $\mathcal{O}(\epsilon^4)$. Note that at each order in ϵ, the terms of highest harmonic weight are the same for both quark and gluon form-factor. This is guaranteed by the equivalence of the coefficient of the leading pole in eqs. (3.20) and (3.21).

3.2.2 Results at two-loops

Written in terms of the two-loop master integrals (listed in the appendix), the unrenormalised two-loop gluon form factor is given by

$$\begin{aligned}
\mathcal{F}_2^q/S_R^2 = C_F^2\Bigg[& B_{4,2}\left(\frac{16}{(D-4)^2} + \frac{8}{(D-4)} + D^2 - 6D + 17\right) \\
& - C_{4,1}\left(\frac{7D^2}{8} - \frac{983D}{48} - \frac{565}{32(2D-7)} - \frac{20}{9(3D-8)} - \frac{28}{(D-4)} - \frac{40}{(D-4)^2} + \frac{10693}{288}\right) \\
& + B_{3,1}\left(\frac{27D^2}{8} - \frac{1293D}{16} + \frac{3955}{32(2D-7)} - \frac{17}{2(D-3)} - \frac{476}{(D-4)} - \frac{456}{(D-4)^2} - \frac{288}{(D-4)^3} + \frac{581}{32}\right) \\
& - C_{6,2}\frac{D^3 - 20D^2 + 104D - 176}{8(2D-7)}\Bigg] \\
+ C_F C_A\Bigg[& - C_{4,1}\left(\frac{D^2}{16} + \frac{77D}{32} + \frac{565}{64(2D-7)} + \frac{12}{5(3D-8)} + \frac{23}{15(D-1)} + \frac{8}{3(D-4)} + \frac{16}{(D-4)^2} + \frac{163}{64}\right) \\
& - B_{3,1}\left(\frac{75D^2}{16} - \frac{1837D}{32} + \frac{3955}{64(2D-7)} + \frac{3}{4(D-3)} - \frac{186}{(D-4)} - \frac{144}{(D-4)^2} - \frac{96}{(D-4)^3} + \frac{3845}{64}\right) \\
& + C_{6,2}\frac{D^3 - 20D^2 + 104D - 176}{16(2D-7)}\Bigg]
\end{aligned}$$

$$+C_F N_F\Bigg[\quad -C_{4,1}\frac{(D-2)(3D^3-31D^2+110D-128)}{(3D-8)(D-4)(D-1)}\Bigg] \tag{3.25}$$

$$\begin{aligned}
\mathcal{F}_2^g/S_R^2 = C_A^2\Bigg[\quad & B_{4,2}\left(D^2-20D-\frac{48}{(D-2)}+\frac{32}{(D-4)}+\frac{16}{(D-2)^2}\right.\\
& \left.+\frac{16}{(D-4)^2}+100\right)\\
& +C_{4,1}\left(\frac{27D}{2}+\frac{119}{48(2D-5)}+\frac{75}{16(2D-7)}+\frac{10}{3(D-1)}+\frac{80}{(D-2)}\right.\\
& \left.+\frac{103}{3(D-4)}-\frac{32}{(D-2)^2}+\frac{24}{(D-4)^2}-\frac{609}{8}\right)\\
& +B_{3,1}\left(24D+\frac{107}{144(2D-5)}+\frac{525}{16(2D-7)}+\frac{116}{9(D-1)}+\frac{96}{(D-2)}\right.\\
& -\frac{2}{(D-3)}-\frac{1175}{3(D-4)}-\frac{32}{(D-2)^2}-\frac{1388}{3(D-4)^2}-\frac{192}{(D-4)^3}\\
& \left.-\frac{1955}{8}\right)\\
& +C_{6,2}\frac{3(3D-8)(D-3)}{4(2D-5)(2D-7)}\Bigg]\\
+C_A N_F\Bigg[\quad & C_{4,1}\left(\frac{7D}{8}+\frac{119}{12(2D-5)}+\frac{35}{48(2D-7)}+\frac{20}{3(D-1)}-\frac{40}{3(D-2)}\right.\\
& \left.-\frac{2}{(D-4)}-\frac{45}{16}\right)\\
& -B_{3,1}\left(\frac{19D}{8}-\frac{107}{36(2D-5)}-\frac{245}{48(2D-7)}-\frac{232}{9(D-1)}+\frac{40}{3(D-2)}\right.\\
& \left.-\frac{3}{2(D-3)}+\frac{8}{9(D-4)}-\frac{8}{(D-4)^2}-\frac{61}{16}\right)\\
& +C_{6,2}\frac{(2D^3-25D^2+94D-112)(D-4)}{8(D-2)(2D-5)(2D-7)}\Bigg]\\
+C_F N_F\Bigg[\quad & -C_{4,1}\frac{(46D^4-545D^3+2395D^2-4606D+3248)(D-6)}{2(2D-7)(2D-5)(D-4)(D-2)}\\
& +B_{3,1}\left(\frac{35D}{4}-\frac{107}{18(2D-5)}-\frac{245}{24(2D-7)}+\frac{8}{3(D-2)}-\frac{1}{(D-3)}\right.\\
& \left.-\frac{448}{9(D-4)}-\frac{112}{3(D-4)^2}-\frac{333}{8}\right)
\end{aligned}$$

$$-C_{6,2}\frac{(2D^3-25D^2+94D-112)(D-4)}{4(D-2)(2D-5)(2D-7)}\Bigg] \tag{3.26}$$

which, after re-expressing in terms of N and N_F agrees with eqs. (10) and (11) of ref. [19].

Inserting the expansion of the two-loop master integrals and keeping terms through to $\mathcal{O}(\epsilon^3)$, we find that

$$\begin{aligned}
\mathcal{F}_2^q = C_F^2\Bigg[& \frac{2}{\epsilon^4}+\frac{6}{\epsilon^3}-\frac{1}{\epsilon^2}\left(2\zeta_2-\frac{41}{2}\right)-\frac{1}{\epsilon}\left(\frac{64\zeta_3}{3}-\frac{221}{4}\right) \\
& -\left(13\zeta_2^2-\frac{17\zeta_2}{2}+58\zeta_3-\frac{1151}{8}\right) \\
& -\epsilon\left(\frac{171\zeta_2^2}{5}-\frac{112\zeta_2\zeta_3}{3}-\frac{213\zeta_2}{4}+\frac{839\zeta_3}{3}+\frac{184\zeta_5}{5}-\frac{5741}{16}\right) \\
& +\epsilon^2\left(\frac{223\zeta_2^3}{5}-\frac{3401\zeta_2^2}{20}+54\zeta_2\zeta_3+\frac{2608\zeta_3^2}{9}+\frac{1839\zeta_2}{8}\right. \\
& \quad \left.-\frac{6989\zeta_3}{6}-\frac{462\zeta_5}{5}+\frac{27911}{32}\right) \\
& +\epsilon^3\left(\frac{768\zeta_2^3}{7}+\frac{5488\zeta_2^2\zeta_3}{15}-\frac{29157\zeta_2^2}{40}+\frac{757\zeta_2\zeta_3}{3}+\frac{184\zeta_2\zeta_5}{5}+\frac{2434\zeta_3^2}{3}\right. \\
& \quad \left.+\frac{13773\zeta_2}{16}-\frac{58283\zeta_3}{12}-\frac{3251\zeta_5}{5}+\frac{8942\zeta_7}{7}+\frac{133781}{64}\right)\Bigg] \\
+C_FC_A\Bigg[& -\frac{11}{6\epsilon^3}+\frac{1}{\epsilon^2}\left(\zeta_2-\frac{83}{9}\right)-\frac{1}{\epsilon}\left(\frac{11\zeta_2}{6}-13\zeta_3+\frac{4129}{108}\right) \\
& +\left(\frac{44\zeta_2^2}{5}-\frac{119\zeta_2}{9}+\frac{467\zeta_3}{9}-\frac{89173}{648}\right) \\
& +\epsilon\left(\frac{1891\zeta_2^2}{60}-\frac{89\zeta_2\zeta_3}{3}-\frac{6505\zeta_2}{108}+\frac{6586\zeta_3}{27}+51\zeta_5-\frac{1775893}{3888}\right) \\
& -\epsilon^2\left(\frac{809\zeta_2^3}{70}-\frac{2639\zeta_2^2}{18}+\frac{397\zeta_2\zeta_3}{9}+\frac{569\zeta_3^2}{3}+\frac{146197\zeta_2}{648}\right. \\
& \quad \left.-\frac{159949\zeta_3}{162}-\frac{3491\zeta_5}{15}+\frac{33912061}{23328}\right) \\
& +\epsilon^3\left(\frac{3817\zeta_2^3}{140}-\frac{7103\zeta_2^2\zeta_3}{30}+\frac{638441\zeta_2^2}{1080}-\frac{4358\zeta_2\zeta_3}{27}-\frac{497\zeta_2\zeta_5}{5}-\frac{16439\zeta_3^2}{27}\right. \\
& \quad \left.-\frac{2996725\zeta_2}{3888}+\frac{3709777\zeta_3}{972}+\frac{49786\zeta_5}{45}-372\zeta_7-\frac{632412901}{139968}\right)\Bigg] \\
+C_FN_F\Bigg[& \frac{1}{3\epsilon^3}+\frac{14}{9\epsilon^2}+\frac{1}{\epsilon}\left(\frac{\zeta_2}{3}+\frac{353}{54}\right)+\left(\frac{14\zeta_2}{9}-\frac{26\zeta_3}{9}+\frac{7541}{324}\right)
\end{aligned}$$

$$
\begin{aligned}
&-\epsilon\left(\frac{41\zeta_2^2}{30}-\frac{353\zeta_2}{54}+\frac{364\zeta_3}{27}-\frac{150125}{1944}\right)\\
&-\epsilon^2\left(\frac{287\zeta_2^2}{45}+\frac{26\zeta_2\zeta_3}{9}-\frac{7541\zeta_2}{324}+\frac{4589\zeta_3}{81}+\frac{242\zeta_5}{15}-\frac{2877653}{11664}\right)\\
&+\epsilon^3\left(-\frac{127\zeta_2^3}{14}-\frac{14473\zeta_2^2}{540}-\frac{364\zeta_2\zeta_3}{27}+\frac{338\zeta_3^2}{27}\right.\\
&\qquad\left.+\frac{150125\zeta_2}{1944}-\frac{98033\zeta_3}{486}-\frac{3388\zeta_5}{45}+\frac{53933309}{69984}\right)\Bigg],
\end{aligned}
\tag{3.27}
$$

which agrees through to $\mathcal{O}(\epsilon^2)$ with eq. (3.6) of ref. [15] and provides the next term in the expansion.

Similarly we find that the two-loop expansion of the gluon form factor is given by

$$
\begin{aligned}
\mathcal{F}_2^g = C_A^2\Bigg[&\quad\frac{2}{\epsilon^4}-\frac{11}{6\epsilon^3}-\frac{1}{\epsilon^2}\left(\zeta_2+\frac{67}{18}\right)+\frac{1}{\epsilon}\left(\frac{11\zeta_2}{2}-\frac{25\zeta_3}{3}+\frac{68}{27}\right)\\
&-\left(\frac{21\zeta_2^2}{5}-\frac{67\zeta_2}{6}-\frac{11\zeta_3}{9}-\frac{5861}{162}\right)\\
&-\epsilon\left(\frac{77\zeta_2^2}{60}-\frac{23\zeta_2\zeta_3}{3}-\frac{106\zeta_2}{9}+\frac{1139\zeta_3}{27}-\frac{71\zeta_5}{5}-\frac{158201}{972}\right)\\
&+\epsilon^2\left(\frac{2313\zeta_2^3}{70}-\frac{1943\zeta_2^2}{60}-\frac{55\zeta_2\zeta_3}{3}+\frac{901\zeta_3^2}{9}+\frac{481\zeta_2}{54}\right.\\
&\qquad\left.-\frac{26218\zeta_3}{81}+\frac{341\zeta_5}{15}+\frac{3484193}{5832}\right)\\
&+\epsilon^3\left(\frac{2057\zeta_2^3}{60}+\frac{1291\zeta_2^2\zeta_3}{10}-\frac{28826\zeta_2^2}{135}+\frac{335\zeta_2\zeta_3}{9}-\frac{313\zeta_2\zeta_5}{5}+\frac{5137\zeta_3^2}{27}\right.\\
&\qquad\left.-\frac{4019\zeta_2}{324}-\frac{397460\zeta_3}{243}-\frac{5963\zeta_5}{45}+\frac{6338\zeta_7}{7}+\frac{70647113}{34992}\right)\Bigg]\\
+C_A N_F\Bigg[&\quad\frac{1}{3\epsilon^3}+\frac{5}{9\epsilon^2}-\frac{1}{\epsilon}\left(\zeta_2+\frac{26}{27}\right)-\left(\frac{5\zeta_2}{3}+\frac{74\zeta_3}{9}+\frac{808}{81}\right)\\
&-\epsilon\left(\frac{51\zeta_2^2}{10}+\frac{16\zeta_2}{9}+\frac{604\zeta_3}{27}+\frac{23131}{486}\right)\\
&-\epsilon^2\left(\frac{257\zeta_2^2}{18}-\frac{50\zeta_2\zeta_3}{3}-\frac{28\zeta_2}{27}+\frac{3962\zeta_3}{81}+\frac{542\zeta_5}{15}+\frac{540805}{2916}\right)\\
&+\epsilon^3\left(-\frac{253\zeta_2^3}{210}-\frac{103\zeta_2^2}{3}+\frac{380\zeta_2\zeta_3}{9}+\frac{2306\zeta_3^2}{27}\right.\\
&\qquad\left.+\frac{3157\zeta_2}{162}-\frac{30568\zeta_3}{243}-\frac{854\zeta_5}{9}-\frac{11511241}{17496}\right)\Bigg]
\end{aligned}
$$

$$
\begin{aligned}
+C_F N_F \Bigg[\quad & -\frac{1}{\epsilon} + \left(8\zeta_3 - \frac{67}{6}\right) + \epsilon \left(+\frac{16\zeta_2^2}{3} + \frac{7\zeta_2}{3} + \frac{92\zeta_3}{3} - \frac{2027}{36}\right) \\
& + \epsilon^2 \left(\frac{184\zeta_2^2}{9} - \frac{40\zeta_2\zeta_3}{3} + \frac{209\zeta_2}{18} + \frac{1124\zeta_3}{9} + 32\zeta_5 - \frac{47491}{216}\right) \\
& + \epsilon^3 \left(-\frac{176\zeta_2^3}{35} + \frac{22147\zeta_2^2}{270} - \frac{460\zeta_2\zeta_3}{9} - 120\zeta_3^2 \right. \\
& \left. + \frac{4273\zeta_2}{108} + \frac{15284\zeta_3}{27} + \frac{368\zeta_5}{3} - \frac{987995}{1296}\right) \Bigg] ,
\end{aligned}
\tag{3.28}
$$

which agrees through to $\mathcal{O}(\epsilon^2)$ with eq. (8) of ref. [16] and provides the next term in the expansion. Expressions for the renormalized one-loop and two-loop form factors, expanded to the appropriate order in ϵ, can be found in [19].

3.3 Calculation of the three-loop form factors

To compute the three-loop quark and gluon form factors, we evaluate the relevant three-loop vertex functions within dimensional regularisation. At this loop order, there are 244 Feynman diagrams contributing to the quark form factor, and 1586 diagrams contributing to the gluon form factor. We generated these diagrams using QGRAF [50]. After contraction with the projectors (3.1)–(3.2), each diagram can be expressed as a linear combination of (typically hundreds of) scalar three-loop Feynman integrals. The three-loop integrals appearing in the form factors have up to nine different propagators. The integrands can depend on the three loop momenta, and the two on-shell external momenta, such that 12 different scalar products involving loop momenta can be formed. Consequently, not all scalar products can be cancelled against combinations of denominators, and we are left with irreducible scalar products in the numerator of the integrand. We denote the number of different propagators in an integral by t, the total number of propagators by r and the total number of irreducible scalar products by s. The topology of each integral is fixed by specifying the set of t different propagators and subtopologies are obtained by removing one or more of the propagators.

Using relations between different integrals based on integration-by-parts (IBP) [51] and Lorentz invariance (LI) [52], one can express the large number of different integrals in terms of a small number of so-called master integrals. These identities yield large linear systems of equations, which are solved in an iterative manner using lexicographic ordering [34]. To carry out the reduction in a systematic manner, we introduce so-called auxiliary topologies. Each auxiliary topology is a set of 12 linearly independent propagators. Within the auxiliary topology, the integrand of a three-loop form factor integral with (r, s, t) is expressed by r propagators (with exactly t different propagators) in the denominator, and s propagators (with at most 12-t different propagators) in the

numerator. All three-loop form factor integrals can be cast into one of three auxiliary topologies, which are listed in Table 3.1. The first auxiliary topology contains planar integrals only.

Three-loop integrals with $4 \leq t \leq 9$ and $t \leq r \leq 9$ appear in the form factors. These come with up to $s = 4$ irreducible scalar products for the quark form factor and up to $s = 5$ for the gluon form factor. For a fixed topology and given (r, s, t), there are in total

$$N_{r,s,t} = \binom{r-1}{t-1} \binom{11-t+s}{s}$$

different integrals.

To obtain a reduction, one has to solve very large systems of equations. Already for $s \leq 4$, the system for a given auxiliary topology contains 900000 equations, and its solution is feasible only with dedicated computer algebra tools. For this reduction, we used the Mathematica-based package FIRE [36] and the C++ package Reduze [37] (see Chapter 4).

With Reduze, the reduction and its performance are as follows. The topologies with more than 4 propagators are reduced after inserting the results of the sub-topologies into the system. With increasing t the number of equations decrease as (in general) does the time taken to solve the system which is in the range of a few days to less than an hour with the program Reduze on a modern desktop computer. The total computing time for all the planar diagrams is more than 2 months. However, the parallelization of topologies with an equal number of propagators reduced the overall reduction time to a few weeks.

The three-loop form factors contain in total 22 master integrals, of which 14 are genuine three-loop vertex functions, 4 are three-loop propagator integrals and 4 are products of one-loop and two-loop integrals. They are described in detail in the following section.

3.4 Three-loop form factor master integrals

Our notation for the master integrals follows [38], and we distinguish three topological types of master integrals: genuine three-loop triangles ($A_{t,i}$-type), bubble integrals ($B_{t,i}$-type) and integrals that contain two-loop triangles ($C_{t,i}$-type). In this notation, the index t denotes the number of propagators, and i is simply enumerating the topologically different integrals with the same number of propagators.

The one-loop and two-loop master integrals appearing in the form factors at these loop orders are displayed in Figure 3.1. Their expansions to finite order have been known for a long time, all-orders expressions were derived in [19], they can for example be expanded using HypExp [53]. $B_{t,i}$-type and $C_{t,i}$-type three-loop integrals are listed in Figure 3.2. The $B_{t,i}$-type integrals were computed to finite order in [51, 54], and

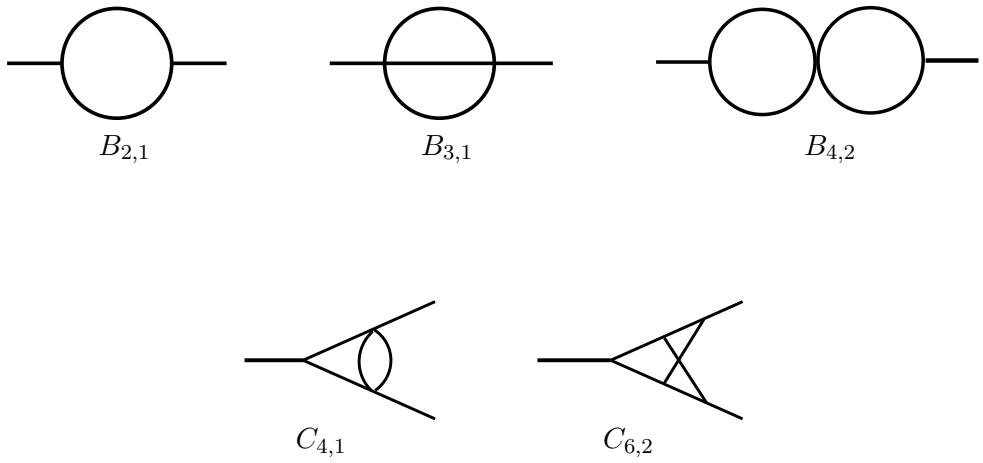

Figure 3.1: One and two-loop master integrals appearing in the quark and gluon form factors.

supplemented by the higher order terms in [55]. Finally, the genuine three-loop vertex integrals are shown in Figure 3.3, their expansions to finite order were derived in [38–41].

The calculation of the nine-line three-loop integrals was the last missing ingredient to the form factor calculation for a long time. The full result for $A_{9,1}$ and most of the pole parts of $A_{9,2}$ and $A_{9,4}$ were computed analytically in [40]. Analytical expressions for the remaining pieces of the latter two integrals were subsequently obtained in [41]. In [40], it was pointed out that for each of these three integrals one can find an integral from the same topology with an irreducible scalar product, which has homogeneous transcendentality. These integrals were named $A_{9,1n}$, $A_{9,2n}$ and $A_{9,4n}$, and are defined in [40]. Compared to [40] we increased the numerical precision of the remaining coefficients, both for $A_{9,2}$ and $A_{9,4}$, by means of conventional packages like `MB.m` [56]. We reproduce thirteen significant digits of the analytic result of [41] in the case of $A_{9,2}$, and fourteen in the case of $A_{9,4}$. We also converted our numerical results for these two integrals into the corresponding integrals of homogeneous transcendentality, $A_{9,2n}$ and $A_{9,4n}$. On the coefficients of these integrals, a PSLQ [57] determination was attempted. For the pole coefficients, the PSLQ algorithm converged to a unique solution in agreement with [41]. For the finite coefficients, the numerical precision that we obtained is yet insufficient for PSLQ to yield a unique solution.

An analytic result for $A_{9,2}$ and $A_{9,4}$, derived by purely analytic steps and without fitting rational coefficients to numerical values, is still a desirable task, and remains to be investigated in the future. This goal is definitely within reach in the case of $A_{9,4}$, whereas the situation is less clear for $A_{9,2}$.

Expansions of all master integrals to the order in ϵ where transcendentality six first appears are listed in the Appendix of the publication [1].

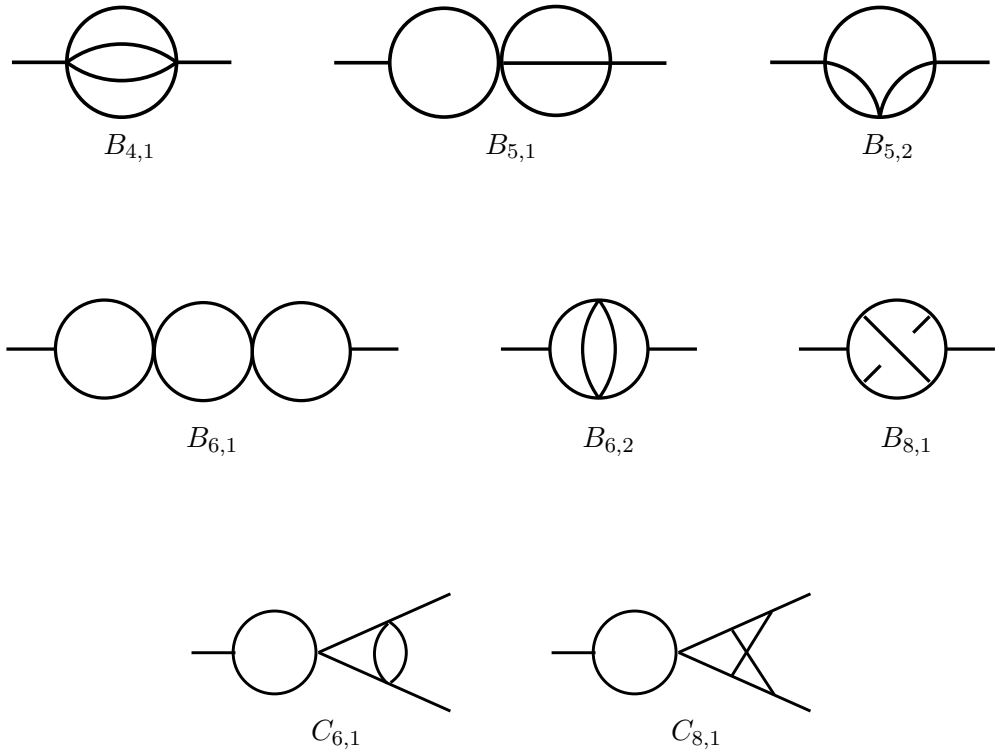

Figure 3.2: Three-loop two-point and factorizable three-point integrals.

3.5 Three-loop form factors

The unrenormalised three-loop form factors can be decomposed into different colour structures as follows:

$$\begin{aligned}\mathcal{F}_3^q/S_R^3 &= C_F^3\ X^q_{C_F^3} + C_F^2 C_A\ X^q_{C_F^2 C_A} + C_F C_A^2\ X^q_{C_F C_A^2} + C_F^2 N_F\ X^q_{C_F^2 N_F} \\ &\quad + C_F C_A N_F\ X^q_{C_F C_A N_F} + C_F N_F^2\ X^q_{C_F N_F^2} + C_F N_{F,V} \left(\frac{N^2-4}{N}\right)\ X^q_{C_F N_{F,V}} \end{aligned} \tag{3.29}$$

and

$$\begin{aligned}\mathcal{F}_3^g/S_R^3 &= C_A^3\ X^g_{C_A^3} + C_A^2 N_F\ X^g_{C_A^2 N_F} + C_A C_F N_F\ X^g_{C_A C_F N_F} + C_F^2 N_F\ X^g_{C_F^2 N_F} \\ &\quad + C_A N_F^2\ X^g_{C_A N_F^2} + C_F N_F^2\ X^g_{C_F N_F^2}\,, \end{aligned} \tag{3.30}$$

where the last term in the quark form factor is generated by graphs where the virtual gauge boson does not couple directly to the final-state quarks. This contribution is denoted by $N_{F,V}$ and is proportional to the charge weighted sum of the quark flavours. In the case of purely electromagnetic interactions, we find,

$$N_{F,\gamma} = \frac{\sum_q e_q}{e_q}. \tag{3.31}$$

The coefficient of each colour structure is a linear combination of master integrals, resulting from the reduction of the integrals appearing in the Feynman diagrams. All coefficients are listed in the appendix of the publication [1].

Inserting the expansion of the three-loop master integrals and keeping terms through to $\mathcal{O}(\epsilon^0)$, we find that the three-loop coefficients are given by

$$
\begin{aligned}
\mathcal{F}_3^q = C_F^3 \Bigg[& -\frac{4}{3\epsilon^6} - \frac{6}{\epsilon^5} + \frac{1}{\epsilon^4}\left(2\zeta_2 - 25\right) + \frac{1}{\epsilon^3}\left(-3\zeta_2 + \frac{100\zeta_3}{3} - 83\right) \\
& + \frac{1}{\epsilon^2}\left(\frac{213\zeta_2^2}{10} - \frac{77\zeta_2}{2} + 138\zeta_3 - \frac{515}{2}\right) \\
& + \frac{1}{\epsilon}\left(\frac{1461\zeta_2^2}{20} - \frac{214\zeta_2\zeta_3}{3} - \frac{467\zeta_2}{2} + \frac{2119\zeta_3}{3} + \frac{644\zeta_5}{5} - \frac{9073}{12}\right) \\
& + \left(-\frac{53675}{24} - \frac{13001\zeta_2}{12} + \frac{12743\zeta_2^2}{40} - \frac{9095\zeta_2^3}{252} + 2669\zeta_3 + 61\zeta_3\zeta_2 \right. \\
& \left. - \frac{1826\zeta_3^2}{3} + \frac{4238\zeta_5}{5}\right)\Bigg] \\
+ C_F^2 C_A \Bigg[& \frac{11}{3\epsilon^5} + \frac{1}{\epsilon^4}\left(-2\zeta_2 + \frac{431}{18}\right) + \frac{1}{\epsilon^3}\left(-\frac{7\zeta_2}{6} - 26\zeta_3 + \frac{6415}{54}\right) \\
& + \frac{1}{\epsilon^2}\left(-\frac{83\zeta_2^2}{5} + \frac{1487\zeta_2}{36} - 210\zeta_3 + \frac{79277}{162}\right) \\
& + \frac{1}{\epsilon}\left(-\frac{9839\zeta_2^2}{72} + \frac{215\zeta_2\zeta_3}{3} + \frac{38623\zeta_2}{108} - \frac{6703\zeta_3}{6} - 142\zeta_5 + \frac{1773839}{972}\right) \\
& + \left(\frac{37684115}{5832} + \frac{664325\zeta_2}{324} - \frac{1265467\zeta_2^2}{2160} - \frac{18619\zeta_2^3}{1260} \right. \\
& \left. - \frac{96715\zeta_3}{18} + \frac{46\zeta_2\zeta_3}{9} + \frac{1616\zeta_3^2}{3} - \frac{46594\zeta_5}{45}\right)\Bigg] \\
+ C_F C_A^2 \Bigg[& -\frac{242}{81\epsilon^4} + \frac{1}{\epsilon^3}\left(\frac{88\zeta_2}{27} - \frac{6521}{243}\right) + \frac{1}{\epsilon^2}\left(-\frac{88\zeta_2^2}{45} - \frac{553\zeta_2}{81} + \frac{1672\zeta_3}{27} - \frac{40289}{243}\right) \\
& + \frac{1}{\epsilon}\left(\frac{802\zeta_2^2}{15} - \frac{88\zeta_2\zeta_3}{9} - \frac{68497\zeta_2}{486} + \frac{12106\zeta_3}{27} - \frac{136\zeta_5}{3} - \frac{1870564}{2187}\right) \\
& + \left(-\frac{52268375}{13122} - \frac{767320\zeta_2}{729} + \frac{152059\zeta_2^2}{540} - \frac{6152\zeta_2^3}{189} \right. \\
& \left. + \frac{1341553\zeta_3}{486} - \frac{710\zeta_2\zeta_3}{9} - \frac{1136\zeta_3^2}{9} + \frac{2932\zeta_5}{9}\right)\Bigg] \\
+ C_F^2 N_F \Bigg[& -\frac{2}{3\epsilon^5} - \frac{37}{9\epsilon^4} + \frac{1}{\epsilon^3}\left(-\frac{\zeta_2}{3} - \frac{545}{27}\right) + \frac{1}{\epsilon^2}\left(-\frac{133\zeta_2}{18} + \frac{146\zeta_3}{9} - \frac{6499}{81}\right)
\end{aligned}
$$

$$
\begin{aligned}
&+\frac{1}{\epsilon}\left(\frac{337\zeta_2^2}{36}-\frac{2849\zeta_2}{54}+\frac{2557\zeta_3}{27}-\frac{138865}{486}\right)\\
&+\left(\frac{8149\zeta_2^2}{216}-\frac{343\zeta_2\zeta_3}{9}-\frac{45235\zeta_2}{162}+\frac{51005\zeta_3}{81}+\frac{278\zeta_5}{45}-\frac{2732173}{2916}\right)\Bigg]\\
+C_FC_AN_F\Bigg[&\quad\frac{88}{81\epsilon^4}+\frac{1}{\epsilon^3}\left(-\frac{16\zeta_2}{27}+\frac{2254}{243}\right)+\frac{1}{\epsilon^2}\left(\frac{316\zeta_2}{81}-\frac{256\zeta_3}{27}+\frac{13679}{243}\right)\\
&+\frac{1}{\epsilon}\left(-\frac{44\zeta_2^2}{5}+\frac{11027\zeta_2}{243}-\frac{6436\zeta_3}{81}+\frac{623987}{2187}\right)\\
&+\left(-\frac{1093\zeta_2^2}{27}+\frac{368\zeta_2\zeta_3}{9}+\frac{442961\zeta_2}{1458}-\frac{45074\zeta_3}{81}-\frac{208\zeta_5}{3}+\frac{8560052}{6561}\right)\Bigg]\\
+C_FN_F^2\Bigg[&\quad-\frac{8}{81\epsilon^4}-\frac{188}{243\epsilon^3}+\frac{1}{\epsilon^2}\left(-\frac{4\zeta_2}{9}-\frac{124}{27}\right)+\frac{1}{\epsilon}\left(-\frac{94\zeta_2}{27}+\frac{136\zeta_3}{81}-\frac{49900}{2187}\right)\\
&+\left(-\frac{83\zeta_2^2}{135}-\frac{62\zeta_2}{3}+\frac{3196\zeta_3}{243}-\frac{677716}{6561}\right)\Bigg]\\
+C_FN_{F,V}&\quad\left(\frac{N^2-4}{N}\right)\left[4-\frac{2\zeta_2^2}{5}+10\zeta_2+\frac{14\zeta_3}{3}-\frac{80\zeta_5}{3}\right]. \qquad (3.32)
\end{aligned}
$$

The pole contributions of $\mathcal{F}_3^q$ are given in eq. (3.7) of ref. [15] while the finite parts of the N_F^2, C_AN_F and C_FN_F contributions are given in eq. (6) of ref. [16]. The finite $N_{F,V}$ contribution can be obtained from the $\delta(1-x)$ contribution to the $d^{abc}d_{abc}$ colour factor in eq. (6.6) of ref. [58]. The remaining finite contributions are given in eqs. (8) and (9) of ref. [42].

Similarly, the expansion of the gluon form factor at three-loops is given by

$$
\begin{aligned}
\mathcal{F}_3^g = C_A^3\Bigg[&\quad-\frac{4}{3\epsilon^6}+\frac{11}{3\epsilon^5}+\frac{361}{81\epsilon^4}+\frac{1}{\epsilon^3}\left(-\frac{517\zeta_2}{54}+\frac{22\zeta_3}{3}-\frac{3506}{243}\right)\\
&+\frac{1}{\epsilon^2}\left(\frac{247\zeta_2^2}{90}+\frac{481\zeta_2}{162}-\frac{209\zeta_3}{27}-\frac{17741}{243}\right)\\
&+\frac{1}{\epsilon}\left(-\frac{3751\zeta_2^2}{360}-\frac{85\zeta_2\zeta_3}{9}+\frac{20329\zeta_2}{243}+\frac{241\zeta_3}{9}-\frac{878\zeta_5}{15}-\frac{145219}{2187}\right)\\
&+\left(\frac{14474131}{13122}+\frac{307057\zeta_2}{1458}+\frac{8459\zeta_2^2}{1080}-\frac{22523\zeta_2^3}{270}\right.\\
&\left.\quad-\frac{68590\zeta_3}{243}+\frac{77\zeta_2\zeta_3}{18}-\frac{1766\zeta_3^2}{9}+\frac{20911\zeta_5}{45}\right)\Bigg]\\
+C_A^2N_F\Bigg[&\quad-\frac{2}{3\epsilon^5}-\frac{2}{81\epsilon^4}+\frac{1}{\epsilon^3}\left(\frac{47\zeta_2}{27}+\frac{1534}{243}\right)+\frac{1}{\epsilon^2}\left(-\frac{425\zeta_2}{81}+\frac{518\zeta_3}{27}+\frac{4280}{243}\right)
\end{aligned}
$$

$$
\begin{aligned}
&+\frac{1}{\epsilon}\left(\frac{2453\zeta_2^2}{180}-\frac{7561\zeta_2}{243}+\frac{1022\zeta_3}{81}-\frac{92449}{2187}\right)\\
&+\left(\frac{437\zeta_2^2}{60}-\frac{439\zeta_2\zeta_3}{9}-\frac{37868\zeta_2}{729}-\frac{754\zeta_3}{27}+\frac{3238\zeta_5}{45}-\frac{10021313}{13122}\right)\Bigg]\\
+C_AC_FN_F\Bigg[&\frac{20}{9\epsilon^3}+\frac{1}{\epsilon^2}\left(-\frac{160\zeta_3}{9}+\frac{526}{27}\right)+\frac{1}{\epsilon}\left(-\frac{176\zeta_2^2}{15}-\frac{22\zeta_2}{3}-\frac{224\zeta_3}{27}+\frac{2783}{81}\right)\\
&+\left(-\frac{16\zeta_2^2}{5}+48\zeta_2\zeta_3-\frac{41\zeta_2}{3}+\frac{11792\zeta_3}{81}+\frac{32\zeta_5}{9}-\frac{155629}{486}\right)\Bigg]\\
+C_F^2N_F\Bigg[&\frac{2}{3\epsilon}+\left(\frac{296\zeta_3}{3}-160\zeta_5+\frac{304}{9}\right)\Bigg]\\
+C_AN_F^2\Bigg[&-\frac{8}{81\epsilon^4}-\frac{80}{243\epsilon^3}+\frac{1}{\epsilon^2}\left(\frac{20\zeta_2}{27}+\frac{8}{9}\right)+\frac{1}{\epsilon}\left(\frac{200\zeta_2}{81}+\frac{664\zeta_3}{81}+\frac{34097}{2187}\right)\\
&+\left(\frac{797\zeta_2^2}{135}+\frac{76\zeta_2}{27}+\frac{11824\zeta_3}{243}+\frac{1479109}{13122}\right)\Bigg]\\
+C_FN_F^2\Bigg[&\frac{8}{9\epsilon^2}+\frac{1}{\epsilon}\left(-\frac{32\zeta_3}{3}+\frac{424}{27}\right)+\left(-\frac{112\zeta_2^2}{15}-\frac{16\zeta_2}{3}-\frac{704\zeta_3}{9}+\frac{10562}{81}\right)\Bigg] \qquad (3.33)
\end{aligned}
$$

The divergent parts agree with eq. (8) of ref. [16] while the finite contributions agree with eq. (10) of ref. [42].

Using our knowledge of the three-loop form factors, we can also write down the $\mathcal{O}(\epsilon)$ contributions to the N_F parts of the quark and gluon form factors. For the quark form-factor we find that,

$$
\begin{aligned}
\mathcal{F}_3^q|_{N_F} \;=\;& C_FN_F^2\epsilon\left(-\frac{2913928}{6561}+\frac{2248}{135}\zeta_5+\frac{2108}{27}\zeta_3-\frac{24950}{243}\zeta_2+\frac{68}{9}\zeta_2\zeta_3-\frac{3901}{810}\zeta_2^2\right)\\
&+C_FC_AN_F\epsilon\left(\frac{24570881}{4374}-\frac{28156}{45}\zeta_5-\frac{2418896}{729}\zeta_3+\frac{10816}{27}\zeta_3^2+\frac{7137385}{4374}\zeta_2\right.\\
&\left.+\frac{2674}{27}\zeta_2\zeta_3-\frac{352559}{1620}\zeta_2^2+\frac{17324}{945}\zeta_2^3\right)\\
&+C_F^2N_F\epsilon\left(-\frac{50187205}{17496}+\frac{5863}{135}\zeta_5+\frac{929587}{243}\zeta_3-\frac{5771}{9}\zeta_3^2-\frac{1263505}{972}\zeta_2\right.\\
&\left.-\frac{8515}{54}\zeta_2\zeta_3+\frac{821749}{3240}\zeta_2^2-\frac{875381}{7560}\zeta_2^3\right)\\
&+C_FN_{F,V}\left(\frac{N^2-4}{N}\right)\epsilon\left(\frac{170}{3}+\frac{752}{9}\zeta_5+\frac{94}{9}\zeta_3-\frac{344}{3}\zeta_3^2+\frac{260}{3}\zeta_2\right.
\end{aligned}
$$

$$+30\zeta_2\zeta_3 - \frac{196}{15}\zeta_2^2 - \frac{9728}{315}\zeta_2^3\Bigg) , \tag{3.34}$$

and for the gluon form factor

$$\begin{aligned}
\mathcal{F}_3^g|_{N_F} \;=\; & C_A N_F^2 \epsilon \left(\frac{16823771}{26244} + \frac{9368}{135}\zeta_5 + \frac{5440}{27}\zeta_3 - \frac{30283}{1458}\zeta_2 - \frac{988}{27}\zeta_2\zeta_3 + \frac{14018}{405}\zeta_2^2 \right) \\
& + C_A^2 N_F \epsilon \left(-\frac{48658741}{8748} - \frac{10066}{45}\zeta_5 + \frac{349918}{729}\zeta_3 - \frac{11657}{27}\zeta_3^2 + \frac{904045}{4374}\zeta_2 \right. \\
& \left. + \frac{791}{9}\zeta_2\zeta_3 - \frac{34931}{1620}\zeta_2^2 - \frac{52283}{1080}\zeta_2^3 \right) \\
& + C_F N_F^2 \epsilon \left(\frac{196900}{243} - \frac{800}{9}\zeta_5 - \frac{4208}{9}\zeta_3 - 54\zeta_2 + \frac{112}{3}\zeta_2\zeta_3 - \frac{2464}{45}\zeta_2^2 \right) \\
& + C_F C_A N_F \epsilon \left(-\frac{10508593}{2916} + \frac{17092}{27}\zeta_5 + \frac{240934}{243}\zeta_3 + \frac{4064}{9}\zeta_3^2 + \frac{8869}{54}\zeta_2 \right. \\
& \left. + \frac{640}{9}\zeta_2\zeta_3 + \frac{28823}{270}\zeta_2^2 + \frac{23624}{315}\zeta_2^3 \right) \\
& + C_F^2 N_F \epsilon \left(\frac{18613}{54} - \frac{3080}{3}\zeta_5 + \frac{10552}{9}\zeta_3 - 272\zeta_3^2 - \frac{74}{3}\zeta_2 \right. \\
& \left. - 16\zeta_2\zeta_3 + \frac{328}{5}\zeta_2^2 - \frac{35648}{315}\zeta_2^3 \right)
\end{aligned} \tag{3.35}$$

The UV-renormalization of the form factors is derived in Section 3.2 above. Applying (3.17) and (3.18) yields the expansion coefficients of the renormalized form factors. These are in the space-like kinematics:

$$\begin{aligned}
F_3^q = C_F^3 \Bigg[& -\frac{4}{3\epsilon^6} - \frac{6}{\epsilon^5} + \frac{1}{\epsilon^4}\left(2\zeta_2 - 25\right) - \frac{1}{\epsilon^3}\left(3\zeta_2 - \frac{100\zeta_3}{3} + 83\right) \\
& + \frac{1}{\epsilon^2}\left(\frac{213\zeta_2^2}{10} - \frac{77\zeta_2}{2} + 138\zeta_3 - \frac{515}{2}\right) \\
& + \frac{1}{\epsilon}\left(\frac{1461\zeta_2^2}{20} - \frac{214\zeta_2\zeta_3}{3} - \frac{467\zeta_2}{2} + \frac{2119\zeta_3}{3} + \frac{644\zeta_5}{5} - \frac{9073}{12}\right) \\
& + \left(-\frac{53675}{24} - \frac{13001\zeta_2}{12} + \frac{12743\zeta_2^2}{40} - \frac{9095\zeta_2^3}{252} + 2669\zeta_3 + 61\zeta_3\zeta_2 \right. \\
& \left. - \frac{1826\zeta_3^2}{3} + \frac{4238\zeta_5}{5}\right)\Bigg] \\
+ C_F^2 C_A \Bigg[& -\frac{11}{\epsilon^5} - \frac{1}{\epsilon^4}\left(\frac{361}{18} + 2\zeta_2\right) + \frac{1}{\epsilon^3}\left(-\frac{1703}{54} - 26\zeta_3 + \frac{27\zeta_2}{2}\right)
\end{aligned}$$

$$
\begin{aligned}
&+\frac{1}{\epsilon^2}\left(\frac{6820}{81}-\frac{482\zeta_3}{9}+\frac{1487\zeta_2}{36}-\frac{83\zeta_2^2}{5}\right)\\
&+\frac{1}{\epsilon}\left(\frac{374149}{486}-142\zeta_5+\frac{215\zeta_3\zeta_2}{3}-\frac{4151\zeta_3}{6}+\frac{31891\zeta_2}{108}-\frac{2975\zeta_2^2}{72}\right)\\
&+\left(\frac{11169211}{2916}-\frac{6890\zeta_5}{9}-\frac{806\zeta_3\zeta_2}{3}-\frac{19933\zeta_3}{6}\right.\\
&\qquad\left.+\frac{1616\zeta_3^2}{3}+\frac{537803\zeta_2}{324}-\frac{723739\zeta_2^2}{2160}-\frac{18619\zeta_2^3}{1260}\right)\Bigg]\\
+C_FC_A^2\Bigg[&-\frac{1331}{81\epsilon^4}+\frac{1}{\epsilon^3}\left(\frac{2866}{243}-\frac{110\zeta_2}{27}\right)+\frac{1}{\epsilon^2}\left(\frac{11669}{486}-\frac{902\zeta_3}{27}+\frac{1625\zeta_2}{81}-\frac{88\zeta_2^2}{45}\right)\\
&+\frac{1}{\epsilon}\left(-\frac{139345}{8748}-\frac{136\zeta_5}{3}-\frac{88\zeta_3\zeta_2}{9}+\frac{3526\zeta_3}{27}-\frac{7163\zeta_2}{243}-\frac{166\zeta_2^2}{15}\right)\\
&+\left(-\frac{51082685}{52488}-\frac{434\zeta_5}{9}+\frac{416\zeta_3\zeta_2}{3}+\frac{505087\zeta_3}{486}\right.\\
&\qquad\left.-\frac{1136\zeta_3^2}{9}-\frac{412315\zeta_2}{729}+\frac{22157\zeta_2^2}{270}-\frac{6152\zeta_2^3}{189}\right)\Bigg]\\
+C_F^2N_F\Bigg[&\frac{2}{\epsilon^5}+\frac{35}{9\epsilon^4}+\frac{1}{\epsilon^3}\left(\frac{139}{27}-3\zeta_2\right)+\frac{1}{\epsilon^2}\left(-\frac{775}{81}-\frac{110\zeta_3}{9}-\frac{133\zeta_2}{18}\right)\\
&+\frac{1}{\epsilon}\left(-\frac{24761}{243}+\frac{469\zeta_3}{27}-\frac{2183\zeta_2}{54}-\frac{287\zeta_2^2}{36}\right)\\
&+\left(-\frac{691883}{1458}-\frac{386\zeta_5}{9}+\frac{35\zeta_3\zeta_2}{3}+\frac{21179\zeta_3}{81}-\frac{16745\zeta_2}{81}-\frac{8503\zeta_2^2}{1080}\right)\Bigg]\\
+C_FC_AN_F\Bigg[&\frac{484}{81\epsilon^4}+\frac{1}{\epsilon^3}\left(-\frac{752}{243}+\frac{20\zeta_2}{27}\right)+\frac{1}{\epsilon^2}\left(-\frac{2068}{243}+\frac{212\zeta_3}{27}-\frac{476\zeta_2}{81}\right)\\
&+\frac{1}{\epsilon}\left(-\frac{8659}{2187}-\frac{964\zeta_3}{81}+\frac{2594\zeta_2}{243}+\frac{44\zeta_2^2}{15}\right)\\
&+\left(\frac{1700171}{6561}-\frac{4\zeta_5}{3}+\frac{4\zeta_3\zeta_2}{3}-\frac{4288\zeta_3}{27}+\frac{115555\zeta_2}{729}+\frac{2\zeta_2^2}{27}\right)\Bigg]\\
+C_FN_F^2\Bigg[&-\frac{44}{81\epsilon^4}-\frac{8}{243\epsilon^3}+\frac{1}{\epsilon^2}\left(\frac{46}{81}+\frac{4}{9}\zeta_2\right)+\frac{1}{\epsilon}\left(\frac{2417}{2187}-\frac{8}{81}\zeta_3-\frac{20}{27}\zeta_2\right)\\
&+\left(-\frac{190931}{13122}-\frac{416}{243}\zeta_3-\frac{824}{81}\zeta_2-\frac{188}{135}\zeta_2^2\right)\Bigg]\\
+C_FN_{F,V}&\left(\frac{N^2-4}{N}\right)\left[4-\frac{2\zeta_2^2}{5}+10\zeta_2+\frac{14\zeta_3}{3}-\frac{80\zeta_5}{3}\right], \qquad (3.36)
\end{aligned}
$$

$$
\begin{aligned}
F_3^g = C_A^3 \Bigg[& -\frac{4}{3\epsilon^6} - \frac{55}{3\epsilon^5} - \frac{9079}{162\epsilon^4} + \frac{1}{\epsilon^3}\left(\frac{5453}{486} + \frac{22\zeta_3}{3} + \frac{77\zeta_2}{54}\right) \\
& + \frac{1}{\epsilon^2}\left(-\frac{4277}{243} + \frac{2266\zeta_3}{27} - \frac{1393\zeta_2}{81} + \frac{247\zeta_2^2}{90}\right) \\
& + \frac{1}{\epsilon}\left(-\frac{1307704}{2187} - \frac{878\zeta_5}{15} - \frac{85\zeta_3\zeta_2}{9} + \frac{1814\zeta_3}{9} - \frac{27301\zeta_2}{486} + \frac{12881\zeta_2^2}{360}\right) \\
& + \left(-\frac{23496187}{26244} + \frac{13882\zeta_5}{45} - \frac{1441\zeta_3\zeta_2}{18} + \frac{24893\zeta_3}{243}\right. \\
& \left. - \frac{1766\zeta_3^2}{9} + \frac{118165\zeta_2}{1458} + \frac{126071\zeta_2^2}{1080} - \frac{22523\zeta_2^3}{270}\right)\Bigg] \\
+ C_A^2 N_F \Bigg[& \frac{10}{3\epsilon^5} + \frac{1780}{81\epsilon^4} + \frac{1}{\epsilon^3}\left(\frac{2344}{243} - \frac{7\zeta_2}{27}\right) + \frac{1}{\epsilon^2}\left(-\frac{1534}{243} + \frac{68\zeta_3}{27} + \frac{169\zeta_2}{81}\right) \\
& + \frac{1}{\epsilon}\left(\frac{854467}{4374} + \frac{3002\zeta_3}{81} + \frac{3536\zeta_2}{243} + \frac{941\zeta_2^2}{180}\right) \\
& + \left(\frac{2143537}{13122} + \frac{4516\zeta_5}{45} - \frac{301\zeta_3\zeta_2}{9} + \frac{1414\zeta_3}{9} - \frac{6440\zeta_2}{729} + \frac{527\zeta_2^2}{20}\right)\Bigg] \\
+ C_A C_F N_F \Bigg[& -\frac{34}{9\epsilon^3} + \frac{1}{\epsilon^2}\left(\frac{427}{27} - \frac{160\zeta_3}{9}\right) + \frac{1}{\epsilon}\left(\frac{13655}{81} - \frac{2600\zeta_3}{27} - \frac{13\zeta_2}{3} - \frac{176\zeta_2^2}{15}\right) \\
& + \left(\frac{284929}{972} + \frac{32\zeta_5}{9} + 48\zeta_3\zeta_2 - \frac{14398\zeta_3}{81} - \frac{118\zeta_2}{3} - \frac{928\zeta_2^2}{15}\right)\Bigg] \\
+ C_F^2 N_F \Bigg[& -\frac{1}{3\epsilon} + \left(\frac{304}{9} - 160\zeta_5 + \frac{296\zeta_3}{3}\right)\Bigg] \\
+ C_A N_F^2 \Bigg[& -\frac{170}{81\epsilon^4} - \frac{998}{243\epsilon^3} + \frac{1}{\epsilon^2}\left(\frac{92}{27} + \frac{2\zeta_2}{27}\right) + \frac{1}{\epsilon}\left(-\frac{37133}{4374} - \frac{164\zeta_3}{81} - \frac{70\zeta_2}{81}\right) \\
& + \left(\frac{125059}{13122} + \frac{952\zeta_3}{243} - \frac{20\zeta_2}{27} - \frac{157\zeta_2^2}{135}\right)\Bigg] \\
+ C_F N_F^2 \Bigg[& \frac{14}{9\epsilon^2} + \frac{1}{\epsilon}\left(-\frac{212}{27} + \frac{16\zeta_3}{3}\right) + \left(\frac{2881}{162} - \frac{152\zeta_3}{9} - \frac{2\zeta_2}{3} + \frac{16\zeta_2^2}{5}\right)\Bigg] \\
+ N_F^3 \Bigg[& \frac{8}{27\epsilon^3}\Bigg]
\end{aligned}
\tag{3.37}
$$

The $\mathcal{O}(\epsilon)$ contributions to the N_F parts of the UV-renormalized space-like quark

and gluon form factors are given by,

$$
\begin{aligned}
F_3^q|_{N_F} &= +C_F N_F^2 \epsilon \left(-\frac{3769249}{26244} + \frac{88}{135}\zeta_5 + \frac{2632}{243}\zeta_3 - \frac{5515}{81}\zeta_2 + \frac{8}{3}\zeta_2\zeta_3 - \frac{952}{81}\zeta_2^2 \right) \\
&\quad + C_F C_A N_F \epsilon \left(\frac{1552436}{729} - \frac{11596}{45}\zeta_5 - \frac{1214351}{729}\zeta_3 + \frac{3988}{27}\zeta_3^2 + \frac{4933141}{4374}\zeta_2 \right. \\
&\quad \left. + \frac{1966}{27}\zeta_2\zeta_3 + \frac{4579}{405}\zeta_2^2 + \frac{2762}{945}\zeta_2^3 \right) \\
&\quad + C_F^2 N_F \epsilon \left(-\frac{15199979}{8748} - \frac{10769}{135}\zeta_5 + \frac{553882}{243}\zeta_3 - \frac{6881}{27}\zeta_3^2 - \frac{961699}{972}\zeta_2 \right. \\
&\quad \left. - \frac{4627}{54}\zeta_2\zeta_3 + \frac{94747}{3240}\zeta_2^2 - \frac{425813}{7560}\zeta_2^3 \right) \\
&\quad + C_F N_{F,V} \left(\frac{N^2-4}{N} \right) \epsilon \left(\frac{170}{3} + \frac{752}{9}\zeta_5 + \frac{94}{9}\zeta_3 - \frac{344}{3}\zeta_3^2 + \frac{260}{3}\zeta_2 \right. \\
&\quad \left. + 30\zeta_2\zeta_3 - \frac{196}{15}\zeta_2^2 - \frac{9728}{315}\zeta_2^3 \right) , \qquad (3.38)
\end{aligned}
$$

and for the gluon form factor

$$
\begin{aligned}
F_3^g|_{N_F} &= +C_A N_F^2 \epsilon \left(\frac{6599393}{26244} + \frac{1844}{135}\zeta_5 + \frac{8396}{81}\zeta_3 - \frac{25315}{1458}\zeta_2 - \frac{172}{27}\zeta_2\zeta_3 + \frac{2453}{405}\zeta_2^2 \right) \\
&\quad + C_A^2 N_F \epsilon \left(-\frac{18825781}{8748} + \frac{1682}{45}\zeta_5 + \frac{270232}{729}\zeta_3 - \frac{6251}{27}\zeta_3^2 + \frac{867919}{4374}\zeta_2 \right. \\
&\quad \left. - \frac{881}{9}\zeta_2\zeta_3 + \frac{33403}{405}\zeta_2^2 + \frac{133627}{7560}\zeta_2^3 \right) \\
&\quad + C_F N_F^2 \epsilon \left(\frac{360181}{972} - \frac{224}{9}\zeta_5 - \frac{1960}{9}\zeta_3 - \frac{277}{9}\zeta_2 + \frac{32}{3}\zeta_2\zeta_3 - \frac{208}{15}\zeta_2^2 \right) \\
&\quad + C_F C_A N_F \epsilon \left(-\frac{7017335}{5832} + \frac{7588}{27}\zeta_5 - \frac{92894}{243}\zeta_3 + \frac{4064}{9}\zeta_3^2 + \frac{986}{54}\zeta_2 \right. \\
&\quad \left. + \frac{1960}{9}\zeta_2\zeta_3 - \frac{59987}{540}\zeta_2^2 + \frac{23624}{315}\zeta_2^3 \right) \\
&\quad + C_F^2 N_F \epsilon \left(\frac{18613}{54} - \frac{3080}{3}\zeta_5 + \frac{10552}{9}\zeta_3 - 272\zeta_3^2 - \frac{74}{3}\zeta_2 \right. \\
&\quad \left. - 16\zeta_2\zeta_3 + \frac{328}{5}\zeta_2^2 - \frac{35648}{315}\zeta_2^3 \right) . \qquad (3.39)
\end{aligned}
$$

3.6 Infrared pole structure

According to ref. [14, 21], the general infrared pole structure of a renormalised QCD amplitude is related to the ultraviolet behaviour of an effective operator in soft-collinear effective theory. These poles can therefore be subtracted by means of a multiplicative renormalization factor **Z**. This means that the finite remainders of a scattering amplitude $\mathbf{M^F}$ is obtained from the full amplitude **M** via the relation,

$$\mathbf{M^F} = \mathbf{Z}^{-1}\mathbf{M}. \tag{3.40}$$

In general, the scattering amplitude **M** and **Z** are matrices in colour space. However, in the context of the quark and gluon form factors, the colour matrix is trivial. The UV renormalised amplitudes M and M_F have perturbative expansions,

$$M = 1 + \sum_{i=1} \left(\frac{\alpha_s(\mu^2)}{4\pi}\right)^i M_i, \tag{3.41}$$

$$M^F = 1 + \sum_{i=1} \left(\frac{\alpha_s(\mu^2)}{4\pi}\right)^i M_i^F, \tag{3.42}$$

while

$$\log(Z) = \sum_{i=1} \left(\frac{\alpha_s(\mu^2)}{4\pi}\right)^i Z_i. \tag{3.43}$$

We can now solve eq. (3.40) order by order in the strong coupling,

$$\mathcal{P}oles(M_1) = Z_1, \tag{3.44}$$

$$\mathcal{P}oles(M_2) = Z_2 + \frac{M_1^2}{2}, \tag{3.45}$$

$$\mathcal{P}oles(M_3) = Z_3 - \frac{M_1^3}{3} + M_2 M_1, \tag{3.46}$$

$$\mathcal{P}oles(M_4) = Z_4 + \frac{M_1^4}{4} - M_1^2 M_2 + M_1 M_3 + \frac{M_2^2}{2}, \tag{3.47}$$

$$\mathcal{P}oles(M_5) = Z_5 - \frac{M_1^5}{5} + M_1^3 M_2 - M_1^2 M_3 - M_1 M_2^2 + M_1 M_4 + M_2 M_3. \tag{3.48}$$

The deepest infrared pole for the i-loop amplitude is ϵ^{-2i}. However, the deepest pole in the Z_i-factor is ϵ^{-i-1}. All of the deepest poles are obtained directly from the lower loop amplitudes - which must be known to an appropriately high order in ϵ. For example, to obtain the correct pole structure for M_i, one needs knowledge of M_1 through to $\mathcal{O}(\epsilon^{2i-3})$.

We find that the infrared pole structure of the renormalised form factors is given by ($i = q, g$ and $C_q = C_F$, $C_g = C_A$ for the cusp anomalous dimension):

$$\mathcal{P}oles(F_1^i) = -\frac{C_i \gamma_0^{\text{cusp}}}{2\epsilon^2} + \frac{\gamma_0^i}{\epsilon}, \tag{3.49}$$

$$\mathcal{P}oles(F_2^i) = \frac{3C_i\gamma_0^{\rm cusp}\beta_0}{8\epsilon^3} + \frac{1}{\epsilon^2}\left(-\frac{\beta_0\gamma_0^i}{2} - \frac{C_i\gamma_1^{\rm cusp}}{8}\right) + \frac{\gamma_1^i}{2\epsilon} + \frac{\left(F_1^i\right)^2}{2}\,, \tag{3.50}$$

$$\begin{aligned}\mathcal{P}oles(F_3^i) &= -\frac{11\beta_0^2C_i\gamma_0^{\rm cusp}}{36\epsilon^4} + \frac{1}{\epsilon^3}\left(\frac{5\beta_0C_i\gamma_1^{\rm cusp}}{36} + \frac{\beta_0^2\gamma_0^i}{3} + \frac{2C_i\gamma_0^{\rm cusp}\beta_1}{9}\right)\\ &\quad + \frac{1}{\epsilon^2}\left(-\frac{\beta_0\gamma_1^i}{3} - \frac{C_i\gamma_2^{\rm cusp}}{18} - \frac{\beta_1\gamma_0^i}{3}\right) + \frac{\gamma_2^i}{3\epsilon} - \frac{\left(F_1^i\right)^3}{3} + F_2^qF_1^q\,.\end{aligned} \tag{3.51}$$

Note that the full (all-orders) expressions for F_i^q are recycled on the right-hand-side. The coefficients of the cusp soft anomalous dimension $\gamma_i^{\rm cusp}$ are known to three-loop order [15] and are given by:

$$\gamma_0^{\rm cusp} = 4\,, \tag{3.52}$$

$$\gamma_1^{\rm cusp} = C_A\left(\frac{268}{9} - \frac{4\pi^2}{3}\right) - \frac{40N_F}{9}\,, \tag{3.53}$$

$$\begin{aligned}\gamma_2^{\rm cusp} &= C_A^2\left(\frac{490}{3} - \frac{536\pi^2}{27} + \frac{44\pi^4}{45} + \frac{88\zeta_3}{3}\right) + C_AN_F\left(-\frac{836}{27} + \frac{80\pi^2}{27} - \frac{112\zeta_3}{3}\right)\\ &\quad + C_FN_F\left(-\frac{110}{3} + 32\zeta_3\right) - \frac{16N_F^2}{27}\,.\end{aligned} \tag{3.54}$$

while the quark and gluon collinear anomalous dimensions γ_i^q and γ_i^g in the conventional dimensional regularisation scheme are also known to three-loop order [20, 21] and are given by:

$$\gamma_0^q = -3C_F\,, \tag{3.55}$$

$$\begin{aligned}\gamma_1^q &= C_F^2\left(-\frac{3}{2} + 2\pi^2 - 24\zeta_3\right) + C_FC_A\left(-\frac{961}{54} - \frac{11\pi^2}{6} + 26\zeta_3\right)\\ &\quad + C_FN_F\left(\frac{65}{27} + \frac{\pi^2}{3}\right),\end{aligned} \tag{3.56}$$

$$\begin{aligned}\gamma_2^q &= C_F^2N_F\left(\frac{2953}{54} - \frac{13\pi^2}{9} - \frac{14\pi^4}{27} + \frac{256\zeta_3}{9}\right) + C_FN_F^2\left(\frac{2417}{729} - \frac{10\pi^2}{27} - \frac{8\zeta_3}{27}\right)\\ &\quad + C_FC_AN_F\left(-\frac{8659}{729} + \frac{1297\pi^2}{243} + \frac{11\pi^4}{45} - \frac{964\zeta_3}{27}\right)\\ &\quad + C_F^3\left(-\frac{29}{2} - 3\pi^2 - \frac{8\pi^4}{5} - 68\zeta_3 + \frac{16\pi^2\zeta_3}{3} + 240\zeta_5\right)\\ &\quad + C_AC_F^2\left(-\frac{151}{4} + \frac{205\pi^2}{9} + \frac{247\pi^4}{135} - \frac{844\zeta_3}{3} - \frac{8\pi^2\zeta_3}{3} - 120\zeta_5\right)\\ &\quad + C_A^2C_F\left(-\frac{139345}{2916} - \frac{7163\pi^2}{486} - \frac{83\pi^4}{90} + \frac{3526\zeta_3}{9} - \frac{44\pi^2\zeta_3}{9} - 136\zeta_5\right),\end{aligned} \tag{3.57}$$

$$\gamma_0^g = -\frac{11C_A}{3} + \frac{2N_F}{3}\,, \tag{3.58}$$

$$\gamma_1^g = C_A^2\left(-\frac{692}{27}+\frac{11\pi^2}{18}+2\zeta_3\right)+C_A N_F\left(\frac{128}{27}-\frac{\pi^2}{9}\right)+2C_F N_F \tag{3.59}$$

$$\begin{aligned}\gamma_2^g = {} & C_A^3\left(-\frac{97186}{729}+\frac{6109\pi^2}{486}-\frac{319\pi^4}{270}+\frac{122\zeta_3}{3}-\frac{20\pi^2\zeta_3}{9}-16\zeta_5\right), \\ & +C_A^2 N_F\left(\frac{30715}{1458}-\frac{599\pi^2}{243}+\frac{41\pi^4}{135}+\frac{356\zeta_3}{27}\right) \\ & +C_F C_A N_F\left(\frac{1217}{27}-\frac{\pi^2}{3}-\frac{4\pi^4}{45}-\frac{152\zeta_3}{9}\right)-C_F^2 N_F \\ & +C_A N_F^2\left(-\frac{269}{1458}+\frac{10\pi^2}{81}-\frac{56\zeta_3}{27}\right)-\frac{11 C_F N_F^2}{9}\,.\end{aligned} \tag{3.60}$$

Taking this one step further, we find that the pole structure of the renormalised four-loop quark form factor is given by

$$\begin{aligned}\mathcal{P}oles(F_4^i) = {} & \frac{25\beta_0^3 C_i\gamma_0^{\rm cusp}}{96\epsilon^5}-\frac{\beta_0(24\beta_0^2\gamma_0^i+13\beta_0 C_i\gamma_1^{\rm cusp}+40 C_i\gamma_0^{\rm cusp}\beta_1)}{96\epsilon^4} \\ & +\frac{1}{\epsilon^3}\left(\frac{7\beta_0 C_i\gamma_2^{\rm cusp}}{96}+\frac{3\beta_1 C_i\gamma_1^{\rm cusp}}{32}+\frac{\beta_0^2\gamma_1^i}{4}+\frac{\beta_1\beta_0\gamma_0^i}{2}+\frac{5 C_i\gamma_0^{\rm cusp}\beta_2}{32}\right) \\ & +\frac{1}{\epsilon^2}\left(-\frac{\beta_1\gamma_1^i}{4}-\frac{C_i\gamma_3^{\rm cusp}}{32}-\frac{\beta_0\gamma_2^i}{4}-\frac{\beta_2\gamma_0^i}{4}\right)+\frac{\gamma_3^i}{4\epsilon} \\ & +\frac{\left(F_1^i\right)^4}{4}+\left(F_1^i\right)^2 F_2^i-\frac{\left(F_2^i\right)^2}{2}-F_1^i F_3^i\,.\end{aligned} \tag{3.61}$$

In this expression, we assume Casimir scaling of the cusp anomalous dimension to hold at four loops [21, 22], such that only a universal $\gamma_3^{\rm cusp}$ appears. If, contrary to expectations, Casimir scaling should be violated at this order, different $\gamma_3^{\rm cusp}$ would appear in the double pole terms of the quark and gluon form factors at four loops.

Eq. (3.61) shows that in order to make use of a calculation of the pole parts of the four-loop form factors to extract the cusp and collinear anomalous dimensions, one requires the finite parts of the three-loop form factor for $\gamma_3^{\rm cusp}$, and of the subleading $\mathcal{O}(\epsilon)$ parts for $\gamma_3^{q,g}$. For all colour-factor contributions proportional to N_F, these are provided in the previous section. The required subleading terms in higher orders in ϵ from the one-loop and two-loop form factors were summarized in Section 3.2 above.

3.7 Effective Theory Matching Coefficients

It is well known that fixed-order perturbation theory is not reliable for physical quantities involving several disparate scales. In such cases, higher-order corrections are enhanced by large logarithms of scale ratios. Experimentally relevant examples are the Drell-Yan and Higgs production processes in hadron-hadron colliders. When the phase

space for soft gluon emission is constrained, large logarithmic threshold corrections appear of the form

$$\alpha_s^k \left[\frac{\ln^{m-1}(1-z)}{(1-z)} \right]_+, \qquad (m \leq 2k), \tag{3.62}$$

where $(1-z)$ is the fraction of centre-of-mass energy of the initial partons available for soft gluon radiation. These spoil the convergence of the perturbative series. The resummation of these so-called Sudakov-logarithms has been accomplished to fourth logarithmic order [8], using the exponentiation properties of the coefficient functions in moment space [59].

An alternative resummation framework is provided by soft-collinear effective field theory (SCET), which is based on the idea to split the calculation into a series of single-scale problems by successively integrating out the physics associated with the largest remaining scale. The SCET framework [10] originated in the study of heavy quarks, and has been subsequently generalized to massless collider processes [60]. The infrared poles in the high energy theory (QCD) get transformed into ultraviolet poles in the effective theory [9, 14] and can then be resummed by renormalization-group (RG) evolution from the larger scales to the smaller ones. Of course the SCET must match precisely onto the high energy theory, and this is achieved by computing matrix elements in both the SCET and QCD and adjusting the Wilson coefficients so that they agree. If the matching is performed on-shell, then the matching coefficients relevant for Drell Yan and Higgs production can be obtained from the quark and gluon form factors respectively. Therefore, we can utilise the results presented in the previous sections to compute the matching conditions through to three-loops. Results up to two loops were obtained previously in [11–13].

The renormalised form-factors are infrared divergent. In the effective field theory, these infrared divergences are transformed into ultraviolet poles. The matching coefficient C^i $(i = q, g)$ is obtained by extracting the poles using a renormalisation factor such that,

$$C^i(\alpha_s(\mu^2), s_{12}, \mu^2) = \lim_{\epsilon \to 0} Z_i^{-1}(\epsilon, s_{12}, \mu) F^i(\epsilon, s_{12}, \mu^2). \tag{3.63}$$

The matching coefficients have the perturbative expansion,

$$C^i(\alpha_s(\mu^2), s_{12}, \mu^2) \;=\; 1 + \sum_{n=1}^{\infty} \left(\frac{\alpha_s(\mu^2)}{4\pi} \right)^n C_n^i(s_{12}, \mu^2). \tag{3.64}$$

They are are known to two loop order for Drell-Yan [11, 12] and Higgs [13] production,

$$\begin{aligned} C_1^q &= C_F \left(-L^2 + 3L - 8 + \zeta_2 \right), \qquad (3.65) \\ C_2^q &= C_F^2 \left(\frac{1}{2} L^4 - 3L^3 + \left(\frac{25}{2} - \zeta_2 \right) L^2 + \left(-\frac{45}{2} + 24\zeta_3 - 9\zeta_2 \right) L \right. \end{aligned}$$

$$+\frac{255}{8} - 30\zeta_3 + 21\zeta_2 - \frac{83}{10}\zeta_2^2\Big)$$
$$+C_F C_A\Big(\frac{11}{9}L^3 + \Big(-\frac{233}{18} + 2\zeta_2\Big)L^2 + \Big(\frac{2545}{54} - 26\zeta_3 + \frac{22}{3}\zeta_2\Big)L$$
$$-\frac{51157}{648} + \frac{313}{9}\zeta_3 - \frac{337}{18}\zeta_2 + \frac{44}{5}\zeta_2^2\Big)$$
$$+C_F N_F\Big(-\frac{2}{9}L^3 + \frac{19}{9}L^2 + \Big(-\frac{209}{27} - \frac{4}{3}\zeta_2\Big)L + \frac{4085}{324} + \frac{2}{9}\zeta_3 + \frac{23}{9}\zeta_2\Big) \quad (3.66)$$

$$C_1^g = C_A\Big(-L^2 + \zeta_2\Big), \quad (3.67)$$

$$C_2^g = C_A^2\Big(\frac{1}{2}L^4 + \frac{11}{9}L^3 + \Big(-\frac{67}{9} + \zeta_2\Big)L^2 + \Big(\frac{80}{27} - 2\zeta_3 - \frac{22}{3}\zeta_2\Big)L$$
$$+\frac{5105}{162} - \frac{143}{9}\zeta_3 + \frac{67}{6}\zeta_2 + \frac{1}{2}\zeta_2^2\Big)$$
$$+C_A N_F\Big(-\frac{2}{9}L^3 + \frac{10}{9}L^2 + \Big(\frac{52}{27} + \frac{4}{3}\zeta_2\Big)L - \frac{916}{81} - \frac{46}{9}\zeta_3 - \frac{5}{3}\zeta_2\Big)$$
$$+C_F N_F\Big(2L - \frac{67}{6} + 8\zeta_3\Big) \quad (3.68)$$

where $L = \log(-s_{12}/\mu^2)$.

Exploiting the expressions for the renormalised quark and gluon form factors given in eqs. (3.36) and (3.37) respectively, we find that the three-loop matching coefficients are

$$C_3^q = C_F^3\Big(-\frac{1}{6}L^6 + \frac{3}{2}L^5 + \Big(-\frac{17}{2} + \frac{1}{2}\zeta_2\Big)L^4 + \Big(9\zeta_2 + 27 - 24\zeta_3\Big)L^3$$
$$+\Big(102\zeta_3 - \frac{507}{8} - \frac{105}{2}\zeta_2 + \frac{83}{10}\zeta_2^2\Big)L^2$$
$$+\Big(-214\zeta_3 - 240\zeta_5 - 8\zeta_2\zeta_3 + \frac{357}{2}\zeta_2 + \frac{207}{10}\zeta_2^2 + \frac{785}{8}\Big)L$$
$$-\frac{413}{5}\zeta_2^2 + 664\zeta_5 - \frac{6451}{24}\zeta_2 + \frac{37729}{630}\zeta_2^3 - 470\zeta_3 + 250\zeta_2\zeta_3 - \frac{2539}{12} + 16\zeta_3^2\Big)$$
$$+C_F^2 C_A\Big(-\frac{11}{9}L^5 + \Big(\frac{299}{18} - 2\zeta_2\Big)L^4 + \Big(-\frac{2585}{27} + 26\zeta_3 - \frac{1}{9}\zeta_2\Big)L^3$$
$$+\Big(\frac{206317}{648} - \frac{1807}{9}\zeta_3 + \frac{502}{9}\zeta_2 - \frac{34}{5}\zeta_2^2\Big)L^2$$
$$+\Big(-\frac{13805}{24} + 120\zeta_5 + \frac{2441}{3}\zeta_3 - \frac{11260}{27}\zeta_2 - 10\zeta_2\zeta_3 + \frac{162}{5}\zeta_2^2\Big)L$$
$$+\frac{415025}{648} - \frac{2756}{9}\zeta_5 - \frac{18770}{27}\zeta_3 + \frac{296}{3}\zeta_3^2 + \frac{538835}{648}\zeta_2 - \frac{3751}{9}\zeta_2\zeta_3$$

$$
\begin{aligned}
&\quad -\frac{4943}{270}\zeta_2^2 - \frac{12676}{315}\zeta_2^3\Big) \\
&+C_F^2 N_F\Big(\frac{2}{9}L^5 - \frac{25}{9}L^4 + \Big(\frac{410}{27} + \frac{10}{9}\zeta_2\Big)L^3 + \Big(-\frac{12815}{324} + \frac{70}{9}\zeta_3 - \frac{112}{9}\zeta_2\Big)L^2 \\
&\quad +\Big(\frac{3121}{108} - \frac{610}{9}\zeta_3 + \frac{1618}{27}\zeta_2 + \frac{28}{5}\zeta_2^2\Big)L \\
&\quad +\frac{41077}{972} - \frac{416}{9}\zeta_5 + \frac{13184}{81}\zeta_3 - \frac{31729}{324}\zeta_2 - \frac{38}{9}\zeta_2\zeta_3 - \frac{331}{27}\zeta_2^2\Big) \\
&+C_F C_A^2\Big(-\frac{121}{54}L^4 + \Big(\frac{2869}{81} - \frac{44}{9}\zeta_2\Big)L^3 + \Big(-\frac{18682}{81} + 88\zeta_3 + \frac{26}{9}\zeta_2 - \frac{44}{5}\zeta_2^2\Big)L^2 \\
&\quad +\Big(\frac{1045955}{1458} + 136\zeta_5 - \frac{17464}{27}\zeta_3 + \frac{17366}{81}\zeta_2 + \frac{88}{3}\zeta_2\zeta_3 - \frac{94}{3}\zeta_2^2\Big)L \\
&\quad -\frac{51082685}{52488} - \frac{434}{9}\zeta_5 + \frac{505087}{486}\zeta_3 - \frac{1136}{9}\zeta_3^2 - \frac{412315}{729}\zeta_2 + \frac{416}{3}\zeta_2\zeta_3 \\
&\quad +\frac{22157}{270}\zeta_2^2 - \frac{6152}{189}\zeta_2^3\Big) \\
&+C_F C_A N_F\Big(\frac{22}{27}L^4 + \Big(-\frac{974}{81} + \frac{8}{9}\zeta_2\Big)L^3 + \Big(\frac{5876}{81} - 8\zeta_3 + \frac{16}{3}\zeta_2\Big)L^2 \\
&\quad +\Big(-\frac{154919}{729} + \frac{724}{9}\zeta_3 - \frac{5864}{81}\zeta_2 + \frac{44}{15}\zeta_2^2\Big)L \\
&\quad +\frac{1700171}{6561} - \frac{4}{3}\zeta_5 - \frac{4288}{27}\zeta_3 + \frac{115555}{729}\zeta_2 + \frac{4}{3}\zeta_2\zeta_3 + \frac{2}{27}\zeta_2^2\Big) \\
&+C_F N_F^2\Big(-\frac{2}{27}L^4 + \frac{76}{81}L^3 + \Big(-\frac{406}{81} - \frac{8}{9}\zeta_2\Big)L^2 + \Big(\frac{9838}{729} + \frac{16}{27}\zeta_3 + \frac{152}{27}\zeta_2\Big)L \\
&\quad -\frac{190931}{13122} - \frac{416}{243}\zeta_3 - \frac{824}{81}\zeta_2 - \frac{188}{135}\zeta_2^2\Big) \\
&+C_F N_{F,V}\left(\frac{N^2-4}{N}\right)\left(4 - \frac{80}{3}\zeta_5 + \frac{14}{3}\zeta_3 + 10\zeta_2 - \frac{2}{5}\zeta_2^2\right)
\end{aligned}
\tag{3.69}
$$

and,

$$
\begin{aligned}
C_3^g \;=\; & C_A^3\Big(-\frac{1}{6}L^6 - \frac{11}{9}L^5 + \Big(\frac{281}{54} - \frac{3}{2}\zeta_2\Big)L^4 + \Big(\frac{11}{3}\zeta_2 + \frac{1540}{81} + 2\zeta_3\Big)L^3 \\
&\quad +\Big(\frac{143}{9}\zeta_3 - \frac{6740}{81} + \frac{685}{18}\zeta_2 - \frac{73}{10}\zeta_2^2\Big)L^2 \\
&\quad +\Big(\frac{2048}{27}\zeta_3 + 16\zeta_5 + \frac{34}{3}\zeta_2\zeta_3 - \frac{13420}{81}\zeta_2 + \frac{176}{5}\zeta_2^2 - \frac{373975}{1458}\Big)L \\
&\quad -\frac{1939}{270}\zeta_2^2 + \frac{2222}{9}\zeta_5 + \frac{105617}{729}\zeta_2 - \frac{24389}{1890}\zeta_2^3 - \frac{152716}{243}\zeta_3 - \frac{605}{9}\zeta_2\zeta_3 \\
&\quad +\frac{29639273}{26244} - \frac{104}{9}\zeta_3^2\Big)
\end{aligned}
$$

$$
\begin{aligned}
&+C_A^2 N_F \left(\frac{2}{9}L^5 - \frac{8}{27}L^4 + \left(-\frac{734}{81} - \frac{2}{3}\zeta_2\right)L^3 + \left(\frac{377}{27} + \frac{118}{9}\zeta_3 - \frac{103}{9}\zeta_2\right)L^2\right.\\
&\qquad + \left(\frac{133036}{729} + \frac{28}{9}\zeta_3 + \frac{3820}{81}\zeta_2 - \frac{48}{5}\zeta_2^2\right)L\\
&\qquad \left. - \frac{3765007}{6561} + \frac{428}{9}\zeta_5 - \frac{460}{81}\zeta_3 - \frac{14189}{729}\zeta_2 - \frac{82}{9}\zeta_2\zeta_3 + \frac{73}{45}\zeta_2^2\right)\\
&+C_A N_F^2 \left(-\frac{2}{27}L^4 + \frac{40}{81}L^3 + \left(\frac{116}{81} + \frac{8}{9}\zeta_2\right)L^2 + \left(-\frac{14057}{729} - \frac{128}{27}\zeta_3 - \frac{80}{27}\zeta_2\right)L\right.\\
&\qquad \left. + \frac{611401}{13122} + \frac{4576}{243}\zeta_3 + \frac{4}{9}\zeta_2 + \frac{4}{27}\zeta_2^2\right)\\
&+C_F N_F^2 \left(\frac{4}{3}L^2 + \left(-\frac{52}{3} + \frac{32}{3}\zeta_3\right)L + \frac{4481}{81} - \frac{112}{3}\zeta_3 - \frac{20}{9}\zeta_2 - \frac{16}{45}\zeta_2^2\right)\\
&+C_F C_A N_F \left(-\frac{8}{3}L^3 + \left(13 - 16\zeta_3\right)L^2 + \left(\frac{3833}{54} - \frac{376}{9}\zeta_3 + 6\zeta_2 + \frac{16}{5}\zeta_2^2\right)L\right.\\
&\qquad \left. - \frac{341219}{972} + \frac{608}{9}\zeta_5 + \frac{14564}{81}\zeta_3 - \frac{68}{9}\zeta_2 + \frac{64}{3}\zeta_2\zeta_3 - \frac{64}{45}\zeta_2^2\right)\\
&+C_F^2 N_F \left(-2L + \frac{304}{9} - 160\zeta_5 + \frac{296}{3}\zeta_3\right). \qquad (3.70)
\end{aligned}
$$

These matching coefficients allow to perform the three-loop matching of the SCET-based resummation onto the full QCD calculation.

3.8 Conclusions

In this chapter, we described the calculation of the three-loop quark and gluon form factors in detail. Our results confirm earlier expressions obtained by Baikov et al. [42], which we extended by subleading terms in the fermionic corrections.

The form factors are the simplest QCD objects with non-trivial infrared structure. Recent findings on the relation between massless on-shell QCD amplitudes and operators in soft-collinear effective theory [27], combined with constraints from factorization, has led to the conjecture [21] that their pole terms at a given loop level contain all information needed to predict the pole structure of massless on-shell multi-leg amplitudes at the same loop order. In particular, the cusp anomalous dimension can be extracted from the double pole, and the collinear anomalous dimension from the single pole. At a given loop order, finite and subleading terms from lower loop orders are also required. In this respect, the finite terms presented here will be instrumental for the extraction of the four-loop cusp anomalous dimension, while the subleading terms contribute to the four-loop quark and gluon collinear anomalous dimension.

The three-loop form factors are key ingredients for the fourth order ($\mathrm{N^3LO}$) corrections to the inclusive Drell-Yan and Higgs boson production cross sections. The

calculation of these, at least in an improvement to the soft approximation [8, 12], could be envisaged in future work. In view of this application, we derived the hard matching coefficients of the SCET operators to this order. Inclusion of these corrections will lead to a further stabilization of the perturbative prediction under scale variations, and are thus important for precision physics at hadron colliders.

AuxTopo 1	AuxTopo 2	AuxTopo3
k_1^2	k_1^2	k_1^2
k_2^2	k_2^2	k_2^2
k_3^2	k_3^2	k_3^2
$(k_1-k_2)^2$	$(k_1-k_2)^2$	$(k_1-k_2)^2$
$(k_1-k_3)^2$	$(k_1-k_3)^2$	$(k_1-k_3)^2$
$(k_2-k_3)^2$	$(k_2-k_3)^2$	$(k_1-k_2-k_3)^2$
$(k_1-p_1)^2$	$(k_1-k_3-p_2)^2$	$(k_1-p_1)^2$
$(k_1-p_1-p_2)^2$	$(k_1-p_1-p_2)^2$	$(k_1-p_1-p_2)^2$
$(k_2-p_1)^2$	$(k_2-p_1)^2$	$(k_2-p_1)^2$
$(k_2-p_1-p_2)^2$	$(k_1-k_2-p_2)^2$	$(k_2-p_1-p_2)^2$
$(k_3-p_1)^2$	$(k_3-p_1)^2$	$(k_3-p_1)^2$
$(k_3-p_1-p_2)^2$	$(k_3-p_1-p_2)^2$	$(k_3-p_1-p_2)^2$

Table 3.1: Propagators in the three different auxiliary topologies used to represent all three-loop form factor integrals.

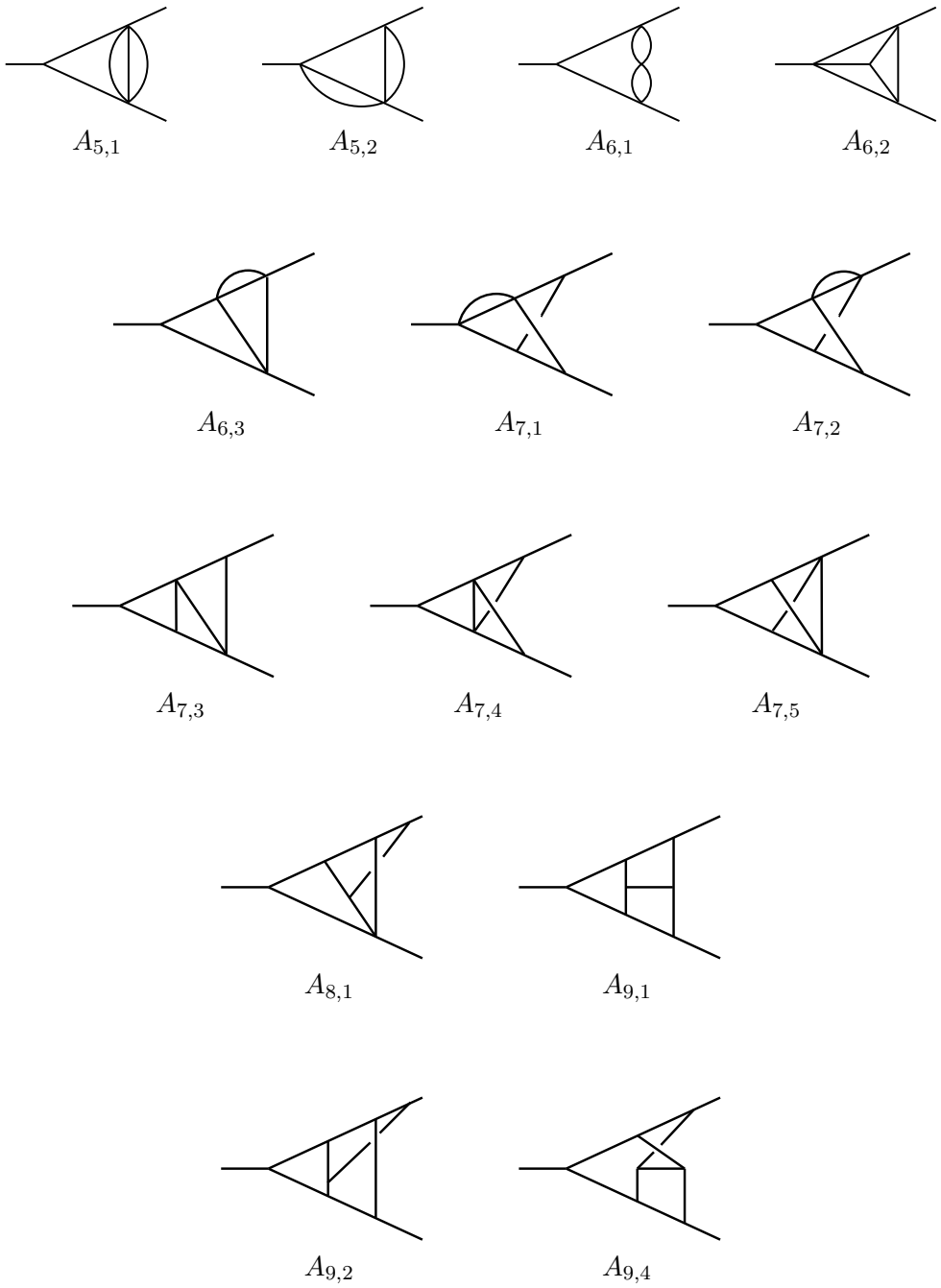

Figure 3.3: Three-point integrals listed in Refs. [38–40].

Bibliography

[1] T. Gehrmann, E. W. N. Glover, T. Huber, N. Ikizlerli and C. Studerus, arXiv:1004.3653 [hep-ph].

[2] G. Altarelli, R. K. Ellis and G. Martinelli, Nucl. Phys. B **157** (1979) 461.

[3] R. Hamberg, W. L. van Neerven and T. Matsuura, Nucl. Phys. B **359** (1991) 343; B **644** (2002) 403(E).

[4] S. Dawson, Nucl. Phys. B **359** (1991) 283.

[5] D. Graudenz, M. Spira and P.M. Zerwas, Phys. Rev. Lett. **70** (1993) 1372;
M. Spira, A. Djouadi, D. Graudenz and P. M. Zerwas, Nucl. Phys. B **453** (1995) 17 [hep-ph/9504378];
A. Djouadi, M. Spira and P.M. Zerwas, Z. Phys. C **70** (1996) 427 [hep-ph/9511344];
M. Spira, Fortsch. Phys. **46** (1998) 203 [hep-ph/9705337].

[6] S. Catani, D. de Florian and M. Grazzini, JHEP **0105** (2001) 025 [hep-ph/0102227];
R.V. Harlander and W. B. Kilgore, Phys. Rev. Lett. **88** (2002) 201801 [hep-ph/0201206];
C. Anastasiou and K. Melnikov, Nucl. Phys. B **646** (2002) 220 [hep-ph/0207004];
V. Ravindran, J. Smith and W. L. van Neerven, Nucl. Phys. B **665** (2003) 325 [hep-ph/0302135], **704** (2005) 332 [hep-ph/0408315].

[7] L. Magnea and G. Sterman, Phys. Rev. D **42** (1990) 4222.

[8] S. Moch and A. Vogt, Phys. Lett. B **631** (2005) 48 [hep-ph/0508265];
E. Laenen and L. Magnea, Phys. Lett. B **632** (2006) 270 [hep-ph/0508284];
V. Ravindran, Nucl. Phys. B **746** (2006) 58 [hep-ph/0512249].

[9] G. P. Korchemsky, Phys. Lett. B **217** (1989) 330.

[10] C.W. Bauer, S. Fleming and M.E. Luke, Phys. Rev. D **63** (2000) 014006 [hep-ph/0005275];
C.W. Bauer, S. Fleming, D. Pirjol and I.W. Stewart, Phys. Rev. D **63** (2001) 114020 [hep-ph/0011336];
C.W. Bauer and I.W. Stewart, Phys. Lett. B **516** (2001) 134 [hep-ph/0107001];
C.W. Bauer, D. Pirjol and I.W. Stewart, Phys. Rev. D **65** (2002) 054022 [hep-ph/0109045];
M. Beneke, A. P. Chapovsky, M. Diehl and T. Feldmann, Nucl. Phys. B **643** (2002) 431 [hep-ph/0206152];
M. Beneke and T. Feldmann, Phys. Lett. B **553** (2003) 267 [hep-ph/0211358].

[11] A. Idilbi and X. Ji, Phys. Rev. D **72** (2005) 054016 [hep-ph/0501006].

[12] A. Idilbi, X. Ji and F. Yuan, Nucl. Phys. B **753** (2006) 42 [hep-ph/0605068].

[13] V. Ahrens, T. Becher, M. Neubert and L. L. Yang, Eur. Phys. J. C **62** (2009) 333 [arXiv:0809.4283].

[14] G. P. Korchemsky and A. V. Radyushkin, Phys. Lett. B **171** (1986) 459; Nucl. Phys. B **283** (1987) 342.

[15] S. Moch, J. A. M. Vermaseren and A. Vogt, JHEP **0508** (2005) 049 [hep-ph/0507039].

[16] S. Moch, J. A. M. Vermaseren and A. Vogt, Phys. Lett. B **625**, 245 (2005) [hep-ph/0508055].

[17] G. Kramer and B. Lampe, Z. Phys. C **34** (1987) 497; **42** (1989) 504(E);
T. Matsuura and W.L. van Neerven, Z. Phys. C **38** (1988) 623;
T. Matsuura, S.C. van der Maarck and W.L. van Neerven, Nucl. Phys. B **319** (1989) 570.

[18] R.V. Harlander, Phys. Lett. B **492** (2000) 74 [hep-ph/0007289].

[19] T. Gehrmann, T. Huber and D. Maître, Phys. Lett. B **622** (2005) 295 [hep-ph/0507061].

[20] T. Becher, M. Neubert and B. D. Pecjak, JHEP **0701** (2007) 076 [hep-ph/0607228].

[21] T. Becher and M. Neubert, JHEP **0906** (2009) 081 [arXiv:0903.1126].

[22] G. P. Korchemsky, Mod. Phys. Lett. A **4** (1989) 1257.

[23] S. Moch, J. A. M. Vermaseren and A. Vogt, Nucl. Phys. B **688** (2004) 101 [hep-ph/0403192].

[24] A. V. Kotikov, L. N. Lipatov, A. I. Onishchenko and V. N. Velizhanin, Phys. Lett. B **595** (2004) 521 [Erratum-ibid. B **632** (2006) 754] [hep-th/0404092].

[25] L. F. Alday and J. M. Maldacena, JHEP **0711** (2007) 019 [arXiv:0708.0672].

[26] J. Frenkel and J. C. Taylor, Nucl. Phys. B **246** (1984) 231.

[27] T. Becher and M. Neubert, Phys. Rev. Lett. **102** (2009) 162001 [arXiv:0901.0722].

[28] E. Gardi and L. Magnea, JHEP **0903** (2009) 079 [arXiv:0901.1091].

[29] S. Catani, Phys. Lett. B **427** (1998) 161 [hep-ph/9802439].

[30] G. Sterman and M. E. Tejeda-Yeomans, Phys. Lett. B **552** (2003) 48 [hep-ph/0210130].

[31] S. M. Aybat, L. J. Dixon and G. Sterman, Phys. Rev. D **74** (2006) 074004 [hep-ph/0607309].

[32] S. M. Aybat, L. J. Dixon and G. Sterman, Phys. Rev. Lett. **97** (2006) 072001 [hep-ph/0606254].

[33] L. J. Dixon, E. Gardi and L. Magnea, JHEP **1002** (2010) 081 [arXiv:0910.3653].

[34] S. Laporta, Int. J. Mod. Phys. A **15** (2000) 5087 [arXiv:hep-ph/0102033].

[35] C. Anastasiou and A. Lazopoulos, JHEP **0407** (2004) 046 [hep-ph/0404258].

[36] A. V. Smirnov, JHEP **0810** (2008) 107 [arXiv:0807.3243].

[37] C. Studerus, Comput. Phys. Commun. **181** (2010) 1293 [arXiv:0912.2546 [physics.comp-ph]].

[38] T. Gehrmann, G. Heinrich, T. Huber and C. Studerus, Phys. Lett. B **640** (2006) 252 [hep-ph/0607185].

[39] G. Heinrich, T. Huber and D. Maître, Phys. Lett. B **662** (2008) 344 [arXiv:0711.3590].

[40] G. Heinrich, T. Huber, D. A. Kosower and V. A. Smirnov, Phys. Lett. B **678** (2009) 359 [arXiv:0902.3512].

[41] R.N. Lee, A.V. Smirnov and V.A. Smirnov, JHEP **1004** (2010) 020 [arXiv:1001.2887].

[42] P. A. Baikov, K. G. Chetyrkin, A. V. Smirnov, V. A. Smirnov and M. Steinhauser, Phys. Rev. Lett. **102** (2009) 212002 [arXiv:0902.3519].

[43] F. Wilczek, Phys. Rev. Lett. **39** (1977) 1304;
M.A. Shifman, A.I. Vainshtein and V.I. Zakharov, Phys. Lett. B **78** (1978) 443;
J.R. Ellis, M.K. Gaillard, D.V. Nanopoulos and C.T. Sachrajda, Phys. Lett. B **83** (1979) 339;
T. Inami, T. Kubota and Y. Okada, Z. Phys. C **18** (1983) 69.

[44] K.G. Chetyrkin, B.A. Kniehl and M. Steinhauser, Phys. Rev. Lett. **79** (1997) 353 [hep-ph/9705240].

[45] B.A. Kniehl and M. Spira, Z. Phys. C **69** (1995) 77 [hep-ph/9505225];
K.G. Chetyrkin, B.A. Kniehl and M. Steinhauser, Nucl. Phys. B **510** (1998) 61 [hep-ph/9708255].

[46] W. A. Bardeen, A. J. Buras, D. W. Duke and T. Muta, Phys. Rev. D **18** (1978) 3998.

[47] D. J. Gross and F. Wilczek, Phys. Rev. Lett. **30** (1973) 1343;
H. D. Politzer, Phys. Rev. Lett. **30** (1973) 1346.

[48] W. E. Caswell, Phys. Rev. Lett. **33** (1974) 244;
D. R. T. Jones, Nucl. Phys. B **75** (1974) 531;
E. Egorian and O. V. Tarasov, Teor. Mat. Fiz. **41** (1979) 26 [Theor. Math. Phys. **41** (1979) 863].

[49] O. V. Tarasov, A. A. Vladimirov and A. Y. Zharkov, Phys. Lett. B **93** (1980) 429;
S. A. Larin and J. A. M. Vermaseren, Phys. Lett. B **303** (1993) 334 [hep-ph/9302208].

[50] P. Nogueira, J. Comput. Phys. **105** (1993) 279.

[51] K.G. Chetyrkin and F.V. Tkachov, Nucl. Phys. **B192** (1981) 159.

[52] T. Gehrmann and E. Remiddi, Nucl. Phys. **B580** (2000) 485 [hep-ph/9912329].

[53] T. Huber and D. Maître, Comput. Phys. Commun. **175** (2006) 122 [hep-ph/0507094].

[54] S.G. Gorishnii, S.A. Larin, L.R. Surguladze and F.V. Tkachov, Comput. Phys. Comm. **55** (1989) 381;
S.A. Larin, F.V. Tkachov and J.A.M. Vermaseren, NIKHEF-H-91-18.

[55] S. Bekavac, Comput. Phys. Commun. **175** (2006) 180 [hep-ph/0505174].

[56] M. Czakon, Comput. Phys. Commun. **175** (2006) 559 [hep-ph/0511200].

[57] H.R.P. Ferguson, D.H. Bailey and S. Arno, *Analysis of PSLQ, An Integer Relation Finding Algorithm*, *Math. Comput.* **68** (1999) 351

[58] J. A. M. Vermaseren, A. Vogt and S. Moch, Nucl. Phys. B **724** (2005) 3 [hep-ph/0504242].

[59] G. Sterman, Nucl. Phys. B **281** (1987) 310;
S. Catani and L. Trentadue, Nucl. Phys. B **327** (1989) 323; Nucl. Phys. B **353** (1991) 183;
S. Catani, M. L. Mangano, P. Nason and L. Trentadue, Nucl. Phys. B **478** (1996) 273 [hep-ph/9604351];
H. Contopanagos, E. Laenen and G. Sterman, Nucl. Phys. B **484** (1997) 303 [hep-ph/9604313].

[60] C.W. Bauer, S. Fleming, D. Pirjol, I.Z. Rothstein and I.W. Stewart, Phys. Rev. D **66** (2002) 014017 [hep-ph/0202088].

4

Reduze

4.1 Introduction

The calculation of loop amplitudes in perturbative quantum field theory is usually done by generating the Feynman diagrams for the desired physical process and interfering the corresponding analytical expressions, working out the Dirac and/or color structure. The amplitude is then a sum of many dimensionally regularized integrals [1] which have to be computed. These integrals are not independent of each other but related by the Integration by Parts (IBP) Identities [2, 3] and the Lorentz Invariance (LI) Identities [4]. These identities form a homogeneous system of linear equations with the integrals as unknowns and algebraic prefactors which are rational polynomials in the kinematic invariants and the dimension. Using the IBP and LI identities one can express most of the integrals in terms of a small set of integrals, called master integrals.

These identities also exist for phase-space integrals after replacing the delta functions by a difference of propagators with an opposite sign prescription of the imaginary part [6].

The procedure of solving this system of equations is called a reduction. Since one often has to solve systems with thousands of equations, computers have to be used and because the prefactors in front of each integral are rational polynomials, computer algebra systems become indispensable.

`Reduze` is a computer program written in C++ which generates the IBP and optionally the LI identities and then reduces the integrals to master integrals. `Reduze` uses the `GiNaC` library [8] to perform the simplification of the prefactors.

The reduction algorithm is a Laporta algorithm [5] which is essentially the Gauss algorithm with additional rules to determine the next equation which should be solved and inserted into the others. To get the reduction of a certain Feynman diagram one first defines a set of integrals by restricting the exponents of the propagators. `Reduze` then generates the identities from this set and starts solving the system of equations.

For a reduction of several diagrams `Reduze` can treat different diagrams (with the same number of propagators) simultaneously. One defines how many cores or processors are available and then `Reduze` will automatically launch some reductions simultaneously. The more cores there are available the more diagrams one can reduce in parallel.

Other published reduction programs are AIR [11] and FIRE [12]. AIR is a `Maple` package that implements the Laporta algorithm. FIRE is a `Mathematica` package that implements the Laporta algorithm and also a method that uses techniques from Gröbner basis calculations. Then there are also several other private codes.

The advantage of `Reduze` is that it is completely open source, has a low memory footprint and can do reductions in parallel.

4.1.1 License

4.2 Theoretical background

4.2.1 Propagators, Sectors and Integrals

A propagator P with momentum flow q and mass m is the expression $q^2 - m^2$ where q^2 denotes the Minkowski scalar product with the metric in the convention $g = \text{diag}\,(1, -1, -1, -1)$. The momentum q is a linear combination of loop momenta k_i and external momenta p_i.

An auxiliary topology is an ordered set of propagators $A_n = \{P_1, \ldots, P_n\}$ such that all scalar products $k_i\,k_j$ and $k_i\,p_j$ containing at least one loop momentum k_i can be expressed by a linear combination of propagators from A_n. The auxiliary topology is called an l-loop auxiliary topology if there are l different loop momenta appearing in the momenta q of the propagators. Denoting the number of independent external momenta by m, the auxiliary topology must contain exactly $l\,(l+1)/2 + l\,m$ propagators where the first term counts the scalar products between loop momenta only and the second term the products involving both loop and external momenta.

Every subset of t propagators of a given auxiliary topology A_n defines a sector T_t with an unique identification number ID. Physically relevant sectors which correspond to diagrams are also called topologies. Assuming the sector has the propagators $P_{j_1}, \ldots, P_{j_t}$ with $\{j_1, \ldots, j_t\} \subset \{1, \ldots, n\}$, then its identification number is defined as

$$ID = \sum_{k=1}^{t} 2^{j_k - 1} \,. \tag{4.1}$$

There are in general $\binom{n}{t}$ different t-propagator sectors T_t and $\sum_{t=1}^{n} \binom{n}{t} = 2^n - 1$ sectors that one can build out of an auxiliary topology A_n. Their identification numbers fulfill $1 \leq ID \leq 2^n - 1$.

A sub-sector T_{t-1} of a sector T_t is a sector where one propagator is removed. There are in general t different sub-sectors for a sector T_t. The sub-sector tree of a sector T_t is the set of all sub-sectors of T_t and recursively all sub-sectors of all these sub-sectors. All sectors of an auxiliary topology A_n, which is the main sector, are in the sub-sector tree of A_n.

To every t-propagator sector T_t with propagators P_{j_1}, ..., P_{j_t} belongs a infinite set of d-dimensionally regularized l-loop integrals [1] which all share the same propagators in the denominator of the integrand. They have the generic form

$$\int \mathrm{d}^d k_1 \ldots \int \mathrm{d}^d k_l \, \frac{P_{j_{t+1}}^{s_1} \ldots P_{j_n}^{s_{n-t}}}{P_{j_1}^{r_1} \ldots P_{j_t}^{r_t}} \tag{4.2}$$

with integer exponents $r_i \geq 1$ and $s_i \geq 0$. In `Reduze` such an integral is represented by a vector $v = \{v_1, \ldots, v_n\}$ containing the exponents of the propagators or, more precisely,

$$\mathrm{INT}[t, r, s, ID, \{v_1, \ldots, v_n\}] \tag{4.3}$$

where $r = \sum_{i=1}^{t} r_i \geq t$ is the sum of the propagators in the denominator and $s = \sum_{i=1}^{n-t} s_i \geq 0$ is the sum of the propagators in the numerator. The value v_i is the exponent of propagator $P_i \in A_n$. It is positive if P_i is in the denominator, negative if P_i comes with a (positive) exponent in the numerator and zero if the propagator is not present. The numbers t, r, s as well as the identification number ID of the sector, to which the integral belongs, can be calculated from the vector v.

Consider an n-propagator auxiliary topology A_n with a t-propagator sector T_t. The number of integrals that one can build for certain values of r and s is given by

$$\mathcal{N}(n, t, r, s) = \binom{r-1}{t-1} \binom{s+n-t-1}{n-t-1} \,. \tag{4.4}$$

The two binomial factors count all possible ways to arrange the exponents of the propagators in the denominator and numerator, respectively.

4.2.2 Integration By Parts (IBP) Identities

In dimensional regularization [1] the integral over a total derivative is zero. Let $\mathbf{I}'$ be the integrand of an integral of the form (4.2). Then, working out the differentiation in

$$\int \mathrm{d}^d k_i \, \frac{\partial}{\partial k_i^\mu} \left[q^\mu \, \mathbf{I}'(p_1, \ldots, p_m, k_1, \ldots, k_l) \right] = 0 \tag{4.5}$$

leads to the integration by parts (IBP) identities [2, 3]. The momentum q is an arbitrary loop or external momentum. The index μ is summed over but the index i is not. If there are l loop momenta and m independent external momenta one can therefore build $l\,(l+m)$ equations from one integral (the seed integral).

4.2.3 Lorentz Invariance (LI) Identities

One can also use the Lorentz Invariance of the integrals [4]. Taking an integral $\mathbf{I}(p_1, \ldots, p_m)$ the following equation holds

$$\sum_{n=1}^{m} \left(p_n^\nu \frac{\partial}{\partial p_{n\mu}} - p_n^\mu \frac{\partial}{\partial p_{n\nu}} \right) \mathbf{I}(p_1, \ldots, p_m) = 0 \,. \tag{4.6}$$

The derivatives can be shifted directly to the integrand of the integral $\mathbf{I}$. This equation can be contracted with all possible antisymmetric combinations of the external momenta, e.g. $p_{1\mu} p_{2\nu} - p_{1\nu} p_{2\mu}$, which leads to $m\,(m-1)/2$ equations where m denotes the number of independent external momenta. As it was shown in [7] the LIs do not give new linear independent equations in addition to the IBPs. However, they can accelerate the convergence in a reduction, since in general an LI identity generated from one seed integral cannot be reproduced with the IBP identities generated from the same seed integral alone. `Reduze` offers the possibility to use the LIs.

4.2.4 Symmetry Relations

Often there are relations between integrals coming from symmetries which can lead to an identification of integrals and even whole sectors.

All integrals are invariant under permutations of the loop momenta and translations of a loop momentum with other momenta. Such a transformation can be used to transform an integral I to an equivalent integral I' and leads to the identity $I = I'$. However, since the integrals are expressed with propagators of an auxiliary topology, the transformations that actually can be used must leave the set of propagators of the auxiliary topology invariant. This means that such an symmetry transformation must lead to a permutation of the propagators and then two equivalent integrals differ only in a permutation of the propagator exponents.

A permutation of the propagator exponents of an integral can alter the sector (sector identification number) it belongs to. This is then valid for all integrals of this sector and one can completely get rid of one of the sectors. These sectors correspond to the same topology.

Sometimes the integrals of an auxiliary topology are invariant under the permutation of external momenta but this permutation leads to propagators which are not contained in the auxiliary topology. One then has to find a transformation on the propagators which transforms the propagators back into the auxiliary topology.

In `Reduze` one can explicitly declare some transformation rules which leave the integrals invariant. Since only transformations that lead to a permutation of propagators can be used, they must be given as permutations. According to these declarations `Reduze` automatically identifies equivalent integrals in the system of equations and also only uses one of them to generate the equations.

4.2.5 Zero Sectors

It is possible that a whole sector is zero which means that all integrals belonging to this sector are zero. In `Reduze` a sector is set to zero if the solutions of all IBP identities generated from the integral I of this sector with $r = t$ and $s = 0$ (no additional propagators in the numerator and denominator) contain the equation $I = 0$.

4.2.6 Reduction

To reduce a sector up to $r = r_{max}$ and $s = s_{max}$ means solving the homogeneous system of linear equations which have been built with the IBP and/or LI identities out of the integrals of this sector that have $r \in [r_{min}, r_{max}]$ and $s \in [s_{min}, s_{max}]$. It is not possible to solve the system completely since the rank of every finite set of equations is smaller than the number of unknown integrals it contains. However, the aim of the reduction is to express most of the integrals by a linear combination of only a few (less complicated) integrals, the so-called master integrals.

In a typical reduction of a t-propagator sector one takes the smallest possible values $r_{min} = t$ and $s_{min} = 0$. If one then generates the equations from all integrals with $r \in [r_{min}, r_{max}]$ and $s \in [s_{min}, s_{max}]$ and reduces this system of equations, one usually gets the solutions for all the integrals that have been chosen to build the system, meaning that all these integrals are expressed as a linear combination of some master integrals.

The equations built to reduce a sector can contain not only integrals of the sector itself but also integrals from sub-sectors. If one tries to reduce the system of equations, the results then still depend on a lot of unsolved integrals of the sub-sectors which also have to be reduced by solving a system of equations built with integrals from the

sub-sector considered. Sub-sectors appear as long as the number of propagators does not go below a minimal value.

4.3 Reduction Algorithm

For a reduction of a certain sector including its sub-sectors `Reduze` first determines the whole sub-sector tree, then reduces the sub-sectors with the smallest number of propagators, inserts the results in the equations of the sectors that depend on these sub-sectors, reduces these sectors, continuing until the desired sector with the largest number of propagators can be reduced. For a reduction of a single sector `Reduze` first will generate the equations and insert the results of the sub-sectors into them if they are available in the default `results`-directory.

`Reduze` is not able to find a solution for a single integral of a sector, instead it employs all integrals in a user-defined range of r and s for building the equations and then reduces the whole system.

Since the reduction of a single sector often involves a huge amount of equations, the system must be divided into smaller parts. Dividing the equations in subsets, each generated from a set of integrals for a certain value for r and s, can still lead to systems which are too big. In `Reduze` the system of equations is divided into smaller sets with a default number of equations. The number of equations per set can be adjusted by the user. To decide which equation goes in which set, the equations are first sorted in descending order with respect to the most complicated integral each equation contains and then simply divided into smaller sets and stored in temporary files.

The reduction of a sector is now done by first loading the temporary file containing the simplest equations. Then this system is reduced according to the algorithm below and the results are inserted in all the other files. Then the equations from the second file will be reduced and the results again inserted in all other files. This procedure is done for all files. Finally, the results from the temporary files are collected and saved in a single result file.

To give a precise meaning for the instance that an integral is simpler or less complicated than another integral a lexicographic ordering can be defined [5]: For an integral

$$I = \mathrm{INT}[t, r, s, ID, \{v_1, \ldots, v_n\}] \tag{4.7}$$

take the vector $\tilde{v}_I = \{t, r, s, ID, v_1, \ldots, v_n\}$ with length $n + 4$. Then for two integrals I and J the comparison $I < J$ is true if and only if there exists an $m \in \{1, \ldots, n + 4\}$ such that $\tilde{v}_I[m] < \tilde{v}_J[m]$ and $\tilde{v}_I[k] = \tilde{v}_J[k]$ for all $k \in \{1, \ldots, m - 1\}$.

This operator can be extended to equations: Equation e_1 is less complicated than equation e_2, $e_1 < e_2$, if the most complicated integral of e_1 is less complicated than the most complicated integral of e_2. For a set L of equations that contains the integral I in

at least one equation the set $[I]_L$ is defined as the subset of L such that all equations have I as the most complicated integral. In addition, the set $(I)_L$ is defined as the subset of equations of $[I]_L$ with the smallest number of integrals. This set is the subset of L which contains the shortest equations and all equations contain the most complicated integral I as their own most complicated integral. For an equation e the expression $*e$ denotes the same equation but solved for its most complicated integral.

The first part of the reduction algorithm (see is to bring the system in a triangular form and the second part of the algorithm is the back substitution.

Algorithm 1 Reduction

$L = \{e_1, \ldots, e_n\}$ // list of equations.
$I = \{I_1, \ldots, I_m\}$ // all integrals in L, sorted in descending order.
$S = \{\}$ // empty list.
// Triangularization:
for $i = 1$ to m **do**
  choose $e \in (I_i)_L$
  $L = L \setminus e$
  replace matching integrals in L by the r.h.s of $*e$
  $S = \{*e, S\}$
end for
// $S = \{S(1), \ldots, S(l)\}$ contains now l equations sorted in ascending order.
// Back substitution:
for $i = 1$ to l **do**
  $e = S(i)$
  for $j = i + 1$ to l **do**
    replace matching integrals in $S(j)$ by r.h.s of $*e$
  end for
end for

4.4 Usage

4.4.1 Finding an Auxiliary Topology

Before a reduction can be launched the user has to find an appropriate auxiliary topology which contains the topologies from given Feynman diagrams as sub-sectors. The auxiliary topology should cover as many diagrams as possible and also allows for as many as possible symmetry relations in order to minimize the number of sectors which finally have to be reduced (see section 4.2.4). The diagrams under consideration need a certain maximal amount of propagators. By building these propagators one has some freedom how to choose the momentum flow and, if the number of propagators of the diagram is smaller than the number of propagators needed for the auxiliary topology,

one must introduce additional auxiliary propagators. This freedom of choosing how the propagators exactly look like and which additional propagators are introduced can be used to set up an auxiliary topology that has as many as possible symmetries.

4.4.2 Reduction

Since `Reduze` reads and writes a lot to files, it should be run on the local hard disc. For the following it is assumed that the current working directory is a local directory. A reduction is now done in three steps: set up an auxiliary topology, prepare the reduction and run the reduction.

4.4.2.1 Set up an Auxiliary Topology

First one has to define an auxiliary topology, where momenta, propagators, etc. are declared. For this one creates a file with suffix `.in`, e.g. `topoA.in`, with all the inputs needed. The syntax of this input file is described in section (4.5.1). There are also some input files in the `example` directory of the package. Then one sets up the auxiliary topology (topoA) with the command

```
reduze --setup topoA.in
```

This creates the directory `topoA` and initializes the auxiliary topology. It derives the rules to express scalar products by propagators, finds the sectors that are equivalent due to symmetry relations and finds most of the zero sectors by doing a small reduction ($r = t$, $s = 0$) of all sectors which have vanishing sub-sectors only.

The new created directory `topoA` contains the directories `reduction` and `results` and a log file `setup.log`. The log file contains some information about the auxiliary topology, e.g at the end of this file there is a list of all sectors that have not been found to be zero and can be reduced. The `reduction` directory will later be used for the reduction. It contains the directory `include` in which the information about the auxiliary topology is stored. One should not edit it directly. If the setup file `topoA.in` was modified, the setup has to be done again. The `results` directory is used for the results after a reduction has completed.

4.4.2.2 Prepare a Reduction

To prepare a reduction one needs a second input file, e.g. `prepareA.in`, in that one writes which sectors (ID numbers) should be reduced and which class of integrals ($R2 = r_{max}, S2 = s_{max}$) one wants to use for building the system of equations. Also the maximum number of processes that will run in parallel can be defined here. The allowed commands of this file are described in section (4.5.2). There are also some example files in the `example` directory. Typing

```
reduze --prepare prepareA.in
       --auxtop /path/to/topoA
```

should evaluate very quickly. It initializes the input data as well as the inputs of the auxiliary topology `topoA`, checks them for consistency and creates the script `run.sh`. Every time one changes this input file it must be reprocessed with `reduze --prepare`. The script `run.sh` will then be overwritten. The option `--auxtop` followed by an absolute or relative path to the directory of the auxiliary topology which is going to be used can be omitted if one already works in the directory of this auxiliary topology.

The input data for the reduction are copied to the directory `reduction/include`. Avoid editing them directly.

4.4.2.3 Run the Reduction

The last step is the reduction. To start it one launches

```
./run.sh
```

This script starts the reduction of the sectors declared in the input file `prepareA.in` and controls the number of processes running in parallel. For every sector that has to be reduced a new directory will be created in the directory `reduction` with the identification number of the sector as name. This directory is used for log files and temporary data. When a reduction is complete the results are written to the directory `results`. If there are already results for this sector they will be overwritten.

The script `run.sh` copies the executable `reduze` from the installation directory and renames it to `reduzeID`, where ID is the identification number of the sector that has to be reduced. If one kills this script with

```
killall run.sh
```

the reductions of the sectors that have been started already will continue, but no further reductions are started anymore. Single reduction processes can be killed with

```
killall reduzeID
```

where ID corresponds to the sector number.

4.4.3 Manipulating the Results

`Reduze` writes the results of a reduction in an internal format which is not well suited for further processing with another algebra system. Also, if symmetry relations are used, the result-files only contain the solutions for one of all equivalent integrals. To get all the desired solutions the user must provide a list of integrals for which the solutions

should be extracted or generated due to symmetry relations. Then these results can be converted to a Mathematica- or FORM-readable format [9, 10].

To do this, Reduze offers the options --select, --FORM and --MMA. These options should be used together with the option --auxtop to tell Reduze which auxiliary topology is going to be used.

4.4.3.1 Select solutions

Reduze can pick the solutions for some user defined integrals from all the results generated during the reduction. Launching

```
reduze --select MyIntegrals
```

where MyIntegrals is a file containing a semicolon separated list of the integrals for which one wants to extract the solution. The format of the integrals is the same as in formula (4.3), however, the numbers t, r, s and ID can be omitted or replaced by any other character, which does not match the bracket '{'. A minimalistic example looks like

```
INT[{v1, ..., vn}];
```

The output is written to the file MyIntegrals.sol. Integrals for which no solution has been found (e.g. master integrals) will be written to the file MyIntegrals.rest.

4.4.3.2 Convert to FORM and Mathematica format

Invoking reduze with the options

```
reduze --FORMAT <files>
```

where --FORMAT is either --FORM or --MMA converts results from Reduze format to a FORM or Mathematica readable format respectively. The parameters given in <files> are interpreted as the names of files containing results in the format of Reduze. For each input file a new output file is created in the current working directory with the extension .inc and .m respectively. Usually, one first uses reduze --select to extract only the results that one actually needs and then converts them to the desired output format.

The Mathematica format is a list of rules and the FORM-format is a table of id statements. Positive integer powers of non-integer denominators in the prefactors of the FORM output are written with the function Den, where Den(a)^k equals to a^{-k}.

Often one wants to expand the results, or more precisely the prefactors, in a Laurent series around $d-4$. With Reduze one can do this expansion on the fly when creating the Mathematica and FORM outputs. If such an expansion is desired, the user has to declare this in the reduction input file. The syntax is explained in section (4.5.2.1).

4.5 Input Files

4.5.1 Auxiliary Topology Input File

The input file, which defines an auxiliary topology, is read in to the main program at run time. It must have the suffix `.in`. The input file consists of lines starting with a keyword followed by some values and a semicolon. Keywords and values are separated by white spaces or tabulators. Comments that will not be interpreted by `Reduze` are entered after a double slash and empty lines are ignored.

```
Keyword value; // don't forget the ';'
```

In the following the keywords are explained using an explicit example. The first declarations define the symbols and must be written at the very beginning of the input file.

```
LoopMomenta k1 k2;
ExtMomenta p1 p2 p3;
Symbol s t m;
Dimension d;
```

The keyword `LoopMomenta` defines the loop momenta k_1 and k_2, `ExtMomenta` the external momenta p_1, p_2, p_3 and `Symbols` declares the symbols s, t and m. `Dimension d` sets the name of the dimension d; however, if this line is missing the default is also taken to be d.

The keyword `Propagator` takes as the first parameter the momentum flow and as the second parameter the mass (not squared). In `Reduze` a propagator with momentum q and mass m is the term $q^2 - m^2$. If one wants to work with the convention of the metric $g = \mathrm{diag}(-1, 1, 1, 1)$, and therefore wants to have a propagator $q^2 + m^2$ one has to replace the mass `m` by `I*m`.

```
Propagator k1 0;
Propagator k2 0;
Propagator k1-k2 0;
Propagator k1-p1 0;
Propagator k2-p1 0;
Propagator k1-p1-p2 0;
Propagator k2-p1-p2 0;
Propagator k1-p3 m;
Propagator k2-p3 m;
```

These lines define nine propagators of which two have the mass m. The order of the declarations is the same order that will be used in the integral representation INT[t, $r, s, ID, \{v_1, \ldots, v_n\}$], where v_i is the exponent of the i-th propagator declared above.

There must be nine propagators because there are nine scalar products containing loop momenta: $k_i^2, k_1\,k_2, k_i\,p_j$ for $1 \leq i \leq 2$ and $1 \leq j \leq 3$. If these scalar products cannot uniquely be replaced by propagators `Reduze` will abort.

For diagrams with cuts only the (sub-)sectors which still contain all cut propagators in the denominator of the integrand are non-zero. In other words: for diagrams with cuts one wants to set to zero all integrals, which either miss one or more cut propagators completely or where a cut propagator appears in the numerator of the integrand only. To achieve this one declares the cut propagators with the keyword `CutPropagator` instead of `Propagator`.

With the keyword `Kinematic` all Lorentz scalar products between the external momenta must be replaced by algebraic expressions of the the symbols defined above, otherwise `Reduze` will abort.

```
Kinematic p1^2 = 0;
Kinematic p2^2 = 0;
Kinematic p3^2 = m^2;
Kinematic p1*p2 = s/2;
Kinematic p2*p3 = (s+t-m^2)/2;
Kinematic p1*p3 = (m^2-t)/2;
```

`Reduze` will also abort if the left hand side of the equations is not a product of exactly two external momenta or not a squared external momentum or if the right hand side still contains some loop or external momenta. For the process of two incoming massless particles with momenta p_1 and p_2 to two outgoing massive particles with momenta p_3 and $p_4 = p_1 + p_2 - p_3$ with squared mass $p_3^2 = p_4^2 = m^2$ the scalar product between different momenta are replaced by the Mandelstam invariants $s = (p_1 + p_2)^2$ and $t = (p_1 - p_3)^2$ in this example.

There are several additional options one can give. One can set a variable, e.g. the mass m, equal to one.

```
SetToOne m;
```

to reduce the number of variables in the rational polynomials by one.

Some integrals with different propagators are equal because the integrands only differ by a shift of a combination of loop/external momenta or a permutation of loop momenta. Those transformations that leave the set of propagators of the auxiliary sector invariant can be given explicitly. The notation is adapted from the cycle representation of permutations of the n propagators and starts with the keyword `Permutation` followed by a sequence of the keyword `Cycle` or `Cyc` with values from $\{1, \ldots, n\}$.

```
Permutation Cyc 1 6 Cyc 2 7;
Permutation Cyc 1 2 Cyc 4 5 Cyc 6 7 Cyc 8 9;
```

The first line declares that there is a symmetry transformation which transforms propagator 1 into 6, 6 into 1, and 2 into 7 as well as 7 into 2. This transformation is the translation $k_i \to -k_i + p_1 + p_2$, $i = 1, 2$, together with the exchange of the external momenta p_1 with p_2 and p_3 with $p_4 = p_1 + p_2 - p_3$. The exchange of the external momenta is allowed since it does not alter the Mandelstam invariants s and t on which the integral actually depends. The second line implements the invariance of interchanging k_1 with k_2. `Reduze` automatically finds all combinations of the user defined permutations. In the above case the combination of the two permutations

```
Permutation Cyc 1 7 Cyc 2 6 Cyc 4 5 Cyc 8 9;
```

will automatically be added.

The setup procedure automatically determines the zero sectors. Setting the

```
SetupFindZeros true;
```

on `false` will turn this off. User defined zero or non-zero sectors can be declared explicitly with the keywords

```
SetupZeroTopos    ID1 ID2     IDn;
SetupNonZeroTopos ID1 ID2     IDn;
```

where the keywords are followed by the desired sector identification numbers.

4.5.2 Reduction Input File

To prepare a reduction one creates a file in the directory of the auxiliary topology. It must have the suffix `.in`. The following minimal declarations are necessary to reduce single sectors, where all integrals with $t = R1 \leq r \leq R2$ and $0 = S1 \leq s \leq S2$ are used to generate the equations. This is usually enough to find all solutions of this class of integrals, but the results will still depend on integrals of sub-sectors if they have not been reduced before already.

```
ReduceID 387 385 384 182;
R2 5;
S2 1;
```

The keyword `ReduceID` can be followed by as many sector identification numbers one wants to reduce, the ordering of the numbers plays no role. `Reduze` always begins reducing the sectors with the smallest number t of propagators. It automatically identifies sub-sectors and looks in the directory `results` for solutions for the sub-sectors. If such solutions exist, they will be inserted in the equations of the sector before the reduction starts.

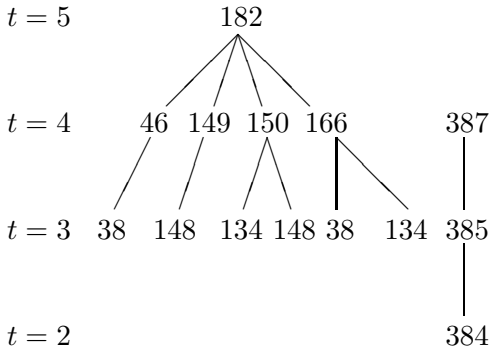

Figure 4.1: Sub-sector trees of sectors 182 and 387

If one wants to reduce some sectors together with their whole trees of sub-sectors they depend on, one can use the keyword `ReduceIDRecursive` followed by the identification numbers. E.g. for the 5-propagator sector 182 and and the 4-propagator sector 387, see Figure (4.1), one simply writes

```
ReduceIDRecursive 182 387;
```

This will first reduce the 2-propagator sector 384 (sub-sector of sector 385), then the 3-propagator sectors 38, 134, 148 (from the sub-sector tree of sector 182) as well as sector 385, then the 4-propagator sub-sectors of sector 182 and sector 387 and finally sector 182. In this example the two sub-sector trees of 182 and 387 do not overlap, but even if they do, each sector is only reduced once.

If one wants to exclude some sectors from the reduction, for example sector 166, which is a sub-sector of sector 182, it can be done with

```
ReduceIDNot 166;
```

Note that the two sub-sectors (38 and 134) of sector 166 still will be reduced.

Excluding a whole sub-sector tree is done with

```
ReduceIDRecursiveNot 166;
```

This will exclude sector 166 and its whole sub-sector tree, in this case sector 38 and 134, from the reduction.

The commands `ReduceID` and `ReduceIDRecursive` for including some sectors as well as `ReduceIDNot` and `ReduceIDRecursiveNot` for excluding some sectors can have as many sectors as arguments as one wants. One can also combine and repeat them as one likes, but one should notice that if a sector is excluded with one of the exclusion commands it cannot be added again with another command. Adding a sector multiple times has no more effect than adding it once.

There is also the possibility to set $R1$ and $S1$ to another value than t and 0 respectively. However, one cannot write $R1 = t$, since t depends on the sector. Therefore the definition $R1 = 0$ (the default) is interpreted as $R1 = t$ with the t of the sector under consideration, but any other declaration $R1 = n$ with $n > 0$ is taken literally.

The equations build from the integrals can be chosen with

```
UseIBP true;
UseLI  false;
```

With this setting, the default, only the IBPs are used.

If the computer used for the reduction has several processors then one can declare

```
Processes n;
```

to tell `Reduze` the number of processes it can run simultaneously. Then, if a reduction is launched with more than one sector with the same t, `Reduze` attempts to run n sectors in parallel.

The system of equations can become quite large, causing memory swapping. To avoid this the system of equations is stored in several files, each holding a certain number of equations, and then only the equations of a single file are loaded into memory and reduced. With the following command one can change the number of the equations per file

```
NrofEqperFile n;
```

where $n = 500$ is the default.

4.5.2.1 Options for the `FORM` and `Mathematica` output

In generating the `FORM` and `Mathematica` results one has the possibility to expand the coefficients in front of each integral in a Laurent series around $\epsilon = 0$, where ϵ is usually defined by $d = 4 - 2\,\epsilon$. One has to tell `Reduze` the name of ϵ and the relation to the dimension d. The following two commands are the default, if omitted.

```
Epsilon ep;
DimensionRule d = 4-2*ep;
```

The next command tells `Reduze` actually to do this expansion.

```
Series n;
```

The integer n is the order up to which the coefficients should be expanded, including the order n term. To generate the output see section (4.4.3.2).

4.6 Installation

4.6.1 Prerequisites

`Reduze` uses the `GiNaC` library [8] for the algebraic manipulations. One must install `GiNaC` version 1.4.1 or higher. If the user's Linux distribution provides a compiled package of `GiNaC`, one simply can install the library and headers with the package manager. Usually, if one wants to use a newer version of `GiNaC`, it has to be compiled and installed by hand.

4.6.2 Building Reduze

The most recent version of `Reduze` can be found at `http://www.itp.uzh.ch/~cedric/reduze/`. Uncompress the package with

```
tar -xzf reduze-version.tgz
```

where `version` is a placeholder for the current version of `Reduze` . Change to the directory `reduze-version` and configure, build, check and install `Reduze` with the commands

```
./configure --prefix=/path/to/inst
make
make check
make install
```

The `--prefix` option can be given if one wants to install `Reduze` in `/path/to/inst/bin` rather than in the default `/usr/local/bin`. The command `make check` sets up an auxiliary topology, does a short reduction and checks if these results are correct by comparing with an internal result file.

The installation directory must be appended to the `PATH` environment variable. If `bash` is used, one writes in the profile file `.bashrc`

```
export PATH=/path/to/inst/bin:$PATH
```

`Reduze` then can be invoked by typing

```
reduze -h
```

which gives a list of options.

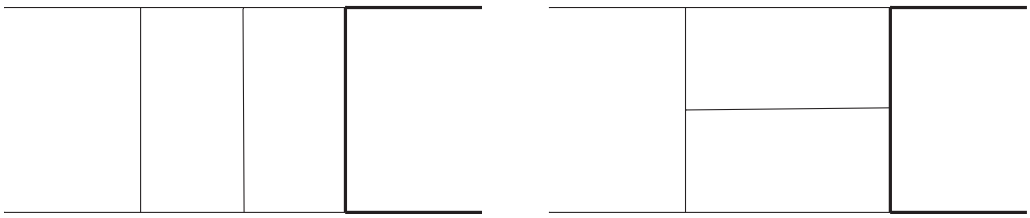

Figure 4.2: 2-loop boxes for the process $q\bar{q} \to t\bar{t}$.

4.7 Performance

Because of internal memory reasons the maximal number of propagators is limited to $N = 16$. The sum of the exponents of the propagators in the numerator and denominator are limited to $R = 16$ and $S = 8$ respectively.

In a reduction most of the time is used for the algebraic manipulations on the prefactors of the system of equations which are rational polynomials. Any additional variable in these polynomials results in larger expressions and makes the calculations slower. It is therefore very useful to put one scale to one.

`Reduze` is implemented in a way that from a given set of integrals all IBP identities are generated and then the whole system is reduced. This system contains a lot of redundant equations, which lead to equations $0 = 0$ during the reduction. If the auxiliary topology allows for symmetry transformations then one cannot only get rid of whole sectors but also some integrals in a specific sector can be identified. This can drastically reduce the number of equations.

4.8 Applications

The program `Reduze` was used to calculate the matrix elements for the leading color coefficient and the fermionic corrections to top-quark pair production in the quark-antiquark channel at NNLO, see Chapter 2. For the leading color coefficient one needs the reduction of the two planar box diagrams in Figure (4.2). These are four-point functions depending on the Mandelstam invariants s, t, the top-mass m and the dimension d. Including all the sub-sectors there are 60 sectors from which the reduction identities of integrals up to three propagators in the numerator are needed. These about 78'000 integrals are used to generate about half a million IBP identities. The reduction of these equations then gives the solutions of all the 78'000 integrals in terms of 35 master integrals. The running time for this reduction using 10 processors (2300 MHz) takes about 30 hours.

`Reduze` was also used to reduce the planar diagrams appearing in the three-loop form factors, see Chapter 3. The reduction was performed for 167 sectors of the auxil-

iary topology AuxTopo 1 (see Table 3.1). The serial computing time would have been more than 2 months but with the parallelization it took a few weeks only.

Bibliography

[1] G. 't Hooft and M. J. G. Veltman, "Regularization And Renormalization Of Gauge Fields," Nucl. Phys. B **44** (1972) 189.

[2] F. V. Tkachov, "A Theorem On Analytical Calculability Of Four Loop Renormalization Group Functions," Phys. Lett. B **100** (1981) 65.

[3] K. G. Chetyrkin and F. V. Tkachov, "Integration By Parts: The Algorithm To Calculate Beta Functions In 4 Loops," Nucl. Phys. B **192** (1981) 159.

[4] T. Gehrmann and E. Remiddi, "Differential equations for two-loop four-point functions," Nucl. Phys. B **580** (2000) 485 [arXiv:hep-ph/9912329].

[5] S. Laporta, "High-precision calculation of multi-loop Feynman integrals by difference equations," Int. J. Mod. Phys. A **15** (2000) 5087 [arXiv:hep-ph/0102033].

[6] C. Anastasiou and K. Melnikov, "Higgs boson production at hadron colliders in NNLO QCD," Nucl. Phys. B **646** (2002) 220 [arXiv:hep-ph/0207004].

[7] R. N. Lee, "Group structure of the integration-by-part identities and its application to the reduction of multiloop integrals," JHEP **0807** (2008) 031 [arXiv:0804.3008 [hep-ph]].

[8] C. W. Bauer, A. Frink and R. Kreckel, "Introduction to the GiNaC Framework for Symbolic Computation within the C++ Programming Language," arXiv:cs/0004015.

[9] Wolfram Research, Inc., Mathematica, Version 7.0, Champaign, IL (2008).

[10] J.A.M. Vermaseren, Symbolic Manipulation with `FORM`, Version 2, CAN, Amsterdam, 1991; "New features of FORM" [math-ph/0010025].

[11] C. Anastasiou and A. Lazopoulos, "Automatic integral reduction for higher order perturbative calculations," JHEP **0407** (2004) 046 [arXiv:hep-ph/0404258].

[12] A. V. Smirnov, "Algorithm FIRE – Feynman Integral REduction," JHEP **0810** (2008) 107 [arXiv:0807.3243 [hep-ph]].

[13] R. Bonciani, A. Ferroglia, T. Gehrmann, D. Maitre and C. Studerus, "Two-Loop Fermionic Corrections to Heavy-Quark Pair Production: the Quark-Antiquark Channel," JHEP **0807** (2008) 129 [arXiv:0806.2301 [hep-ph]].

[14] R. Bonciani, A. Ferroglia, T. Gehrmann and C. Studerus, "Two-Loop Planar Corrections to Heavy-Quark Pair Production in the Quark-Antiquark Channel," JHEP **0908** (2009) 067 [arXiv:0906.3671 [hep-ph]].

Appendix A

Master Integrals for two-loop Heavy Quark Production

A.1 Definition of the Harmonic Polylogarithms

The results presented here are conveniently expressed in terms of one- and two- dimensional HPLs. Nowadays, harmonic polylogarithms are extensively employed in multi-loop computations. Therefore, in this appendix we only briefly review their definition. The reader interested in the algebraic properties of these functions can find detailed discussions about this topic in the available literature [1–4].

In the non-physical region $s < 0$, seven weight functions are needed for the HPLs with argument x. They are[1]

$$f_w(x) = \frac{1}{x-w}\,, \quad \text{with} \quad w \in \left\{0, 1, -1, -y, -\frac{1}{y}, \frac{1}{2} \pm \frac{i\sqrt{3}}{2}\right\}\,. \tag{A.1}$$

For HPLs with argument y, we need six weight functions

$$f_w(y) = \frac{1}{y-w}\,, \quad \text{with} \quad w \in \left\{0, 1, -1, -x, -\frac{1}{x}, 1 - \frac{1}{x} - x\right\}\,. \tag{A.2}$$

The weight-one HPLs are defined as

$$G(0;x) = \ln x\,, \qquad G(w;x) = \int_0^x dt f_w(t)\,. \tag{A.3}$$

HPLs of higher weight are defined by iterated integrations

$$G(w, \cdots;x) = \int_0^x dt f_w(t) G(\cdots;t)\,, \tag{A.4}$$

[1] The last two weights in Eq. (A.1) introduce explicit imaginary parts in the formulae. However, these HPLs appear in such a way that these imaginary parts cancel in the non-physical region, where the result has to be real. Alternatively, one could choose a basis of weight functions in which the pair $\frac{1}{2} \pm \frac{i\sqrt{3}}{2}$ is replaced by the original quadratic expressions in the integrals: $1/(x^2 - x + 1)$ and $x/(x^2 - x + 1)$ [4]. In this case these HPLs are all manifestly real.

with the only exception being the HPLs in which all the weights are zero which are defined as follows

$$G(\underbrace{0,0,\cdots,0}_{n};x) = \frac{1}{n!}\ln^n x\,. \tag{A.5}$$

Analogous definitions hold for HPLs with argument y. The reader should be aware of the fact that in the original definition of Remiddi and Vermaseren, the weight function corresponding to the weight 1 was $f_1 = 1/(1-x)$. In order to translate the HPLs defined with the Remiddi-Vermaseren convention to the ones employed in this work (and vice versa) it is sufficient to multiply each HPL by a factor $(-1)^n$, where n is the number of weights equal to 1.

The weights $-y$ and $-1/y$ were already introduced in [2, 5]. In our results, the two-dimensional harmonic polylogarithms have maximum weight four. Therefore, it was not possible to rewrite all the two-dimensional HPLs in terms of Nielsen polylogarithms, as it was done for the results of Section 2.3, where the two-dimensional HPLs had maximal weight three. However, it is possible to evaluate all the HPLs appearing in the analytic expression of the coefficient A in Eq. (2.5) by employing the `GiNaC` implementation of multiple polylogarithms by Vollinga and Weinzierl [3].

We first obtained the squared matrix elements in the non-physical region $s < 0$. The corresponding quantities in the physical region $s > 4m^2$ could be obtained by analytic continuation to the complex value $s \to s + i\delta$, where $\delta \to 0^+$. For $s > 4m^2$ the variable x becomes

$$x = -x' + i\delta\,, \tag{A.6}$$

where

$$x' = \frac{\sqrt{s} - \sqrt{s-4m^2}}{\sqrt{s} + \sqrt{s-4m^2}}\,, \tag{A.7}$$

So that $0 < x' < 1$ for $4m^2 < s < \infty$. The HPLs of argument x can develop an imaginary part because of analytic continuation[1]. In particular, the imaginary part of the HPLs of argument x for $s > 4m^2$ is defined when the analytic continuation of the logarithm is specified:

$$G(0;x) = G(0;-x'+i\delta) = G(0,x') + i\pi\,. \tag{A.8}$$

For notation convenience, after the analytic continuation we rename x' as x.

[1] The coefficient A is real for $s < 0$. However, because of the weight functions we use, and because of the fact that $0 \le y \le \infty$, individual HPLs can develop imaginary parts also in the non-physical region. The latter cancel out among each other.

A.2 Expansion of the HPLs near the Threshold

We devote this section to a brief discussion of the technique employed to expand the coefficient A near the production threshold $\beta = \sqrt{1-4m^2/s} = 0$.

The first step consists in carrying out the analytic continuation from the non-physical region, $s < 0$, to the physical one, $s > 4m^2$, according to the method outlined above. The one- and two-dimensional HPLs appearing in the analytically continued expression of the coefficient A must then be expanded in the $\beta \to 0$ limit. While the threshold expansion of the ordinary HPLs does not lead to any particular difficulty, the expansion of the two-dimensional HPLs is indeed more delicate. The reason is that, in the latter case, the expansion parameter β appears in both the argument and the weights of the HPLs. In fact, in the physical region one finds:

$$x = \frac{1-\beta}{1+\beta}\,, \qquad y = \frac{1-\beta}{1+\beta} + \frac{4\beta}{1-\beta^2}\xi\,. \tag{A.9}$$

Moreover, the coefficient A depends on two-dimensional HPLs of maximal weight four; therefore it is very challenging to obtain explicit analytic expressions of these functions in terms of logarithms and polylogarithms of complicated arguments, which can be subsequently expanded in $\beta \to 0$. Such an approach should be replaced by a more direct and algorithmic method.

In the following we describe the method which allows to extract directly the expansion of a given two-dimensional HPL of weight n, assuming that the expansion of the HPLs of weight $n-1$ is known. Let us consider, for simplicity, the case in which the HPL has argument x and it has y (or $1/y$) in the weights. Since the dependence of x on β is the one shown in Eq. (A.9), we first use the transformation that relates $G(w,...;(1-\beta)/(1+\beta))$ to $G(w',...;\beta)$. This transformation allows to rewrite the HPL function of x as a combination of HPL functions of β, HPLs with y in the weights but evaluated in $x = 1$, and HPLs (either one- or two-dimensional) of a smaller weight. The series expansion of the HPLs with argument β is found recursively. We write them as the integral between 0 and β of the total derivative with respect to β of the HPLs themselves. The total derivative gives rise to HPLs of lower weight. We insert the expansions of the lower-weight HPLs and then we integrate again. For the HPLs evaluated in $x = 1$ the procedure is analogous. It can happen that in the intermediate steps (expansion followed by an integration) logarithmic divergences occur. These divergences must be regularized and they cancel in the final expressions.

Let us illustrate the algorithm more in detail. To this purpose, we consider the example of a simple two-dimensional HPL of weight two, which appears in the expression of the coefficient A. For $0 < x < 1$ and $x < y < 1/x$ we define

$$G(y,-1;x) = \int_0^x dt \frac{1}{t-y} G(-1,t) = \int_0^x dt \frac{1}{t-y} \ln(1+t)\,. \tag{A.10}$$

This HPL is real in the physical region, however the intermediate stages of the procedure described below require the sum of complex terms. We assume that any ambiguity of this sort is dealt with by assigning an infinitesimal imaginary part to y. We start by rewriting the HPL of argument x in terms of HPLs of argument β; the integral representation in Eq. (A.10) can be rewritten as

$$G(y,-1;x) = G(y,-1;1) + \int_1^x dt \frac{1}{t-y} G(-1,t)\,. \tag{A.11}$$

In the integral in the second term of Eq. (A.11) we carry out a change of integration variable by setting $q = (1-t)/(1+t)$ ($dt = -2/(1+q)^2 dq$)

$$\begin{aligned}\int_1^x dt \frac{1}{t-y} G(-1,t) &= -2\int_0^\beta dq \frac{(1+q)}{(1-q)-y(1+q)} \frac{2}{(1+q)^2} G\left(-1,\frac{1-q}{1+q}\right)\,, \\ &= \int_0^\beta dq \left(\frac{1}{q-\gamma} - \frac{1}{q+1}\right) G\left(-1;\frac{1-q}{1+q}\right)\,,\end{aligned} \tag{A.12}$$

where we employed the relation $\beta = (1-x)/(1+x)$ and we introduced $\gamma = (1-y)/(1+y)$. We emphasize that, given the definitions of x and y in the physical region, γ is a function of β and of the variable ξ defined in Eq. (2.21). The weight one HPLs appearing in the integrand of Eq. (A.12) can also be easily rewritten in terms of HPLs of argument q:

$$G\left(-1;\frac{1-q}{1+q}\right) = -G(-1;q) + \ln 2\,. \tag{A.13}$$

At this stage it is straightforward to integrate in q to finally obtain

$$\begin{aligned}G(y,-1;x) &= G(y,-1;1) - \Big(G(\gamma,-1;\beta) - G(-1,-1;\beta)\Big) \\ &\quad + \ln 2\Big(G(\gamma;\beta) - G(-1;\beta)\Big)\,.\end{aligned} \tag{A.14}$$

In the equation above, there are one- and two-dimensional HPLs of weight one, that we consider to be known, and three HPLs of weight two. Among them, there is a single two-dimensional HPL of weight two, $G\left(\gamma(\beta),-1;\beta\right)$, and two one-dimensional HPLs. One of them, $G(-1,-1;\beta)$, has a trivial expansion in $\beta \to 0$. Let us discuss the method employed to obtain the threshold expansion of the other two: $G\left(\gamma(\beta),-1;\beta\right)$, and $G(y,-1;1)$.

We can rewrite $G\left(\gamma(\beta),-1;\beta\right)$ as follows:

$$G\left(\gamma(\beta),-1;\beta\right) = \int_0^\beta d\beta' \frac{d}{d\beta'} G\left(\gamma(\beta'),-1;\beta'\right) + G\left(\gamma(0),-1;0\right)\,. \tag{A.15}$$

In this simple example the second term in Eq. (A.15) is well defined (and it is actually equal to zero). The derivative in the first term of Eq. (A.15) can be rewritten as

$$\frac{d}{d\beta} G\left(\gamma(\beta),-1;\beta\right) = \frac{1}{\beta-\gamma(\beta)} G(-1;\beta) + \int_0^\beta dt \frac{d}{d\beta}\left(\frac{1}{t-\gamma(\beta)} G(-1;t)\right)$$

$$
\begin{aligned}
&= \frac{1}{\beta-\gamma(\beta)}G(-1;\beta) + \frac{d\gamma(\beta)}{d\beta}\int_0^\beta \frac{dt}{(t-\gamma(\beta))^2}G(-1;t) \\
&= \frac{1}{\beta-\gamma(\beta)}G(-1;\beta) - \frac{d\gamma(\beta)}{d\beta}\int_0^\beta dt\frac{d}{dt}\left(\frac{1}{t-\gamma(\beta)}\right)G(-1;t) \\
&= \frac{1}{\beta-\gamma(\beta)}G(-1;\beta) - \frac{d\gamma(\beta)}{d\beta}\Bigg[\frac{1}{\beta-\gamma(\beta)}G(-1;\beta) \\
&\quad -\frac{1}{1+\gamma(\beta)}\int_0^\beta dt\left(\frac{1}{t-\gamma(\beta)}-\frac{1}{t+1}\right)\Bigg] \\
&= \frac{1}{\beta-\gamma}G(-1;\beta) - \frac{d\gamma}{d\beta}\Bigg[\frac{1}{\beta-\gamma}G(-1;\beta) - \frac{1}{1+\gamma}\Big(G(\gamma;\beta) \\
&\quad -G(-1;\beta)\Big)\Bigg], \qquad \text{(A.16)}
\end{aligned}
$$

where in the last line we dropped the dependence of γ on β. Since the expansion of the HPLs of weight one is assumed to be known, it is straightforward to expand the equation above in the limit $\beta \to 0$ and to insert it in Eq. (A.15) to obtain

$$
G\left(\gamma,-1;\beta\right) = \beta\Big[1+(1-2\xi)\Big(\ln 2+\ln(\xi)-\ln(2\xi-1)\Big)\Big] + \mathcal{O}(\beta^2)\,. \qquad \text{(A.17)}
$$

The formula above is real for $\xi > 1/2$. However, the imaginary parts which arise for $\xi < 1/2$ cancel against the imaginary parts coming from the expansion of $G(y,-1;1)$.

The expansion of $G(y,-1;1)$ can be done with the same algorithm. We write:

$$
G(y(\beta),-1;1) = \int_{0^+}^{\beta}\frac{d}{d\beta'}G(y(\beta'),-1;1) + G(y(0^+),-1;1)\,, \qquad \text{(A.18)}
$$

where 0^+ indicates the fact that we must take the limit $\beta \to 0^+$ both in the integration constant and in the lower boundary of the integration. Both limits are logarithmically divergent, but the divergences cancel between the two terms. We have:

$$
\begin{aligned}
\frac{d}{d\beta'}G(y(\beta'),-1;1) &= \frac{dy(\beta)}{d\beta}\int_0^1\frac{dt}{(t-y)^2}G(-1,t)\,, \\
&= \frac{dy(\beta)}{d\beta}\left[-\frac{1}{t-y}G(-1,t)\Big|_0^1 + \frac{1}{1+y}\int_0^1 dt\left(\frac{1}{t-y}-\frac{1}{1+t}\right)\right], \\
&= \frac{dy(\beta)}{d\beta}\left[-\frac{\ln 2}{1-y}+\frac{1}{1+y}\Big(G(y;1)-\ln 2\Big)\right]. \qquad \text{(A.19)}
\end{aligned}
$$

Expanding Eq. (A.19) in the limit $\beta \to 0$, we find the following Laurent series:

$$
\frac{d}{d\beta'}G(y(\beta'),-1;1) = \frac{\ln 2}{\beta}+\frac{\ln 2}{2\xi-1}+(2\xi-1)\left[\ln(\beta)+\ln(2\xi-1)\right]+\mathcal{O}(\beta)\,. \qquad \text{(A.20)}
$$

Integrating Eq. (A.20), as in Eq. (A.18), we find:

$$\int_{0^+}^{\beta} \frac{d}{d\beta'} G(y(\beta'),-1;1) = \ln 2 \ln(\beta) - \ln 2 \ln(0^+) + \beta \Big\{ \frac{\ln 2}{2\xi - 1} + (2\xi - 1) \Big[\ln(\beta) + \ln(2\xi - 1) - 1 \Big] \Big\} + \mathcal{O}(\beta^2). \tag{A.21}$$

Moreover, one finds:

$$\begin{aligned} G(y(0^+),-1;1) &= G(y(0^+);1) G(-1;1) - G(-1, y(0^+);1)\,, \\ &= \ln 2 \left[\ln(0^+) + \ln 2 + \ln(2\xi - 1) \right] + \frac{1}{2}\zeta_2 - \frac{1}{2}\ln^2 2\,. \end{aligned} \tag{A.22}$$

Finally, we have:

$$\begin{aligned} G(y(\beta),-1;1) &= \ln 2 \ln(\beta) + \ln 2 \ln(2\xi - 1) + \frac{1}{2}\ln^2 2 + \frac{1}{2}\zeta_2 \\ &\quad + \beta \Big\{ \frac{\ln 2}{2\xi - 1} + (2\xi - 1) \Big[\ln(\beta) + \ln(2\xi - 1) - 1 \Big] \Big\} + \mathcal{O}(\beta^2), \end{aligned} \tag{A.23}$$

where the divergences disappeared. Considering also the expansion of the one- and two-dimensional HPLs of weight 1 and the expansion of $G(-1,-1;\beta)$ in Eq. (A.14), we find the final formula:

$$\begin{aligned} G(y,-1;x) &= \ln 2 \ln(\beta) + \ln 2 \ln(\xi) + \frac{3}{2}\ln^2 2 + \frac{1}{2}\zeta_2 \\ &\quad + \beta \Big\{ -2\xi + (2\xi - 1) \big[\ln(\beta) + \ln(\xi) + \ln 2 \big] \Big\} + \mathcal{O}(\beta^2)\,. \end{aligned} \tag{A.24}$$

In the case in which the argument of the HPLs is y and x is present in the weights, $G(w,...;y)$, the procedure is analogous to the one explained above. Since the dependence of y on β involves also the parameter ξ (see Eq. (A.9)), the first step consists in using the scale properties of the HPLs:

$$G(w,...;y) = G(\lambda w,...;\lambda y)\,, \tag{A.25}$$

(valid in the case in which all the trailing zeros have already been extracted) to get rid of the ξ dependence in the argument. To achieve this goal, one multiplies weights and argument by

$$\lambda = \frac{1}{1 + \frac{4\beta}{(1-\beta)^2}\xi}\,. \tag{A.26}$$

In so doing, we fit again in the case illustrated in the example concerning $G(w,...;x)$, since

$$\frac{1}{1 + \frac{4\beta}{(1-\beta)^2}\xi}\, y = \frac{1-\beta}{1+\beta}\,, \tag{A.27}$$

and the expansion proceeds along the same steps as outlined above.

A.3 Master Integrals for the Fermionic Corrections

In this Appendix we collect the MIs for the topologies in Fig. 2.2-(k), Fig. 2.2-(l), Fig. 2.3-(k), and in Fig. 2.3-(l) that are not yet available in the literature.

The explicit expression of the MIs depends on the chosen normalization of the integration measure. The integration on the loop momenta is normalized as follows

$$\int \mathfrak{D}^d k = \frac{1}{C(\varepsilon)} \left(\frac{\mu^2}{m^2}\right)^{-\varepsilon} \int \frac{d^d k}{(4\pi^2)^{(1-\varepsilon)}}\,, \tag{A.28}$$

where $C(\varepsilon)$ was defined in Eq. (2.20). In Eq. (A.28) μ stands for the 't Hooft mass of dimensional regularization. The integration measure in Eq. (A.28) is chosen in such a way that the one-loop massive tadpole becomes

$$\int \mathfrak{D}^d k \, \frac{1}{k^2+m^2} = -\frac{m^2}{4(1-\varepsilon)\varepsilon}\,. \tag{A.29}$$

In calculating the squared matrix element, we multiply our bare results by $(\mu^2/m^2)^\varepsilon$, in order to make explicit the dependence on the top scale. We also point out that, since the squared matrix element still contains soft and collinear divergences regulated by ε, it depends on the normalization of the integration measure. In particular, in order to match our results with the ones of [6, 7], it is necessary to multiply them by the factor

$$\frac{e^{-2\gamma\varepsilon}}{\Gamma\left(1+\varepsilon\right)^2} = 1 - \zeta(2)\varepsilon^2 + \frac{2}{3}\zeta(3)\varepsilon^3 + \mathcal{O}\left(\varepsilon^4\right)\,. \tag{A.30}$$

There is a single MIs belonging to the topology Fig. 2.2-(k) :

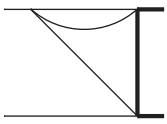

$$= \int \frac{\mathfrak{D}^d k_1 \mathfrak{D}^d k_2}{P_0\left(k_1+p_1\right) P_0\left(k_2\right) P_0\left(k_1-k_2\right) P_m\left(k_1+p_3\right)}\,, \tag{A.31}$$

where we define

$$P_0\left(k\right) \equiv k^2\,, \qquad P_m\left(k\right) \equiv k^2+m^2\,; \tag{A.32}$$

we then find

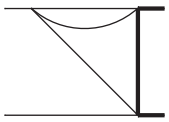

$$= \sum_{i=-2}^{1} A_i\, \varepsilon^i + \mathcal{O}(\varepsilon^2)\,, \tag{A.33}$$

$$A_{-2} \;=\; \frac{1}{32}\,,$$

A. MASTER INTEGRALS FOR TWO-LOOP HEAVY QUARK PRODUCTION

$$
\begin{aligned}
A_{-1} &= \frac{1}{32y}\left[5y - 2\left(1+y\right)G\left(-1;y\right)\right], \\
A_{0} &= \frac{1}{32y}\left[19y + 4y\zeta(2) - 10\left(1+y\right)G\left(-1;y\right)\right. \\
&\quad \left. +8\left(1+y\right)G\left(-1,-1;y\right) - 4G\left(0,-1;y\right) - 4yG\left(0,-1;y\right)\right], \\
A_{1} &= \frac{1}{32y}\Big[65y + 20y\zeta\left(2\right) + 8y\zeta\left(3\right) - 2\left(1+y\right)\left(19 + 4\zeta\left(2\right)\right)G\left(-1;y\right) \\
&\quad +40\left(1+y\right)G\left(-1,-1;y\right) - 20G\left(0,-1,y\right) - 20yG\left(0,-1;y\right) - 32G\left(-1,-1,-1;y\right) \\
&\quad -32yG\left(-1,-1,-1;y\right) + 16G\left(-1,0,-1,y\right) + 16yG\left(-1,0,-1;y\right) \\
&\quad +16G\left(0,-1,-1;y\right) + 16yG\left(0,-1,-1;y\right) - 8G\left(0,0,-1;y\right) - \text{`}8yG\left(0,0,-1;y\right)\Big]
\end{aligned}
\tag{A.34}
$$

Also the four point topology Fig. 2.2-(l) has a single MI:

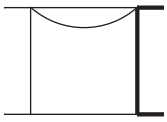

$$
= \int \frac{\mathfrak{D}^d k_1 \mathfrak{D}^d k_2}{P_0\left(k_1+p_1\right) P_0\left(k_1+p_1+p_2\right) P_0\left(k_2\right) P_0\left(k_1-k_2\right) P_m\left(k_1+p_3\right)} \tag{A.35}
$$

with

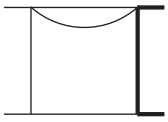

$$
= \frac{1}{m^2}\sum_{i=-3}^{0} A_i\,\varepsilon + \mathcal{O}(\varepsilon), \tag{A.36}
$$

$$
\begin{aligned}
A_{-3} &= \frac{1}{32(y+1)}, \\
A_{-2} &= \frac{1}{32(y+1)}\Big(G(0;x) - 2G(1;x) - 2G(-1;y) + 2\Big), \\
A_{-1} &= \frac{1}{32(y+1)}\Big[-3\zeta(2) + G(0,0;x) - 2G(0,1;x) - 2G(1,0;x) + 4G(1,1;x) \\
&\quad +G(0;x)(2 - 2G(-1;y)) - 4G(-1;y) + G(1;x)(4G(-1;y) - 4) \\
&\quad +4G(-1,-1;y) - 2G(0,-1;y) + 4\Big], \\
A_{0} &= \frac{1}{32(y+1)}\Big[-2(3\zeta(2) + 4\zeta(3) - 4) + G(0,0,0;x) - 2G(0,0,1;x) - 2G(0,1,0;x) \\
&\quad +4G(0,1,1;x) - 2G\left(-1/y,0,0,x\right) + 4G\left(-1/y,0,1,x\right) + 2G\left(-1/y,1,0,x\right) \\
&\quad -4G\left(-1/y,1,1,x\right) + 2G(-y,1,0;x) - 4G(-y,1,1;x) + G(1,1;x)(8 - 16G(-1;y)) \\
&\quad +G(0,0;x)(2 - 2G(-1;y)) + 2(3\zeta(2) - 4)G(-1;y) - 2G\left(-1/y,0,x\right)G(-1;y) \\
&\quad +4G\left(-1/y,1,x\right)G(-1;y) - 2G(-y,0;x)G(-1;y) + 4G(-y,1;x)G(-1;y) \\
&\quad +G(0,1;x)(4G(-1;y) - 4) + G(1,0;x)(8G(-1;y) - 4) \\
&\quad +G(1;x)(2(7\zeta(2) - 4) + 8G(-1;y)) + 8G(-1,-1;y)
\end{aligned}
$$

$$
\begin{aligned}
&+G(0;x)(-3\zeta(2)-4G(-1;y)+4G(-1,-1;y)-2G(0,-1;y)+4)\\
&-4G(0,-1;y)+G(-y;x)(2G(0,-1;y)-4G(-1,-1;y))\\
&+G\left(-1/y,x\right)\left(-8\zeta(2)-4G(-1,-1;y)+2G(0,-1;y)\right)\\
&-8G(-1,-1,-1;y)+4G(-1,0,-1;y)+4G(0,-1,-1;y)-2G(0,0,-1;y)\Big]\,. \qquad \text{(A.37)}
\end{aligned}
$$

We now consider the MIs involved in the calculation of the part of the amplitude proportional to N_h. Topology Fig. 2.3-(k) has two MIs:

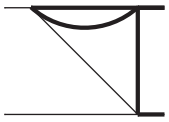

$$
= \int \frac{\mathfrak{D}^d k_1 \mathfrak{D}^d k_2}{P_0\left(k_1+p_1\right) P_m\left(k_2\right) P_m\left(k_1-k_2\right) P_m\left(k_1+p_3\right)}\,, \qquad \text{(A.38)}
$$

with

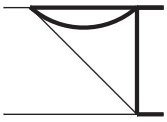

$$
= \sum_{i=-2}^{1} A_i\,\varepsilon + \mathcal{O}\left(\varepsilon\right)\,, \qquad \text{(A.39)}
$$

$$
\begin{aligned}
A_{-2} &= \frac{1}{32},\\
A_{-1} &= \frac{1}{32y}\,\left[5y-2(y+1)G(-1;y)\right],\\
A_0 &= \frac{1}{32y(y+1)}\,\Big[-10G(-1;y)(y+1)^2+4G(-1,-1;y)(y+1)^2-4G(0,-1;y)(y+1)\\
&\quad -4yG(0,0,-1;y)+y\left(19y-4\zeta(3)+19\right)\Big]\,,\\
A_1 &= \frac{1}{32y(y+1)}\,\Big[20G(-1,-1;y)(y+1)^2-8G(-1,-1,-1;y)(y+1)^2\\
&\quad +8G(-1,0,-1;y)(y+1)+8G(0,-1,-1;y)(y+1)-8(y-1)G(1,0,-1;y)(y+1)\\
&\quad +4(y-1)G(1;y)\zeta(2)(y+1)+4(y-2)(2y+1)G(0,0,-1;y)-8yG(-1,0,0,-1;y)\\
&\quad +8yG(0,-1,0,-1;y)+8yG(0,0,-1,-1;y)-12yG(0,0,0,-1;y)\\
&\quad +16yG(0,1,0,-1;y)-8yG(0,1;y)\zeta(2)+4G(0,-1;y)\left(2\zeta(2)y-5y-5\right)\\
&\quad -2G(-1;y)\left(2\zeta(2)y^2+19y^2+4\zeta(3)y+38y-2\zeta(2)+19\right)+\frac{y}{5}\left(6\zeta(2)^2+325y\right.\\
&\quad \left.+20y\zeta(3)-40\zeta(3)+325\right)\Big]\,. \qquad \text{(A.40)}
\end{aligned}
$$

As second MI for the topology Fig. 2.3-(k), we chose

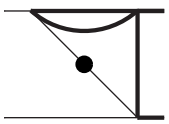

$$
= \int \frac{\mathfrak{D}^d k_1 \mathfrak{D}^d k_2}{P_0^2\left(k_1+p_1\right) P_m\left(k_2\right) P_m\left(k_1-k_2\right) P_m\left(k_1+p_3\right)}\,, \qquad \text{(A.41)}
$$

where

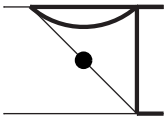

$$= \frac{1}{m^2}\sum_{i=-2}^{1} A_i\,\varepsilon^i + \mathcal{O}\left(\varepsilon^2\right), \tag{A.42}$$

$$\begin{aligned}
A_{-2} &= -\frac{1}{16(y+1)},\\
A_{-1} &= \frac{y-1}{16y(y+1)}G(-1;y),\\
A_0 &= \frac{y-1}{8y(y+1)^2}\Big[(y+1)G(-1;y)-(y+1)G(-1,-1;y)\\
&\quad -G(0,-1;y)+\frac{2y}{1-y}\left(y-\zeta(2)+1\right)\Big],\\
A_1 &= \frac{y-1}{8y(y+1)^2}\Big[-2(y+1)G(-1,-1;y)+2G(0,-1;y)+2(y+1)G(-1,-1,-1;y)\\
&\quad -2G(-1,0,-1;y)-2G(0,-1,-1;y)-2(y-1)G(0,0,-1;y)\\
&\quad +2(y-1)G(1,0,-1;y)-(y-1)G(1;y)\zeta(2)+G(-1;y)\left(\zeta(2)y+2y-\zeta(2)+2\right)\\
&\quad -\frac{y}{y-1}\left(12\ln(2)\zeta(2)-4\zeta(2)+y\zeta(3)-8\zeta(3)\right)\Big].
\end{aligned} \tag{A.43}$$

The box topology Fig. 2.3-(l), has also two MIs: the first one is

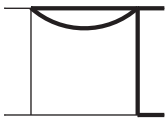

$$= \int \frac{\mathfrak{D}^d k_1 \mathfrak{D}^d k_2}{P_0\left(k_1+p_1\right) P_0\left(k_1+p_1+p_2\right) P_m\left(k_2\right) P_m\left(k_1-k_2\right) P_m\left(k_1+p_3\right)}, \tag{A.44}$$

with

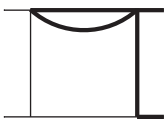

$$= \frac{1}{m^2}\sum_{i=-3}^{0} A_i\,\varepsilon^i + \mathcal{O}\left(\varepsilon\right), \tag{A.45}$$

$$\begin{aligned}
A_{-3} &= \frac{1}{32(y+1)},\\
A_{-2} &= \frac{1}{32(x-1)(y+1)}\Big[-2G(-1;y)(x-1)+2(x-1)-(1+x)G(0;x)\Big],\\
A_{-1} &= \frac{1}{32(x-1)(y+1)}\Big[3\zeta(2)x+4x+6(x+1)G(-1,0;x)+(-5x-1)G(0,0;x)
\end{aligned}$$

$$
\begin{aligned}
&-4(x-1)G(-1;y)+G(0;x)(2(x+1)G(-1;y)-2(x+1))+4(x-1)G(-1,-1;y)\\
&-2(x-1)G(0,-1;y)+3\zeta(2)-4\Big]\,,\\
A_0 \;=\; &\frac{1}{32(x-1)(y+1)}\Big[-36(x+1)G(-1,-1,0;x)+18(x+1)G(-1,0,0;x)\\
&+6(5x+1)G(0,-1,0;x)+(-5x-1)G(0,0,0;x)-2(5x-3)G(1,0,0;x)\\
&+4(x+1)G(1,1,0;x)+2(x+1)G\left(-1/y,0,0,x\right)-2(x+1)G\left(-1/y,1,0,x\right)\\
&-2(x+1)G(-y,1,0;x)-4(x+1)G(1,0;x)G(-1;y)+2(x+1)G\left(-1/y,0,x\right)G(-1;y)\\
&+2(x+1)G(-y,0;x)G(-1;y)+G(-1,0;x)(12(x+1)-12(x+1)G(-1;y))\\
&+G(0,0;x)(2(5x+1)G(-1;y)-2(5x+1))+8(x-1)G(-1,-1;y)\\
&-4(x-1)G(0,-1;y)-2(x+1)G(-y;x)G(0,-1;y)-8(x-1)G(-1,-1,-1;y)\\
&+4(x-1)G(-1,0,-1;y)+4(x-1)G(0,-1,-1;y)-2(3x-1)G(0,0,-1;y)\\
&-18(x+1)G(-1;x)\zeta(2)-4(x+1)G(1;x)\zeta(2)-2G(-1;y)\left(3\zeta(2)x+4x+3\zeta(2)-4\right)\\
&+G(0;x)\big(15\zeta(2)x-4x+4(x+1)G(-1;y)-4(x+1)G(-1,-1;y)\\
&+2(x+1)G(0,-1;y)+3\zeta(2)-4\big)+G\left(-1/y,x\right)\left(2(x+1)G(0,-1;y)+4(x+1)\zeta(2)\right)\\
&+2\left(3\zeta(2)x+12\zeta(3)x+4x+3\zeta(2)+4\zeta(3)-4\right)\Big]\,. \qquad \text{(A.46)}
\end{aligned}
$$

As second MI for topology Fig. 2.3-(l) we chose

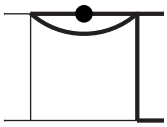

$$
= \int \frac{\mathfrak{D}^d k_1 \mathfrak{D}^d k_2}{P_0\left(k_1+p_1\right) P_0\left(k_1+p_1+p_2\right) P_m^2\left(k_2\right) P_m\left(k_1-k_2\right) P_m\left(k_1+p_3\right)} \qquad \text{(A.47)}
$$

with

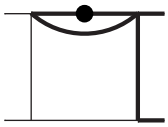

$$
= \frac{1}{m^4}\sum_{i=-2}^{0} A_i\,\varepsilon^i + \mathcal{O}\left(\varepsilon\right)\,, \qquad \text{(A.48)}
$$

$$
\begin{aligned}
A_{-2} \;=\; &\frac{x}{32(x-1)(x+1)(y+1)}\,G(0;x)\,,\\
A_{-1} \;=\; &-\frac{x}{32(x-1)(x+1)(y+1)}\Big[6G(-1,0;x)-3G(0,0;x)+2G(0;x)G(-1;y)+3\zeta(2)\Big]\,,\\
A_0 \;=\; &-\frac{x}{32(x-1)(x+1)(y+1)}\Big[18G(-1,0,0;x)-36G(-1,-1,0;x)+18G(0,-1,0;x)\\
&-3G(0,0,0;x)-2G(1,0,0;x)+4G(1,1,0;x)+2G\left(-1/y,0,0,x\right)-2G\left(-1/y,1,0,x\right)\\
&-2G(-y,1,0;x)-12G(-1,0;x)G(-1;y)+6G(0,0;x)G(-1;y)\\
&-4G(1,0;x)G(-1;y)+2G\left(-1/y,0,x\right)G(-1;y)+2G(-y,0;x)G(-1;y)
\end{aligned}
$$

$$
\begin{aligned}
&-2G(-y;x)G(0,-1;y) - 2G(0,0,-1;y) - 18G(-1;x)\zeta(2) - 4G(1;x)\zeta(2) \\
&-6G(-1;y)\zeta(2) + G\left(-1/y,x\right)\left(2G(0,-1;y) + 4\zeta(2)\right) \\
&+G(0;x)\left(-4G(-1,-1;y) + 2G(0,-1;y) + 9\zeta(2)\right) + 16\zeta(3)\Big] \,. \qquad \text{(A.49)}
\end{aligned}
$$

A.4 Master Integrals for the Planar Corrections

In this Appendix we collect the MIs for the topologies in Fig. 2.2.

The explicit expression of the MIs depends on the chosen normalization of the integration measure. The integration on the loop momenta is normalized as follows:

$$
\int \mathfrak{D}^d k = \frac{1}{C(\varepsilon)} \left(\frac{\mu^2}{m^2}\right)^{-\varepsilon} \mu^{2\varepsilon} \int \frac{d^d k}{(4\pi^2)^{(1-\varepsilon)}} \,, \qquad \text{(A.50)}
$$

where $C(\varepsilon)$ was defined in Eq. (2.20). In Eq. (A.50) μ stands for the 't Hooft mass of dimensional regularization. The integration measure in Eq. (A.50) is chosen in such a way that the one-loop massive tadpole becomes

$$
\int \mathfrak{D}^d k \, \frac{1}{k^2 + m^2} = -\frac{m^2}{4(1-\varepsilon)\varepsilon} \,. \qquad \text{(A.51)}
$$

In calculating the squared matrix element, we multiply our bare results by $(\mu^2/m^2)^\varepsilon$, in order to make explicit the dependence on the 't Hooft scale. We also point out that, since the squared matrix element still contains soft and collinear divergences regulated by ε, it depends on the normalization of the integration measure. In particular, in order to match our results with the ones of [6, 7], it is necessary to multiply the latter by the factor

$$
\frac{e^{-2\gamma\varepsilon}}{\Gamma\left(1+\varepsilon\right)^2} = 1 - \zeta(2)\varepsilon^2 + \frac{2}{3}\zeta(3)\varepsilon^3 + \frac{3}{10}\zeta(2)^2\varepsilon^4 + \mathcal{O}\left(\varepsilon^5\right) \,. \qquad \text{(A.52)}
$$

The MIs are expanded in powers of the dimensional regulator ε; below we collect the analytic expression of the coefficients in the ε expansion up to terms involving HPLs and 2dHPLs of weight three. The coefficients involving HPLs and 2dHPLs of weight four are also needed in order to obtain the finite part of the leading color coefficient, and we calculated them. However, their analytic expressions are too long to be written in this appendix; the interested reader can find them in the text file included in the arXiv submission of the publication [8].

There are two MIs belonging to the topology Fig. 2.2-(a). The first MI is

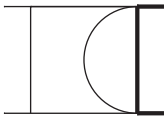

$$
= \int \frac{\mathfrak{D}^d k_1 \mathfrak{D}^d k_2}{P_0\left(k_2\right) P_0\left(k_1 - k_2\right) P_0\left(k_2 - p_1\right) P_0\left(k_2 - p_1 - p_2\right) P_m\left(k_1 - p_3\right)} \qquad \text{(A.53)}
$$

where we define

$$P_0\left(k\right) \equiv k^2\,, \qquad P_m\left(k\right) \equiv k^2 + m^2\,. \tag{A.54}$$

We find

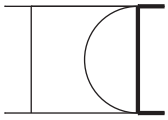

$$= \frac{1}{m^2}\sum_{i=-3}^{0} A_i \varepsilon^i + \mathcal{O}(\varepsilon)\,, \tag{A.55}$$

$$\begin{aligned}
A_{-3} &= \frac{x}{16(1-x)^2}\,,\\
A_{-2} &= -\frac{x}{16(1-x)^2 y}\Big[-2y - yG(0;x) + 2yG(1;x) + (y+1)G(-1;y)\Big]\,,\\
A_{-1} &= -\frac{x}{16(1-x)^2 y}\Big[y(3\zeta(2)-4) + 2(y+1)G(-1;y) - 2yG(0;x)\\
&\quad +(y+1)G(-1;y)G(0;x) + 4yG(1;x) - 2(y+1)G(-1;y)G(1;x)\\
&\quad -2(y+1)G(-1,-1;y) + (y-1)G(0,-1;y) - yG(0,0;x) + 2yG(0,1;x)\\
&\quad +2yG(1,0;x) - 4yG(1,1;x)\Big]\,,\\
A_0 &= -\frac{x}{16(1-x)^2 y}\Big[2y(3\zeta(2)+7\zeta(3)-4) - (7\zeta(2)y - 4y + 11\zeta(2) - 4)G(-1;y)\\
&\quad -y(\zeta(2)+4)G(0;x) + 2(y+1)G(-1;y)G(0;x) - 2y(3\zeta(2)-4)G(1;x)\\
&\quad -4(y+1)G(-1;y)G(1;x) + 4(y+1)\zeta(2)G\left(-1/y;x\right) - 4(y+1)G(-1,-1;y)\\
&\quad -4(y+1)G(0;x)G(-1,-1;y) + 4(y+1)G(1;x)G(-1,-1;y)\\
&\quad +2(y+1)G\left(-1/y;x\right)G(-1,-1;y) + 2(y+1)G(-y;x)G(-1,-1;y)\\
&\quad +2(y-1)G(0,-1;y) + 2yG(0;x)G(0,-1;y) - 2(y-1)G(1;x)G(0,-1;y)\\
&\quad -(y+1)G\left(-1/y;x\right)G(0,-1;y) - (y+1)G(-y;x)G(0,-1;y) - 2yG(0,0;x)\\
&\quad +4yG(0,1;x) + 4yG(1,0;x) - 2(y+1)G(-1;y)G(1,0;x) - 8yG(1,1;x)\\
&\quad +4(y+1)G(-1;y)G(1,1;x) + (y+1)G(-1;y)G\left(-1/y,0;x\right)\\
&\quad -2(y+1)G(-1;y)G\left(-1/y,1;x\right) + (y+1)G(-1;y)G(-y,0;x)\\
&\quad -2(y+1)G(-1;y)G(-y,1;x) + 2(y-1)G(-1,0,-1;y) + 4G(0,-1,-1;y)\\
&\quad -2yG(0,0,-1;y) - 2yG(0,0,0;x) + 4yG(0,0,1;x) + (3y+1)G(0,1,0;x)\\
&\quad -2(3y+1)G(0,1,1;x) + 2yG(1,0,0;x) - 4yG(1,0,1;x) - 4yG(1,1,0;x)\\
&\quad +8yG(1,1,1;x) + (y+1)G\left(-1/y,0,0,x\right) - 2(y+1)G\left(-1/y,0,1;x\right)\\
&\quad -(y+1)G\left(-1/y,1,0;x\right) + 2(y+1)G\left(-1/y,1,1,x\right) - (y+1)G(-y,1,0;x)\\
&\quad +2(y+1)G(-y,1,1;x)\Big]\,.
\end{aligned} \tag{A.56}$$

A. MASTER INTEGRALS FOR TWO-LOOP HEAVY QUARK PRODUCTION

The second MI for the topology in Fig. 2.2-(a) was chosen as

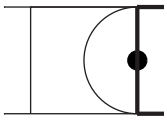

$$= \int \frac{\mathfrak{D}^d k_1 \mathfrak{D}^d k_2}{P_0\left(k_2\right) P_0\left(k_1-k_2\right) P_0\left(k_2-p_1\right) P_0\left(k_2-p_1-p_2\right) P_m^2\left(k_1-p_3\right)} \tag{A.57}$$

Its analytic expression is

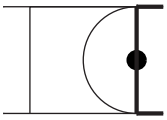

$$= \frac{1}{m^4} \sum_{i=-2}^{0} A_i \varepsilon^i + \mathcal{O}(\varepsilon)\,, \tag{A.58}$$

$$\begin{aligned}
A_{-2} &= \frac{x}{16(1-x)^2 y} G(-1;y)\,, \\
A_{-1} &= -\frac{x}{16(1-x)^2 y}\Big[-G(-1;y)G(0;x) + 2G(-1;y)G(1;x) + 2G(-1,-1;y) \\
&\quad + G(0,-1;y)\Big]\,, \\
A_0 &= -\frac{x}{16(1-x)^2 y}\Big[11\zeta(2)G(-1;y) + 2G(1,0;x)G(-1;y) - 4G(1,1;x)G(-1;y) \\
&\quad - G\left(-1/y,0;x\right)G(-1;y) + 2G\left(-1/y,1;x\right)G(-1;y) - G(-y,0;x)G(-1;y) \\
&\quad + 2G(-y,1;x)G(-1;y) - 4\zeta(2)\; G\left(-1/y;x\right) + 4G(0;x)G(-1,-1;y) \\
&\quad - 4G(1;x)G(-1,-1;y) - 2G\left(-1/y;x\right)G(-1,-1;y) - 2G(-y;x)G(-1,-1;y) \\
&\quad - 2G(1;x)G(0,-1;y) + G\left(-1/y;x\right)G(0,-1;y) + G(-y;x)G(0,-1;y) \\
&\quad + 2G(-1,0,-1;y) - 4G(0,-1,-1;y) - G(0,1,0;x) + 2G(0,1,1;x) \\
&\quad - G\left(-1/y,0,0;x\right) + 2G\left(-1/y,0,1;x\right) + G\left(-1/y,1,0;x\right) \\
&\quad - 2G\left(-1/y,1,1;x\right) + G(-y,1,0;x) - 2G(-y,1,1;x)\Big]\,.
\end{aligned} \tag{A.59}$$

The topology shown in Fig. 2.2-(b) has two MIs. The first one,

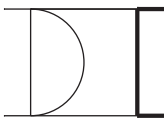

$$= \int \frac{\mathfrak{D}^d k_1 \mathfrak{D}^d k_2}{P_0\left(k_1\right) P_0\left(k_1-k_2\right) P_0\left(k_2-p_1\right) P_0\left(k_1-p_1-p_2\right) P_m\left(k_1-p_3\right)} \tag{A.60}$$

has the following analytic expression:

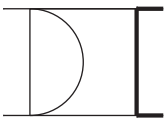

$$= \frac{1}{m^2} \sum_{i=-1}^{0} A_i \varepsilon^i + \mathcal{O}(\varepsilon)\,, \tag{A.61}$$

$$
\begin{aligned}
A_{-1} &= \frac{x}{16(1-x^2)}\left[4\zeta(2)+G(0,0;x)-2G(0,1;x)\right], \\
A_0 &= \frac{x}{16(1-x^2)}\Big[\zeta(2)\Big(16G(-1;x)-G(0;x)-12G(1;x)-4\,G\left(-1/y;x\right)+8\Big) \\
&\quad +7\zeta(3)-2\,G\left(-1/y;x\right)G(-1,-1;y)+2G(-y;x)G(-1,-1;y) \\
&\quad +G(0;x)G(0,-1;y)+G\left(-1/y;x\right)G(0,-1;y)-G(-y;x)G(0,-1;y)+2\,G(0,0;x) \\
&\quad -4G(0,1;x)-G(-1;y)G\left(-1/y,0;x\right)+2G(-1;y)\;G\left(-1/y,1;x\right) \\
&\quad +G(-1;y)G(-y,0;x)-2G(-1;y)\;G(-y,1;x)+4G(-1,0,0;x)-8G(-1,0,1;x) \\
&\quad +2G(0,-1,-1;y)-G(0,0,-1;y)+2\,G(0,0,0;x)-4G(0,0,1;x)-4G(0,1,0;x) \\
&\quad +8G(0,1,1;x)-3G(1,0,0;x)+6\,G(1,0,1;x)-G\left(-1/y,0,0;x\right) \\
&\quad +2G\left(-1/y,0,1;x\right)+G\left(-1/y,1,0;x\right)-2G\;\left(-1/y,1,1;x\right)-G(-y,1,0;x) \\
&\quad +2G(-y,1,1;x)\Big]. \qquad \text{(A.62)}
\end{aligned}
$$

The second MI for the topology in Fig. 2.2-(b) is:

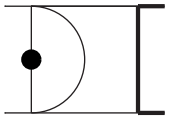

$$
= \int \frac{\mathfrak{D}^d k_1 \mathfrak{D}^d k_2}{P_0\left(k_1\right) P_0^2\left(k_1-k_2\right) P_0\left(k_2-p_1\right) P_0\left(k_1-p_1-p_2\right) P_m\left(k_1-p_3\right)}, \qquad \text{(A.63)}
$$

where

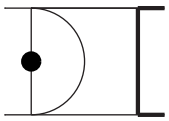

$$
= \frac{1}{m^4}\sum_{i=-3}^{0} A_i \varepsilon^i + \mathcal{O}(\varepsilon), \qquad \text{(A.64)}
$$

$$
\begin{aligned}
A_{-3} &= -\frac{7x}{192(1-x)^2(1+y)}, \\
A_{-2} &= -\frac{x}{96(1-x)^2(1+y)}\Big[-8G(-1;y)+3G(0;x)-6G(1;x)\Big], \\
A_{-1} &= -\frac{x}{24(1-x)^2(1+y)}\Big[-5\zeta(2)-3G(-1;y)G(0;x)+6G(-1;y)G(1;x) \\
&\quad +2G(-1,-1;y)\Big], \\
A_0 &= -\frac{x}{48(1-x)^2(1+y)}\Big[-29\zeta(3)+46\zeta(2)G(-1;y)+3\zeta(2)G(0;x) \\
&\quad +30\zeta(2)G(1;x)-36\zeta(2)G\left(-1/y;x\right)+24G(0;x)G(-1,-1;y) \\
&\quad -12G(1;x)G(-1,-1;y)-18G\left(-1/y;x\right)G(-1,-1;y)-18G(-y;x)G(-1,-1;y) \\
&\quad -9G(0;x)G(0,-1;y)+9G\left(-1/y;x\right)G(0,-1;y)+9G(-y;x)G(0,-1;y)
\end{aligned}
$$

$$
\begin{aligned}
&+18G(-1;y)G(1,0;x) - 36G(-1;y)G(1,1;x) - 9G(-1;y)G\left(-1/y,0;x\right)\\
&+18G(-1;y)G\left(-1/y,1;x\right) - 9G(-1;y)G(-y,0;x) + 18G(-1;y)G(-y,1;x)\\
&+32G(-1,-1,-1;y) - 18G(-1,0,-1;y) - 18G(0,-1,-1;y) + 9G(0,0,-1;y)\\
&+9G(1,0,0;x) - 18G(1,0,1;x) - 18G(1,1,0;x) + 36G(1,1,1;x)\\
&-9G\left(-1/y,0,0;x\right) + 18G\left(-1/y,0,1;x\right) + 9G\left(-1/y,1,0;x\right)\\
&-18G\left(-1/y,1,1;x\right) + 9G(-y,1,0;x) - 18G(-y,1,1;x)\Big] \,. \qquad \text{(A.65)}
\end{aligned}
$$

The are two MIs for the topology in Fig. 2.2-(c). The first one is

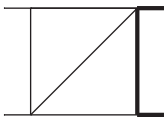

$$
= \int \frac{\mathfrak{D}^d k_1 \mathfrak{D}^d k_2}{P_0\left(k_2\right) P_0\left(k_1-k_2\right) P_0\left(k_2-p_1\right) P_0\left(k_1-p_1-p_2\right) P_m\left(k_1-p_3\right)} \,, \qquad \text{(A.66)}
$$

and the corresponding Laurent expansion in ε is

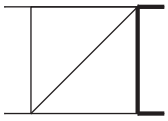

$$
= \frac{1}{m^2}\frac{A_{-1}}{\varepsilon} + \mathcal{O}(\varepsilon^0) \,, \qquad \text{(A.67)}
$$

$$
\begin{aligned}
A_{-1} \;=\; & -\frac{x}{16(1-x+x^2+xy)}\Big[\zeta(3) + \zeta(2)G(-1;y) - 3\zeta(2)G(0;x)\\
&-6\zeta(2)G(1;x) + 4\zeta(2)G\left(-1/y;x\right) - 4G(1;x)G(-1,-1;y)\\
&+2G\left(-1/y;x\right)G(-1,-1;y) + 2G(-y;x)G(-1,-1;y) + G(0;x)G(0,-1;y)\\
&-G\left(-1/y;x\right)G(0,-1;y) - G(-y;x)G(0,-1;y) - 2G(-1;y)G(1,0;x)\\
&+4G(-1;y)G(1,1;x) + G(-1;y)G\left(-1/y,0;x\right) - 2G(-1;y)G\left(-1/y,1;x\right)\\
&+G(-1;y)G(-y,0;x) - 2G(-1;y)G(-y,1;x) + G(-1,0,-1;y)\\
&+2G(0,-1,-1;y) - G(0,0,-1;y) - G(0,0,0;x) + 2G(0,0,1;x)\\
&-G(1,0,0;x) + 2G(1,0,1;x) + 2G(1,1,0;x) - 4G(1,1,1;x)\\
&+G\left(-1/y,0,0;x\right) - 2G\left(-1/y,0,1;x\right) - G\left(-1/y,1,0;x\right)\\
&+2G\left(-1/y,1,1;x\right) - G(-y,1,0;x) + 2G(-y,1,1;x)\Big] \,. \qquad \text{(A.68)}
\end{aligned}
$$

The second MI for the topology in Fig. 2.2-(c) was chosen to be

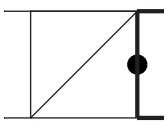

$$
= \int \frac{\mathfrak{D}^d k_1 \mathfrak{D}^d k_2}{P_0\left(k_2\right) P_0\left(k_1-k_2\right) P_0\left(k_2-p_1\right) P_0\left(k_1-p_1-p_2\right) P_m^2\left(k_1-p_3\right)} \,, \qquad \text{(A.69)}
$$

where

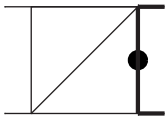

$$= \frac{1}{m^4}\sum_{i=-3}^{0} A_i \varepsilon^i + \mathcal{O}(\varepsilon)\,, \tag{A.70}$$

$$\begin{aligned}
A_{-3} &= -\frac{x}{96(1-x)^2}\,,\\
A_{-2} &= \frac{x}{96(1-x)^2}\Big[-2G(-1;y) - 3G(0;x) + 6G(1;x)\Big]\,,\\
A_{-1} &= \frac{x}{96(1-x)^2}\Big[-11\zeta(2) - 6G(-1;y)G(0;x) + 12G(-1;y)G(1;x) - 4G(-1,-1;y)\\
&\quad -9G(0,0;x) + 18G(0,1;x) + 18G(1,0;x) - 36G(1,1;x)\Big]\,,\\
A_{-0} &= \frac{x}{96(1-x)^2}\Big[-34\zeta(3) + 50\zeta(2)G(-1;y) + 39\zeta(2)G(0;x) + 66\zeta(2)G(1;x)\\
&\quad -72\zeta(2)G\left(-1/y;x\right) + 24G(0;x)G(-1,-1;y) + 24G(1;x)G(-1,-1;y)\\
&\quad -36G\left(-1/y;x\right)G(-1,-1;y) - 36G(-y;x)G(-1,-1;y) - 18G(0;x)G(0,-1;y)\\
&\quad +18G\left(-1/y;x\right)G(0,-1;y) + 18G(-y;x)G(0,-1;y) + 36G(-1;y)G(1,0;x)\\
&\quad -72G(-1;y)G(1,1;x) - 18G(-1;y)G\left(-1/y,0;x\right) + 36G(-1;y)G\left(-1/y,1;x\right)\\
&\quad -18G(-1;y)G(-y,0;x) + 36G(-1;y)G(-y,1;x) + 64G(-1,-1,-1;y)\\
&\quad -36G(-1,0,-1;y) - 36G(0,-1,-1;y) + 18G(0,0,-1;y) - 9G(0,0,0;x)\\
&\quad +18G(0,0,1;x) + 36G(0,1,0;x) - 72G(0,1,1;x) + 54G(1,0,0;x)\\
&\quad -108G(1,0,1;x) - 108G(1,1,0;x) + 216G(1,1,1;x) - 18G\left(-1/y,0,0;x\right)\\
&\quad +36G\left(-1/y,0,1;x\right) + 18G\left(-1/y,1,0;x\right) - 36G\left(-1/y,1,1;x\right)\\
&\quad +18G(-y,1,0;x) - 36G(-y,1,1;x)\Big]\,.
\end{aligned} \tag{A.71}$$

The topology shown in Fig. 2.2-(d) has two MIs. The first one is

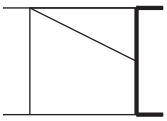

$$= \int \frac{\mathfrak{D}^d k_1 \mathfrak{D}^d k_2}{P_0(k_2)\,P_0(k_1-k_2)\,P_0(k_1-p_1)\,P_0(k_1-p_1-p_2)\,P_m(k_1-p_3)\,P_m(k_2-p_3)} \tag{A.72}$$

with

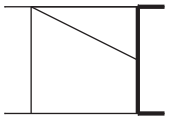

$$= \frac{1}{m^4}\sum_{i=-2}^{-1} A_i \varepsilon^i + \mathcal{O}(\varepsilon^0)\,, \tag{A.73}$$

$$
\begin{aligned}
A_{-2} &= -\frac{x}{32(1-x^2)(1+y)}\Big[-4\zeta(2) - G(0,0;x) + 2G(0,1;x)\Big]\,, \\
A_{-1} &= -\frac{x}{32(1-x^2)(1+y)}\Big[-5\zeta(3) + 8\zeta(2)G(-1;x) + 8\zeta(2)G(-1;y) - 3\zeta(2)G(0;x) \\
&\quad +16\zeta(2)G(1;x) - 8\zeta(2)\ G\left(-1/y;x\right) - 4G\left(-1/y;x\right)\ G(-1,-1;y) \\
&\quad +4G(-y;x)G(-1,-1;y) + 2G(0;x)G(0,-1;y) + 2G\left(-1/y;x\right)G(0,-1;y) \\
&\quad -2G(-y;x)G(0,-1;y) + 2G(-1;y)G(0,0;x) - 4G(-1;y)G(0,1;x) \\
&\quad -2G(-1;y)\ G\left(-1/y,0;x\right) + 4G(-1;y)G\left(-1/y,1;x\right) + 2G(-1;y)G(-y,0;x) \\
&\quad -4G(-1;y)G(-y,1;x) + 2G(-1,0,0;x) - 4G(-1,0,1;x) + 4G(0,-1,-1;y) \\
&\quad -2G(0,0,-1;y) - 3G(0,0,0;x) + 6G(0,0,1;x) + 2G(0,1,0;x) \\
&\quad -4G(0,1,1;x) + 4G(1,0,0;x) - 8G(1,0,1;x) - 2G\left(-1/y,0,0;x\right) \\
&\quad +4G\left(-1/y,0,1;x\right) + 2G\left(-1/y,1,0;x\right) - 4G\left(-1/y,1,1;x\right) - 2G(-y,1,0;x) \\
&\quad +4G(-y,1,1;x)\Big]\,. \qquad \text{(A.74)}
\end{aligned}
$$

The second MI for topology 2.2-(d) is

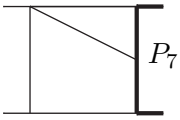

$$
P_7 = \int \frac{\mathfrak{D}^d k_1 \mathfrak{D}^d k_2 (k_2-p_1-p_2)^2}{P_0(k_2)\,P_0(k_1-k_2)\,P_0(k_1-p_1)\,P_0(k_1-p_1-p_2)\,P_m(k_1-p_3)\,P_m(k_2-p_3)} \qquad \text{(A.75)}
$$

where

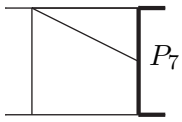

$$
P_7 = \frac{1}{m^2}\sum_{i=-3}^{0} A_i \varepsilon^i + \mathcal{O}(\varepsilon)\,, \qquad \text{(A.76)}
$$

$$
\begin{aligned}
A_{-3} &= \frac{1}{32(1+y)}\,, \\
A_{-2} &= \frac{1}{16(1+y)}\Big[1 - G(-1;y)\Big]\,, \\
A_{-1} &= \frac{1}{16(1+y)(x+1)}\Big[5\zeta(2)x + 2x - 3\zeta(2) + 2 - 2(x+1)G(-1;y) \\
&\quad +2(x+1)G(-1,-1;y) + (x-1)G(0,0;x) - 2(x-1)G(0,1;x)\Big]\,, \\
A_0 &= \frac{1}{16(1+y)(x+1)(1-x+x^2+xy)}\Big[8(x+1)(x-1)^2G(1;x)G(-1,-1;y) \\
&\quad +4(x+1)(x-1)^2G(-1;y)G(1,0;x) - 8(x+1)(x-1)^2G(-1;y)G(1,1;x) \\
&\quad -4(x+1)(x-1)^2G(1,1,0;x) + 8(x+1)(x-1)^2G(1,1,1;x)
\end{aligned}
$$

$$
\begin{aligned}
&-8\left(x^2+yx-x+1\right)(x-1)\zeta(2)G(-1;x)+3\left(3x^2+yx-x-1\right)(x-1)\zeta(2)G(0;x)\\
&-4\left(x^2+4yx-4x+7\right)(x-1)\zeta(2)G(1;x)+8(yx-x+2)(x-1)\zeta(2)G\left(-1/y;x\right)\\
&+4(yx-x+2)(x-1)G\left(-1/y;x\right)G(-1,-1;y)-4x(2x+y-1)\times\\
&\times(x-1)G(-y;x)G(-1,-1;y)-2x(2x+y-1)(x-1)G(0;x)G(0,-1;y)\\
&-2(yx-x+2)(x-1)G\left(-1/y;x\right)G(0,-1;y)+2x(2x+y-1)(x-1)\times\\
&\times G(-y;x)G(0,-1;y)+2\left(x^2+yx-x+1\right)(x-1)G(0,0;x)-2\left(x^2+yx-x+1\right)\times\\
&\times(x-1)G(-1;y)G(0,0;x)-4\left(x^2+yx-x+1\right)(x-1)G(0,1;x)\\
&+4\left(x^2+yx-x+1\right)(x-1)G(-1;y)G(0,1;x)+2(yx-x+2)(x-1)G(-1;y)\\
&G\left(-1/y,0;x\right)-4(yx-x+2)(x-1)G(-1;y)G\left(-1/y,1;x\right)\\
&-2x(2x+y-1)(x-1)G(-1;y)G(-y,0;x)+4x(2x+y-1)(x-1)G(-1;y)\times\\
&\times G(-y,1;x)-2\left(x^2+yx-x+1\right)(x-1)G(-1,0,0;x)+4\left(x^2+yx-x+1\right)\times\\
&\times(x-1)G(-1,0,1;x)+2x(2x+y-1)(x-1)G(0,0,-1;y)+(5x^2+3yx\\
&-3x+1)(x-1)G(0,0,0;x)-2\left(5x^2+3yx-3x+1\right)(x-1)G(0,0,1;x)\\
&-2\left(x^2+yx-x+1\right)(x-1)G(0,1,0;x)+4\left(x^2+yx-x+1\right)(x-1)G(0,1,1;x)\\
&-2\left(x^2+2yx-2x+3\right)(x-1)G(1,0,0;x)+4(x^2+2yx-2x\\
&+3)(x-1)G(1,0,1;x)+2(yx-x+2)G\left(-1/y,0,0;x\right)(x-1)-4(yx-x\\
&+2)(x-1)G\left(-1/y,0,1;x\right)-2(yx-x+2)(x-1)G\left(-1/y,1,0;x\right)+4(yx-x\\
&+2)(x-1)G\left(-1/y,1,1;x\right)+2x(2x+y-1)(x-1)G(-y,1,0;x)-4x(2x+y\\
&-1)(x-1)G(-y,1,1;x)+2\big(5\zeta(2)x^3+4\zeta(3)x^3+2x^3+2yx^2+5y\zeta(2)x^2\\
&-8\zeta(2)x^2+5y\zeta(3)x^2-4\zeta(3)x^2+2yx-3y\zeta(2)x+8\zeta(2)x+6\zeta(3)x-3\zeta(2)-\zeta(3)\\
&+2\big)-2\big(5\zeta(2)x^3+2x^3+2yx^2+4y\zeta(2)x^2-9\zeta(2)x^2+2yx-4y\zeta(2)x+7\zeta(2)x\\
&-3\zeta(2)+2\big)G(-1;y)+4(x+1)\left(x^2+yx-x+1\right)G(-1,-1;y)-4(x+1)\big(x^2\\
&+yx-x+1\big)G(-1,-1,-1;y)+2x(x+1)(y+1)G(-1,0,-1;y)-2\big(5x^3+3yx^2\\
&-6x^2-yx+2x+1\big)G(0,-1,-1;y)\Big]\,.
\end{aligned}
\tag{A.77}
$$

The topology in Fig. 2.2-(e) involves two MIs. One of them is

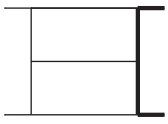

$$
= \int \frac{\mathfrak{D}^d k_1 \mathfrak{D}^d k_2}{P_0(k_2)P_0(k_1-k_2)P_0(k_1-p_1)P_0(k_2-p_1)P_0(k_1-p_1-p_2)P_m(k_1-p_3)P_m(k_2-p_3)}\,, \tag{A.78}
$$

where

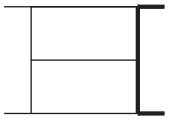

$$
= \frac{1}{m^6}\sum_{i=-4}^{-1} A_i \varepsilon^i + \mathcal{O}(\varepsilon^0)\,, \tag{A.79}
$$

A. MASTER INTEGRALS FOR TWO-LOOP HEAVY QUARK PRODUCTION

$$
\begin{aligned}
A_{-4} &= \frac{x}{12(1-x)^2(1+y)^2}\,, \\
A_{-3} &= \frac{x}{96(1-x)^2(1+y)^2}\Big[-14G(-1;y)+9G(0;x)-18G(1;x)\Big]\,, \\
A_{-2} &= \frac{x}{48(1-x)^2(1+y)^2}\Big[-22\zeta(2)-12G(-1;y)G(0;x)+24G(-1;y)G(1;x) \\
&\quad +4G(-1,-1;y)+3G(0,0;x)-6G(0,1;x)-6G(1,0;x)+12G(1,1;x)\Big]\,, \\
A_{-1} &= \frac{x}{48(1-x)^2(1+y)^2}\Big[-29\zeta(3)+46\zeta(2)G(-1;y)-21\zeta(2)G(0;x) \\
&\quad +66\zeta(2)G(1;x)-24\zeta(2)G\left(-1/y;x\right)+24G(0;x)G(-1,-1;y) \\
&\quad -24G(1;x)G(-1,-1;y)-12G\left(-1/y;x\right)G(-1,-1;y) \\
&\quad -12G(-y;x)G(-1,-1;y)-6G(0;x)G(0,-1;y)+6G\left(-1/y;x\right)G(0,-1;y) \\
&\quad +6G(-y;x)G(0,-1;y)-12G(-1;y)G(0,0;x)+24G(-1;y)G(0,1;x) \\
&\quad +36G(-1;y)G(1,0;x)-72G(-1;y)G(1,1;x)-6G(-1;y)G\left(-1/y,0;x\right) \\
&\quad +12G(-1;y)G\left(-1/y,1;x\right)-6G(-1;y)G(-y,0;x)+12G(-1;y)G(-y,1;x) \\
&\quad +32G(-1,-1,-1;y)-12G(-1,0,-1;y)-12G(0,-1,-1;y) \\
&\quad +6G(0,0,-1;y)+6G(1,0,0;x)-12G(1,0,1;x)-12G(1,1,0;x) \\
&\quad +24G(1,1,1;x)-6G\left(-1/y,0,0;x\right)+12G\left(-1/y,0,1;x\right)+6G\left(-1/y,1,0;x\right) \\
&\quad -12G\left(-1/y,1,1;x\right)+6G(-y,1,0;x)-12G(-y,1,1;x)\Big]\,. \qquad \text{(A.80)}
\end{aligned}
$$

The second MI for the topology in Fig. 2.2-(e) is

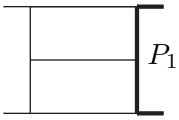

$$
P_1 = \int \frac{\mathfrak{D}^d k_1 \mathfrak{D}^d k_2\, k_1^2}{P_0(k_2)P_0(k_1-k_2)P_0(k_1-p_1)P_0(k_2-p_1)P_0(k_1-p_1-p_2)P_m(k_1-p_3)P_m(k_2-p_3)} \qquad \text{(A.81)}
$$

where

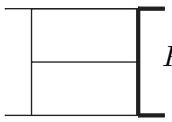

$$
P_1 = \frac{1}{m^4}\sum_{i=-4}^{-1} A_i \varepsilon^i + \mathcal{O}(\varepsilon^0)\,, \qquad \text{(A.82)}
$$

$$
\begin{aligned}
A_{-4} &= \frac{1}{24(1+y)^2}\,, \\
A_{-3} &= \frac{1}{96(1+y)^2}\Big[-10G(-1;y)+3G(0;x)-6G(1;x)\Big]\,, \\
A_{-2} &= \frac{1}{192(1+y)^2}\Big[-47\zeta(2)-24G(-1;y)G(0;x)+48G(-1;y)G(1;x)+32G(-1,-1;y)
\end{aligned}
$$

$$
\begin{aligned}
& -6G(0,-1;y)\Big]\,, \\
A_{-1} \;=\; & \frac{1}{192(1+y)^2}\Big[-85\zeta(3)+188\zeta(2)G(-1;y)+96\zeta(2)G(1;x)-96\zeta(2)\,G\left(-1/y;x\right) \\
& +96G(0;x)G(-1,-1;y)-96G(1;x)G(-1,-1;y)-48G\left(-1/y;x\right)G(-1,-1;y) \\
& -48G(-y;x)G(-1,-1;y)-24G(0;x)G(0,-1;y)+24G\left(-1/y;x\right)G(0,-1;y) \\
& +24G(-y;x)G(0,-1;y)+48G(-1;y)G(1,0;x)-96G(-1;y)G(1,1;x) \\
& -24G(-1;y)G\left(-1/y,0;x\right)+48G(-1;y)G\left(-1/y,1;x\right)-24G(-1;y)G(-y,0;x) \\
& +48G(-1;y)G(-y,1;x)+64G(-1,-1,-1;y)-24G(-1,0,-1;y) \\
& -12G(0,-1,-1;y)+6G(0,0,-1;y)+24G(1,0,0;x)-48G(1,0,1;x) \\
& -48G(1,1,0;x)+96G(1,1,1;x)-24G\left(-1/y,0,0;x\right)+48G\left(-1/y,0,1;x\right) \\
& +24G\left(-1/y,1,0;x\right)-48G\left(-1/y,1,1;x\right)+24G(-y,1,0;x)-48G(-y,1,1;x)\Big] \qquad \text{(A.83)}
\end{aligned}
$$

Finally, the topology in Fig. 2.2-(f) involves three MIs. The first MI we chose is

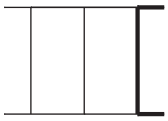

$$
= \int \frac{\mathfrak{D}^d k_1 \mathfrak{D}^d k_2}{P_0(k_1)P_0(k_2)P_0(k_1-k_2)P_0(k_2-p_1)P_0(k_1-p_1-p_2)P_0(k_2-p_1-p_2)P_m(k_1-p_3)} \qquad \text{(A.84)}
$$

where

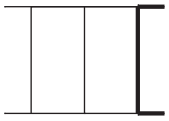

$$
= \frac{1}{m^6}\sum_{i=-4}^{-1} A_i \varepsilon^i + \mathcal{O}(\varepsilon^0)\,, \qquad \text{(A.85)}
$$

$$
\begin{aligned}
A_{-4} \;=\; & \frac{x^2}{24(1-x)^4(1+y)}\,, \\
A_{-3} \;=\; & \frac{x^2}{96(1-x)^4(1+y)}\Big[-10G(-1;y)+3G(0;x)-6G(1;x)\Big]\,, \\
A_{-2} \;=\; & \frac{x^2}{48(1-x)^4(1+y)}\Big[-5\zeta(2)-6G(-1;y)G(0;x)+12G(-1;y)G(1;x)+8G(-1,-1;y)\Big]\,, \\
A_{-1} \;=\; & \frac{x^2}{48(1-x)^4(1+y)}\Big[-13\zeta(3)+38\zeta(2)G(-1;y)+9\zeta(2)G(0;x)+6\zeta(2)G(1;x) \\
& -24\zeta(2)G\left(-1/y;x\right)+24G(0;x)G(-1,-1;y)-24G(1;x)G(-1,-1;y) \\
& -12G\left(-1/y;x\right)G(-1,-1;y)-12G(-y;x)G(-1,-1;y)-6G(0;x)G(0,-1;y) \\
& +6G\left(-1/y;x\right)G(0,-1;y)+6G(-y;x)G(0,-1;y)+12G(-1;y)G(1,0;x) \\
& -24G(-1;y)G(1,1;x)-6G(-1;y)G\left(-1/y,0;x\right)+12G(-1;y)G\left(-1/y,1;x\right) \\
& -6G(-1;y)G(-y,0;x)+12G(-1;y)G(-y,1;x)+16G(-1,-1,-1;y)
\end{aligned}
$$

$$
\begin{aligned}
&-12G(-1,0,-1;y) - 12G(0,-1,-1;y) + 6G(0,0,-1;y) + 6G(1,0,0;x) \\
&-12G(1,0,1;x) - 12G(1,1,0;x) + 24G(1,1,1;x) - 6G\left(-1/y,0,0;x\right) \\
&+12G\left(-1/y,0,1;x\right) + 6G\left(-1/y,1,0;x\right) - 12G\left(-1/y,1,1;x\right) + 6G(-y,1,0;x) \\
&-12G(-y,1,1;x)\Big] \,. \qquad \text{(A.86)}
\end{aligned}
$$

The second MI for the topology Fig. 2.2-(f) was chosen as follows

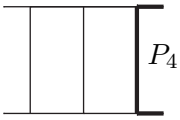

$$
P_4 = \int \frac{\mathfrak{D}^d k_1 \mathfrak{D}^d k_2 \; (k_1-p_1)^2}{P_0(k_1) P_0(k_2) P_0(k_1-k_2) P_0(k_2-p_1) P_0(k_1-p_1-p_2) P_0(k_2-p_1-p_2) P_m(k_1-p_3)} \qquad \text{(A.87)}
$$

where

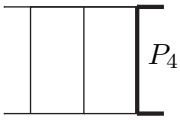

$$
P_4 = \frac{1}{m^4} \sum_{i=-2}^{-1} A_i \varepsilon^i + \mathcal{O}(\varepsilon^0) \,, \qquad \text{(A.88)}
$$

$$
\begin{aligned}
A_{-2} &= \frac{x^2}{16(1-x)^3(1+x)} \Big[4\zeta(2) + G(0,0;x) - 2G(0,1;x) \Big] \,, \\
A_{-1} &= \frac{x^2}{16(1-x)^3(1+x)} \Big[5\zeta(3) + 24\zeta(2) G(-1;x) - \zeta(2) G(0;x) - 8\, \zeta(2) G(1;x) \\
&\quad -8\zeta(2) G\left(-1/y;x\right) - 4G\left(-1/y;x\right) G(-1,-1;y) + 4G(-y;x) G(-1,-1;y) \\
&\quad +2G(0;x) G(0,-1;y) + 2G\left(-1/y;x\right) G(0,-1;y) - 2G(-y;x) G(0,-1;y) \\
&\quad -2G(-1;y) G\left(-1/y,0;x\right) + 4G(-1;y) G\left(-1/y,1;x\right) + 2G(-1;y) G(-y,0;x) \\
&\quad -4G(-1;y) G(-y,1;x) + 6G(-1,0,0;x) - 12G(-1,0,1;x) + 4G(0,-1,-1;y) \\
&\quad -2G(0,0,-1;y) + 2G(0,0,0;x) - 4G(0,0,1;x) - 6G(0,1,0;x) + 12G(0,1,1;x) \\
&\quad -2G(1,0,0;x) + 4G(1,0,1;x) - 2G\left(-1/y,0,0;x\right) + 4G\left(-1/y,0,1;x\right) \\
&\quad +2G\left(-1/y,1,0;x\right) - 4G\left(-1/y,1,1;x\right) - 2G(-y,1,0;x) + 4G(-y,1,1;x) \Big] \,. \qquad \text{(A.89)}
\end{aligned}
$$

The last MI for topology 2.2-(f) is

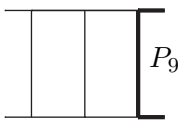

$$
P_9 = \int \frac{\mathfrak{D}^d k_1 \mathfrak{D}^d k_2 \; \left[(k_2-p_3)^2 + m^2 \right]}{P_0(k_1) P_0(k_2) P_0(k_1-k_2) P_0(k_2-p_1) P_0(k_1-p_1-p_2) P_0(k_2-p_1-p_2) P_m(k_1-p_3)} \qquad \text{(A.90)}
$$

with

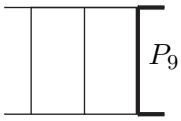

$$P_9 \quad = \quad \frac{1}{m^4} \sum_{i=-4}^{-1} A_i \varepsilon^i + \mathcal{O}(\varepsilon^0)\,, \tag{A.91}$$

$$\begin{aligned}
A_{-4} &= \frac{7x^2}{192(1-x)^4}\,,\\
A_{-3} &= \frac{x^2}{96(1-x)^4}\Big[-8G(-1;y)+3G(0;x)-6G(1;x)\Big]\,,\\
A_{-2} &= \frac{x^2}{24(1-x)^4}\Big[-5\zeta(2)-3G(-1;y)G(0;x)+6G(-1;y)G(1;x)+2G(-1,-1;y)\Big]\,,\\
A_{-1} &= \frac{x^2}{48(1-x)^4}\Big[-29\zeta(3)+58\zeta(2)G(-1;y)+9\zeta(2)G(0;x)+6\zeta(2)\;G(1;x)\\
&\quad -24\zeta(2)G\left(-1/y;x\right)+24G(0;x)G(-1,-1;y)-24G(1;x)G(-1,-1;y)\\
&\quad -12G\left(-1/y;x\right)G(-1,-1;y)-12G(-y;x)G(-1,-1;y)-6G(0;x)G(0,-1;y)\\
&\quad +6G\left(-1/y;x\right)G(0,-1;y)+6G(-y;x)G(0,-1;y)+12G(-1;y)G(1,0;x)\\
&\quad -24G(-1;y)G(1,1;x)-6G(-1;y)G\left(-1/y,0;x\right)+12G(-1;y)G\left(-1/y,1;x\right)\\
&\quad -6G(-1;y)G(-y,0;x)+12G(-1;y)G(-y,1;x)+32G(-1,-1,-1;y)\\
&\quad -12G(-1,0,-1;y)-12G(0,-1,-1;y)+6G(0,0,-1;y)+6G(1,0,0;x)\\
&\quad -12G(1,0,1;x)-12G(1,1,0;x)+24G(1,1,1;x)-6G\left(-1/y,0,0;x\right)\\
&\quad +12G\left(-1/y,0,1;x\right)+6G\left(-1/y,1,0;x\right)-12G\left(-1/y,1,1;x\right)+6G(-y,1,0;x)\\
&\quad -12G(-y,1,1;x)\Big]\,.
\end{aligned} \tag{A.92}$$

A. MASTER INTEGRALS FOR TWO-LOOP HEAVY QUARK PRODUCTION

Bibliography

[1] A B. Goncharov, Math. Res. Lett. 5 (1998), 497-516.
D.J. Broadhurst, Eur. Phys. J. C **8** (1999) 311 [hep-th/9803091].
E. Remiddi and J.A.M. Vermaseren, Int. J. Mod. Phys. A **15** (2000) 725 [hep-ph/9905237].
T. Gehrmann and E. Remiddi, Comput. Phys. Commun. **141** (2001) 296 [hep-ph/0107173].
J. Vollinga and S. Weinzierl, Comput. Phys. Commun. **167** (2005) 177 [hep-ph/0410259].
D. Maître, Comput. Phys. Commun. **174** (2006) 222 [hep-ph/0507152]. hep-ph/0703052.

[2] T. Gehrmann and E. Remiddi, Nucl. Phys. B **601** (2001) 248 [hep-ph/0008287]; Nucl. Phys. B **601** (2001) 287 [hep-ph/0101124]; Comput. Phys. Commun. **144** (2002) 200 [hep-ph/0111255].

[3] J. Vollinga and S. Weinzierl, Comput. Phys. Commun. **167** (2005) 177 [hep-ph/0410259].

[4] U. Aglietti and R. Bonciani, Nucl. Phys. B **698** (2004) 277 [hep-ph/0401193].

[5] R. Bonciani, A. Ferroglia, P. Mastrolia, E. Remiddi and J. J. van der Bij, Nucl. Phys. B **681** (2004) 261 [Erratum-ibid. B **702** (2004) 364] [hep-ph/0310333]; R. Bonciani and A. Ferroglia, Phys. Rev. D **72** (2005) 056004 [hep-ph/0507047]; R. Bonciani, A. Ferroglia and A.A. Penin, Phys. Rev. Lett. **100** (2008) 131601 [arXiv:0710.4775]; JHEP **0802** (2008) 080 [arXiv:0802.2215]; S. Actis, M. Czakon, J. Gluza and T. Riemann, Nucl. Phys. B **786** (2007) 26 [arXiv:0704.2400]; Phys. Rev. Lett. **100** (2008) 131602 [arXiv:0711.3847]; Phys. Rev. D **78** (2008) 085019 [arXiv:0807.4691].

[6] M. Czakon, A. Mitov and S. Moch, Phys. Lett. B **651** (2007) 147 [arXiv:0705.1975].

[7] M. Czakon, Phys. Lett. B **664** (2008) 307 [arXiv:0803.1400].

[8] R. Bonciani, A. Ferroglia, T. Gehrmann and C. Studerus, JHEP **0908** (2009) 067 [arXiv:0906.3671 [hep-ph]].